

## Exact fracture mechanics theory of wood, based on micro crack extension, proving the non-existence of mechanical softening behavior

Exact, according to boundary value- Airy stress function- and limit analysis- approach, for derivations of: “softening”-called yield drop; of mixed mode-, micro-crack-, volume effect-behavior, and the replacement of the current applied insufficient singularity approach.

*T.A.C.M. van der Put,*

*TU-Delft, Civil Engineering and Geosciences, Timber Structures and Wood Technology,*

*Wielengahof 16 NL 2625 LJ Delft, Netherlands Tel: +31 152851980, E-mail: vanderp@xs4all.nl*

### **Delft Wood Science Foundation Publication Series 2016, No 1 - ISSN 1871-675X**

#### **Discussion and extension of all reviewed series C publications (at: [dwsf.nl](http://dwsf.nl) or: [iews.nl](http://iews.nl))**

Tension perpendicular to the grain at notches and joints - C(1990 )

Evaluation of perpendicular to grain failure of beams caused by concentrated loads of joints CIB-C(2000)

“Softening” behavior and correction of the fracture energy - C(2007a)

A new fracture mechanics theory for orthotropic material like wood - C(2007b)

A new fracture mechanics theory of wood - C(2011a)

Fracture mechanics of wood and wood like reinforced polymers - C(2011b)

Discussion of mode II paper of Eng. Frac. Mech. 75 (2008) 4727..- C(2012)

Comment on Mode II critical stress intensity factor paper in *Holzforschung*, Vol. 66, pp 989..- C(2013)

Exact Derivation of the Geometric Correction Factor of the Center Notched Test Specimen, Based On Small Cracks Merging As Explanation of “Softening” - C(2014a)

Limit analysis discussion of design methods for fracture of timber dowel joints loaded perpendicular to grain C(2014b) (Exact and complete Fracture Mechanics of wood” – C(2016).)

#### **Contents**

1. Introduction	2
1.1. References	3
2. The boundary value problem of fracture mechanics	4
2.1. Basic Airy stress function	4
2.2. The elliptical flat crack solution	6
2.2.1. The elliptic hole in an infinite region	6
2.2.2. The mathematical flat crack solution, explaining the singularity approach	7
2.3. Derivation of the mixed I- II- mode equation	8
2.4. Remarks regarding crack propagation	12
2.5. Remarks regarding the empirical confirmation	14
2.6. References	14
3. “Softening”- called, yield drop and hardening like behavior	15
3.1. Introduction	15
3.2. Mode I yield drop behavior	15
3.3. Mode I apparent “softening” behavior, explained by “hardening” behavior	17
3.4. Fracture energy as area under the yield drop curve	19
3.5. Explanation of data and the empirical yield drop curve	21
3.6. Crack merging mechanism	23
3.7. Mode II yield drop behavior	25
3.7.1. Derivation of the mode II critical crack length for yield drop	25
3.7.2. Mode II fracture strength criterion	26
3.8. References	28

# Exact Fracture Mechanics theory

4. Correction of the singularity approach	28
4.1. Introduction	28
4.2. The fictitious crack models	29
4.3. Applied crack growth models	30
4.4. Continuum damage mechanics	31
4.5. Deformation kinetics of fracture	32
4.6. Derivation of the power law:	33
4.7. J-integral application	34
4.8. References	35
5. Energy theory of fracture	35
5.1. Introduction	35
5.2. Critical distortional energy as fracture criterion	35
5.3. Revision of the critical energy release rate equation	37
5.4. References	37
6. Energy approach for fracture of notched beams	38
6.1. Introduction	38
6.2. Energy balance	38
6.3. Experimental verification	40
6.4. References	41
7. Energy approach for fracture of joints loaded perpendicular to the grain.	41
7.1. Introduction	41
7.2. Energy balance	42
7.3. Experimental verification	45
7.4. Design equation of the Eurocode 5	46
7.5. References	46
8. Conclusions chapters 1 to 7	46
9. Weibull size effect in fracture mechanics of wide angle notched timber beams.	47 (51)
9.1. Overview	47
9.2. Introduction	48
9.3. Size effect	49
9.4. Size effect of wide notched beams	50
9.5. Conclusions regarding the size effect	52
9.6. References	52
10. Small cracks fracture mechanics	52
10.1. Introduction.	52
10.2. Derivation of the geometric correction factor of the center notched specimen	53
10.3. Small crack limit strength behavior	55
10.3.1. Small crack limit dimensions	55
10.3.2. Small crack failure criterion	56
10.4. Conclusions regarding small crack fracture mechanics	57
10.5. References	58
11. Conclusions overview	61

## 1. Introduction

Limit analysis is a technical exact approach for reliable upper- and lower bound estimations of the ultimate load. Structural design and strength calculations therefore have to be based on limit analysis, at least on the lower bound equilibrium method by choosing an equilibrium stress system, covering the whole body, which suffices boundary conditions and nowhere surmounts the failure or yield criterion. The high value of  $G_c$ , the critical energy release rate, with respect to the surface energy, shows, that there is sufficient plasticity for a linear elastic- full-plastic approach of limit analysis. Because the isotropic wood-matrix is determining for fracture, linear elastic fracture mechanics (LEFM) applies perfectly for initial fracture of wood. Plastic deformation of the polymeric reinforcement occurs at creases at the crack tip, called fracture process zone. This zone also is the location of micro crack and small crack multiplication and propagation. Wood thus shows local small scale yielding at the crack tip. First yield occurs at the highest elastic stress at the crack boundary, what also is the location of the highest ultimate strain after yield and thus is the location of crack extension. This zone of confined plasticity also can be replaced by the equivalent linear elastic ultimate stress value (similar to the applied linear elastic bending strength diagram to represent full plastic bending compression flow). The difference is an internal equilibrium system, which, as all initial stresses and deformations, does not affect the ultimate load, according to limit analysis theorems, based on the virtual displacements behavior. This explains why, outer regarding the flow stress at the elastic plastic boundary, also LEFM may apply up to failure at the crack boundary. The so called non-linear fracture mechanics approach, which only applies for the singularity approach as correction of infinite stresses, is superfluous, because it is covered by limit analysis, (see chapter 4). The always applied singularity approach is not exact, because e.g. the Airy stress function wrongly predicts failure when whether mode I and/or mode II (without interaction) becomes ultimate at mixed mode fracture. (Thus when  $K_I \leq K_{Ic}$  and/or  $K_{II} \leq K_{IIc}$ ). In Chapter 2, the derivation of the exact, non-singular, mixed mode failure criterion is given. Transformation to polar coordinates, shows that the singularity equations follow directly from the exact non-singular solution. The, in e.g. [1] and [2] given equation:  $\sigma_{ij} = F_{ij}(\theta) \cdot K_I / \sqrt{2\pi r}$  applies for a stress  $\sigma$  perpendicular to crack with a length of  $2c$ . For collinear crack extension is  $\theta=0$  and  $F_{ij}(0)=1$  and is:  $\sigma_{22} = K_I / \sqrt{2\pi r}$  where  $K_I (= \sigma\sqrt{\pi c})$  is an arbitrary shortcut for “ $\sigma\sqrt{\pi c}$ ”, which follows from the exact solution, given in § 2.2.2, (see also: [3], [4]). This is not a necessary parameter following from dimensional analysis, as is stated in [2], page 78, and  $K_I$  is not the limit of  $\sigma_y\sqrt{2\pi r}$ , for crack boundary  $r \rightarrow 0$  and strength  $\sigma_y \rightarrow \infty$ . Both are constant. For small crack extension, (see paragraph 10.2) it is possible, for a freely chosen singularity solution of the Airy stress function, containing points where  $\sigma \rightarrow \infty$ , that then  $c \rightarrow 0$ , with  $K_I$  as limit of  $\sigma\sqrt{\pi c}$ . This is the only possible singularity, which is not a necessary one, but freely chosen, as a possible approximate solution. It is shown that the area under the load-displacement yield drop curve gives the total external work on the test specimen and not the fracture energy as wrongly is assumed. The fracture energy follows from half this area which is equal to the critical strain energy release rate at initial crack extension. For wood this correctly is applied for mode II (see fig. 3.4.3). For mode I however, as for other materials, wrongly the total area is regarded as fracture energy, a factor 2 too high. The finite element method regards the area of the loading-unloading hysteresis loop, Area(OABO) in Fig. 3.4.3, as fracture energy, what indeed, correctly, is equal to half the area under the load displacement curve (0.5·Area(ABCD)).

The derivations lead to an adaption of the energy approach for fracture of beams with square end notches and of joints loaded perpendicular to the grain, providing a simple design method. It further is shown that all, corrective, so called, non-linear fracture mechanics models, as the Dugdale model, the fictitious crack model and the crack growth models, are not exact and thus not reliable. It is shown that failure according to the modes I and II is not simply related to the dissipated stress

## Exact Fracture Mechanics theory

type. The so called mode I may occur by dissipation of elastic shear stress energy only and the so called mode II, by dissipation of bending stress energy only. Determining for the strength is the stress combination at the fracture site (as also follows from the crack closure technique). Therefore, these local stresses should satisfy the derived mixed mode failure criterion, which is shown to follow the critical distortional energy criterion for initial crack extension and follows the Coulomb criterion after “hardening”. It is shown, that strain softening does not exist and thus is not a material property (as assumed by cohesive zone models). This “softening”-called yield drop, is a dynamic elastic unloading process. At loading, in a constant strain rate test, the unloading rate due to the kinetic damage process, [5], is much higher than the loading rate, causing unloading of the specimen. Increasing the loading rate may change this apparent softening behavior into apparent “hardening”. “Softening”-called yield drop behavior therefore is not possible in a constant loading rate test and not in a dead load to failure test, which end in sudden failure (at the speed of sound). This yield drop stress, due to crack extension, is a nominal stress, based on unnotched specimen dimensions, thus is the mean actual stress outside the fractured area, while the actual fracture stress, in the fracture plane (at the ligament), increases and remains ultimate. Apparent and real softening, (e.g. thermal softening), are fully explained by molecular deformation kinetics processes [5], and here, by limit analysis without assuming the impossible negative dissipation, decreasing flow stress, and negative modulus of elasticity of the fictitious crack models. The derivation of the yield drop curve of the “Griffith strength” (which is based on a constant ultimate actual stress in the fracture plane) is given in § 3.3. It appears that small crack extension and crack merging in the high loaded intact clear wood part of the fracture plane explains yield drop and fracture in general, what should replace the Griffith law for overcritical initial crack lengths. In that case the Griffith law only gives the crack closure energy which then is lower than the crack formation energy. The Griffith law only applies for the critical crack length at the top of the initial loading curve. The Griffith stress is a nominal stress, thus based on the intact, uncracked, not ultimate, but elastic loaded section, thus is the actual stress outside the fracture plane, and not the actual ultimate fracture stress on the intact material in the fracture plane.

It is shown in § 2.3, that oblique virtual crack extension in the isotropic matrix, by any stress combination, follows the Coulomb- equation (also called Wu-equation for wood), what implies that failure always occurs by the same actual ultimate uniaxial tensile stress in the matrix, at the crack boundary near the crack tip. This uniaxial tensile failure, as measure of the cohesion strength, leads to the mixed mode Coulomb-equation, eq.(2.3.10), as exact failure criterion. This applies, as initial crack extension, for the isotropic Airy stress function of the isotropic matrix stresses, and for the orthotropic total stresses after multiplication with the derived stiffness factors. Only for mode I loading, is crack extension collinear. For shear, mode II loading, and for combined mode I and II loading, initial, virtual, oblique crack extension is determining providing the lower bound solution, as well as for the isotropic matrix, as for the total orthotropic case.

In the following, is further discussed: the derivation of the power law; the energy method of notched beams and of joints loaded perpendicular to the grain; the explanation of the Weibull size effect in fracture mechanics, and the necessary rejection of the applied crack growth models and fictitious crack models.

### 1.1. References

(See files of [3] to [5] on: [dwsf.nl](http://dwsf.nl), or: [iewws.nl](http://iewws.nl) or: [Researchgate.net](http://Researchgate.net) )

[1] RILEM state of the art report on fracture mechanics, Espoo, 1991.

[2] I. Smith, E. Landis, M. Gong, Fracture and Fatigue in Wood, J. Wiley & Sns, 2003.

[3] van der Put, T.A.C.M., A new fracture mechanics theory of wood”, Nova Science Publishers, New York, 2011. - C(2011a) :

[4] van der Put, T.A.C.M. Adv Mech Eng Res, Vol. 2. Chap. 1: Fracture Mechanics of Wood and Wood like reinforced Polymers, Nova Science Publishers, Inc. New York, 2011 - C(2011b).

[5] van der Put, T.A.C.M., Deformation and damage processes in wood, Delft Univ. press, 1989.

## 2. The boundary value problem of fracture mechanics

### 2.1. Basic Airy stress function

For the solution of the crack-boundary value problem of notches in wood, the orthotropic Airy stress function, is normally based on the spread out of the reinforcement, to act as a continuum, satisfying the equilibrium, compatibility and strength conditions. This behaviour only is possible by interaction of reinforcements through the matrix. Thus also the equilibrium conditions and strength criterion of the matrix, as determining element, have to be satisfied. This also is necessary because the isotropic matrix fails earlier than the reinforcement, and determines initial “flow” behavior. It thus is necessary to solve the Airy stress function for the stresses in the isotropic matrix and then to derive the total (orthotropic) stresses from this solution. This is not applied in other approaches, mentioned e.g. in chapter 2. of [1]. In fact none of the always applied singularity models is exact, leading to the exact, mixed mode failure criterion (The Coulomb- or Wu- equation, eq.(2.5.10)).

In total stresses, the stress-strain relations for the two-dimensional flat crack problem are:

$$\varepsilon_x = c_{11}\sigma_x + c_{12}\sigma_y; \quad \varepsilon_y = c_{12}\sigma_x + c_{22}\sigma_y; \quad \gamma_{xy} = c_{66}\tau_{xy}. \quad (2.1.1)$$

This can be written:

$$\varepsilon_x = \sigma_x / E_x - \nu_{21}\sigma_y / E_y; \quad \varepsilon_y = -\nu_{21}\sigma_x / E_y + \sigma_y / E_y; \quad \gamma_{xy} = \tau_{xy} / G_{xy} \quad (2.1.2)$$

$$\text{The Airy function follows from: } \sigma_x = \frac{\partial^2 U}{\partial y^2}; \quad \sigma_y = \frac{\partial^2 U}{\partial x^2}; \quad \tau_{xy} = -\frac{\partial^2 U}{\partial x \partial y}, \quad (2.1.3)$$

$$\text{satisfying the equilibrium equations: } \frac{\partial \sigma_x}{\partial x} + \frac{\partial \tau}{\partial y} = 0 \quad \text{and} \quad \frac{\partial \tau}{\partial x} + \frac{\partial \sigma_y}{\partial y} = 0 \quad (2.1.4)$$

Substitutions of eq.(2.1.1), using eq.(2.1.3):  $\varepsilon_x = c_{11} \frac{\partial^2 U}{\partial y^2} + c_{12} \frac{\partial^2 U}{\partial x^2}$ , etc., in the compatibility

$$\text{condition: } \frac{\partial^2 \varepsilon_x}{\partial y^2} + \frac{\partial^2 \varepsilon_y}{\partial x^2} = \frac{\partial^2 \gamma_{xy}}{\partial x \partial y}, \quad (2.1.5)$$

$$\text{gives: } c_{22} \frac{\partial^4 U}{\partial x^4} + (c_{66} + 2c_{12}) \frac{\partial^4 U}{\partial x^2 \partial y^2} + c_{11} \frac{\partial^4 U}{\partial y^4} = 0 \quad (2.1.6)$$

The general solution of eq.2.1.6 is:  $U = \sum_i^4 F_i(x + \mu y)$ , where  $\mu$  is a root of the characteristic

equation:  $c_{11}\mu^4 + (c_{66} + 2c_{12})\mu^2 + c_{22} = 0$ , giving:

$$\mu^2 = \frac{c_{66} + 2c_{12}}{2c_{11}} \cdot \left( -1 \pm \sqrt{1 - \frac{4c_{22}c_{11}}{(c_{66} + 2c_{12})^2}} \right), \quad (2.1.7)$$

thus giving 4 imaginary roots. Introducing the complex variables  $z_1$  and  $z_2$ , defined by:

$z_1 = x + \mu_1 y \equiv x' + iy'$  and  $z_2 = x + \mu_2 y \equiv x'' + iy''$ , the solution of eq.2.1.6 assumes the form:

$$U = F_1(z_1) + F_2(z_2) + \bar{F}_1(\bar{z}_1) + \bar{F}_2(\bar{z}_2), \quad (2.1.8)$$

where the bars denote complex conjugate values. The stresses, displacements and boundary conditions now can be written in the general form of the derivatives of these functions. There are standard methods to solve some boundary value problems (e.g. by Fourier transforms of equations of the boundary conditions) but in principle, functions have to be guessed or chosen, or expanded as polynomials, or Fourier series or power series in:  $z$  or  $z^{-1}$ , etc. As alternative, eq.(2.1.6) also can be given as:

$$\left( \frac{\partial^2}{\partial x^2} + \alpha_1 \frac{\partial^2}{\partial y^2} \right) \left( \frac{\partial^2}{\partial x^2} + \alpha_2 \frac{\partial^2}{\partial y^2} \right) U = 0 \quad (2.1.9)$$

where  $\alpha_1 \alpha_2 = c_{11} / c_{22}$  and  $\alpha_1 + \alpha_2 = (c_{66} + 2c_{12}) / c_{22}$ . Introducing 3 sets of polar coordinates for this

## Exact Fracture Mechanics theory

case,  $x + iy = re^{i\theta}$ ,  $x + iy / \sqrt{\alpha_1} = re^{i\theta_1}$ ,  $x + iy / \sqrt{\alpha_2} = re^{i\theta_2}$ , eq.(2.1.9) has e.g. elementary solutions as:  $r_1^{\pm m} \cos(m\theta_1)$ ,  $r_1^{\pm m} \sin(m\theta_1)$ ,  $r_2^{\pm m} \cos(m\theta_2)$ ,  $r_2^{\pm m} \sin(m\theta_2)$ , and solutions may be chosen in the form of series of these types. For wood the elementary solution in  $r^{\pm m}$  are e.g. chosen in [2], what

leads to: 
$$\{\sigma_r, \sigma_\theta, \sigma_{r\theta}\} = \frac{K_A}{(2\pi r)^s} \{f_1(\theta), f_2(\theta), f_3(\theta)\} \quad (2.1.10)$$

and: 
$$\{\sigma_r, \sigma_\theta, \sigma_{r\theta}\} = \frac{K_B}{(2\pi r)^q} \{f_1(\theta), f_2(\theta), f_3(\theta)\} \quad (2.1.11)$$

with  $q \leq s$ . The chosen solution is such, that it applies in the vicinity of the notch root as stress singularity at  $r = 0$ . Because for  $q < s$ , and  $r$  small, the stresses of eq.(2.1.10) are always higher than those of eq.(2.1.11), the solution, eq.(2.1.11), should be rejected based on the boundary conditions at failure, (the highest lower bound solution is also most probable). It thus is not right to mention that there are 2 singular stress fields, only eq.(2.1.10) applies, as approximate solution, only applicable for strength of the uniaxial stress in the main material direction.

Because wood is a reinforced material where the reinforcement interacts through the matrix and also the primary cracking is in the matrix, the failure condition should be based on the strength of the matrix and first the Airy stress function of the matrix-stresses should be solved.

As orthotropic solution, eq.(2.1.10), of  $U$  of eq.(2.1.9), always only smaller powers than  $s = 0.5$  (the value of the common isotropic singularity approach) are found. For instance one finite element solution did show:  $s = 0.45$ , near a rectangular notch, while another investigation of the same notch showed values of  $s = 0.45$  for  $\sigma$  and  $s = 0.10$  for  $\tau$ , while by the finite difference method, powers were found of  $s = 0.437$  for the same rectangular notch of  $90^\circ$  and  $s = 0.363$  and  $0.327$  for wider notch angles of  $153^\circ$  and  $166^\circ$ . This shows that no compatibility, at initial failure, of the (linearly lower) stresses and strains in the isotropic wood matrix are possible. The, now for wood, nearly always applied approach, with (isotropic)  $s = 0.5$ , represents flow of the matrix with the, at that moment, still elastic contribution of reinforcement, thus follows, in principle, the same starting point as the in § 2.3 given derivation of the non-singularity approach.

Wood acts as a reinforced material because lignin is isotropic and hemicellulose and cellulose are transversely isotropic, what means that only one stiffness factor in the main direction has a  $n$ -fold higher stiffness in proportion to the higher stiffness of the reinforcement with respect to the matrix. Thus wood material can be treated to contain a shear-reinforcement and a tensile reinforcement in the main direction, and for equilibrium of the matrix stresses applies:

$$\frac{\sigma_x}{n_1} = \frac{\partial^2 U}{\partial y^2}; \quad \sigma_y = \frac{\partial^2 U}{\partial x^2}; \quad \tau_{xy} = -\frac{\partial^2 U}{\partial x \partial y}, \quad (2.1.12)$$

In stead of using the matrix stresses and the matrix stiffness, also the orthotropic  $n$ -fold higher total stresses and  $n$ -fold higher stiffness can be used to give the same compatibility condition, (thus the same condition for matrix and reinforcement). Inserting, in the compatibility equation, eq.(2.1.5), the total stresses, expressed in the isotropic Airy stress function  $U$  of the matrix stresses, gives:

$$c_{22} \frac{\partial^4 U}{\partial x^4} + (n_6 c_{66} + (1 + n_1) c_{12}) \frac{\partial^4 U}{\partial x^2 \partial y^2} + n_1 c_{11} \frac{\partial^4 U}{\partial y^4} = 0 \quad (2.1.13)$$

For the isotropic matrix is:  $n_1 c_{11} / c_{22} = 1$  and  $(n_6 c_{66} + (1 + n_1) c_{12}) / c_{22} = 2$  giving:

$$\frac{\partial^4 U}{\partial x^4} + 2 \frac{\partial^4 U}{\partial x^2 \partial y^2} + \frac{\partial^4 U}{\partial y^4} = \nabla^2 (\nabla^2 U) = 0 \quad (2.1.14)$$

Thus: 
$$n_1 = \frac{c_{22}}{c_{11}} = \frac{E_x}{E_y}; \quad n_6 = \left( 2 - \frac{c_{12}}{c_{22}} - \frac{c_{12}}{c_{11}} \right) \cdot \frac{c_{22}}{c_{66}} = (2 + \nu_{21} + \nu_{12}) \cdot \frac{G_{xy}}{E_y} \quad (2.1.15)$$

This new orthotropic-isotropic transformation of the Airy stress function and the calculation method based on the stresses of the matrix, is used in the following. It now is possible to use the isotropic

solutions of  $U$  to find the matrix stresses (which should not surmount the matrix strength) and to multiply these matrix stresses with the  $n$ -factors of eq.(2.1.15) for the applied, orthotropic stresses of initial flow of the regarded loading case. This is applied in § 2.2 by solving first the matrix stresses. This is equivalent to the orthotropic solution of the singularity approach, with singularity  $r^{-0.5}$ , what now always is applied.

## 2.2. The elliptical flat crack solution

As shown above, the applied singularity approach with  $s = 0.5$ , only applies for uniaxial loading and thus prevents the solution of mixed mode loading cases and prevents the derivation of a right failure criterion. In stead of such a criterion, critical values are assumed of e.g. the strain energy density, the J-integral, or the maximal principal stress, or a non local stress function, all at a distance away from the crack tip, thus away from the fracture site. A real failure criterion only can be based on the actual ultimate stress in the material which occurs at the crack- boundary. A real, physical possible, crack form is the flat elliptical crack, which is the first expanded of any crack boundary form and because the crack is flat, the higher expanded terms have a negligible, in the limit, zero, contribution. When “flow” occurs around the crack tip, the ultimate strain condition (or ultimate equivalent stress, see chapter 1), at the crack-boundary determines failure and the direction of crack extension. The elastic-plastic boundary (of limit analysis) then acts as an enlarged crack tip boundary. Thus limit analysis approach incorporates linear elastic -, as well as non-linear fracture mechanics. There is no distinction between the two.

### 2.2.1. The elliptic hole in an infinite region

The classical way of analyzing the elliptic crack problem is to use complex variables and elliptic coordinates. The Airy stress function can be expressed in terms of two analytic functions [3], of the complex variable  $z (= x + iy)$  and the transformation to elliptic coordinates in Fig. 2.1, gives:

$$z = x + iy = c \cdot \cosh(\xi + i\eta) \text{ or: } x = c \cdot \cosh(\xi) \cdot \cos(\eta); \quad y = c \cdot \sinh(\xi) \cdot \sin(\eta). \quad (2.2.1)$$

For an elliptic hole,  $\xi = \xi_0$ , in an infinite region with uniaxial stress  $p$  at infinity in a direction inclined at  $\beta$  to the major axis Ox of the ellipse, the Airy stress function  $U$ , satisfying:

$$\nabla^2(\nabla^2 U) = 0, \quad (2.2.2)$$

and satisfying the conditions at infinity and at the surface  $\xi = \xi_0$ , showing no discontinuity of displacement, thus being the solution, is:

$$U = R\{z\phi(z) + \chi(z)\}, \text{ with [3]:} \quad (2.2.3)$$

$$4\phi(z) = p \cdot c \cdot \exp(2\xi_0) \cdot \cos(2\beta) \cdot \cosh(\zeta) + p \cdot c \cdot (1 - \exp(2\xi_0 + 2i\beta)) \cdot \sinh(\zeta) \quad (2.2.4)$$

$$4\chi'(z) = - p \cdot c \cdot [\cosh(2\xi_0) - \cos(2\beta) + \exp(2\xi_0) \cdot \sinh(2\{\zeta - \xi_0 - i\beta\})] \cdot \operatorname{cosech}(\zeta) \quad (2.2.5)$$

where  $\zeta = \xi + i\eta$ .

For the stresses at the boundary, due to a stress  $p$  at an angle  $\beta$  to the crack, is:

$$\sigma_\eta - \sigma_\xi + 2i\tau_{\xi\eta} = 2[\overline{z\phi'(z)} + \chi''(z)]e^{i\delta} \quad \text{and:} \quad \sigma_\xi + \sigma_\eta = 2[\phi'(z) + \overline{\phi'(z)}] = 4R\{\phi'(z)\} \quad (2.2.6)$$

and the tangential stress  $\sigma_t$  at the surface  $\xi = \xi_0$  is simply known from the last equation because

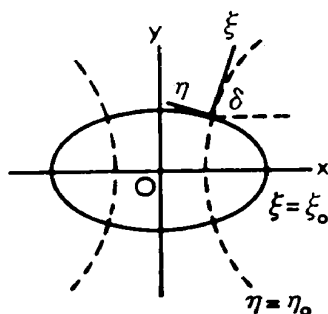


Figure 2.1 - Elliptic hole and coordinates.

## Exact Fracture Mechanics theory

here  $\sigma_\xi = 0$ . Thus: Determining for the strength is the tangential stress  $\sigma_t$  at the crack surface  $\xi = \xi_0$  due to a stress  $p$  at an angle  $\beta$  (of Fig. 2.3.1) to the crack. Thus:

$$\sigma_t = 2[\varphi'(\xi_0 + i\eta) + \varphi'(\xi_0 - i\eta)] = \frac{p(\sinh(2\xi_0) + \cos(2\beta) - \exp(2\xi_0) \cdot \cos(2(\beta - \eta)))}{\cosh(2\xi_0) - \cos(2\eta)} \quad (2.2.7)$$

while  $\chi'(z)$  has to vanish at:  $\xi = \xi_0$ .

Eq.(2.2.7) can be extended for two mutual perpendicular principal stresses  $p_1$  and  $p_2$  (see Fig. 2.3.1) by a simple addition leading to eq.(2.3.1) below.

### 2.2.2. The derivation of the singularity approach

The stresses in the wood-matrix of the limit case of the elliptical notch with  $\xi_0$  approaching zero appear to be comparable with the results of the mathematical flat crack solution of the singularity approach. To derive these singularity equations, (as special case of the general exact solution), new coordinates  $X, Y$  with the origin in the focus of the ellipse are necessary (see Fig. 2.2)

Thus: 
$$X = x - c = c(\xi^2 - \eta^2)/2, \quad Y = y = c\xi\eta \quad (2.2.8)$$

or in polar coordinates: 
$$r = (X^2 + Y^2)^{0.5}, \quad X = r \cdot \cos(\theta), \quad Y = r \cdot \sin(\theta) \quad (2.2.9)$$

and from eq.(2.2.8): 
$$\xi^2 + \eta^2 = 2(X^2 + Y^2)^{0.5} / c = 2r / c \quad (2.2.10)$$

$$\xi = \sqrt{2r/c} \cdot \cos(\theta/2), \quad \eta = \sqrt{2r/c} \cdot \sin(\theta/2), \quad \eta / \xi = \tan(\theta/2) = \tan(\delta) \quad (2.2.11)$$

Using these relation in the stresses  $\sigma_\eta, \sigma_\xi, \tau_{\xi\eta}$  of § 2.2.1 and applying the singularity,  $\xi_0 = 0$  in the general solution of the elliptic Airy stress function, then the tangential stress  $\sigma_\theta$  along a crack boundary  $r_0$ , due to a stress  $p$  at infinity at an angle  $\beta$  with the notch is:

$$(8r/cp^2)^{0.5} \sigma_\theta = -3\sin(\theta/2)\cos^2(\theta/2)\sin(2\beta) + 2\cos^3(\theta/2)\sin^2(\beta) \quad (2.2.12)$$

for a small value of  $r$ , as applies for any flat crack with  $\sqrt{r} \ll \sqrt{2c}$ , so that all terms containing not the factor  $r^{-0.5}$  are negligible and omitted. The other stresses then are:

$$(8r/cp^2)^{0.5} \sigma_r = \sin(\theta/2)(1 - 3\sin^2(\theta/2))\sin(2\beta) + 2\cos(\theta/2)(1 + \sin^2(\theta/2))\sin^2(\beta) \quad (2.2.13)$$

$$(8r/cp^2)^{0.5} \tau_{r\theta} = \cos(\theta/2)(3\cos^2(\theta/2) - 2)\sin(2\beta) + 2\cos^2(\theta/2)\sin(\theta/2)\sin^2(\beta) \quad (2.2.14)$$

For the, for wood always applied, singularity method, the flat crack in the grain direction is supposed to propagate in that direction. Thus  $\theta = 0$ , and eq.(2.2.12) becomes [4]:

$$(8r/cp^2)^{0.5} \sigma_\theta = 2\sin^2(\beta) \quad \text{and is: } \sigma_r = \sigma_\theta \quad \text{and: } \tau_{r\theta} = \sigma_\theta \cotg(\beta). \quad (2.2.15)$$

Mode I failure  $\sigma_\theta = \sigma_t$  occurs when  $\beta = \pi/2$ . Thus when:  $\tau_{r\theta} = 0$  and:

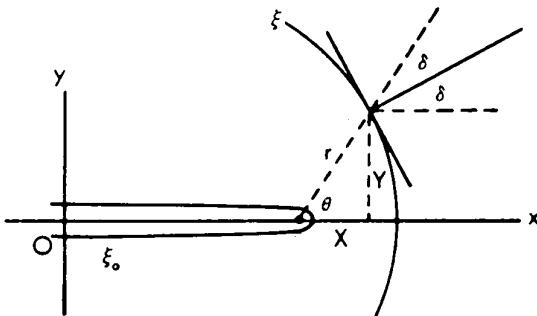


Figure 2.2 - Confocal coordinates

## Exact Fracture Mechanics theory

$$p = \sigma_t \sqrt{(2r/c)} \quad (2.2.16)$$

For pure shear loading, thus for superposition of  $p_1 = S$  at  $\beta = \pi/4$  and  $p_2 = -S$  at  $\beta = 3\pi/4$  in eq.(2.2.12) and in the other equations of the solution, is for crack extension  $\theta = 0$ :

$$(2r/cS^2)^{0.5} \tau_{r\theta} = \left( \cos(\theta/2) \cdot (3\cos^2(\theta/2) - 2) \right)_{\theta=0} = 1 \quad (2.2.17)$$

$$\text{or : } S = \tau_{r\theta} \sqrt{(2r/c)} \quad (2.2.18)$$

with now  $\sigma_r = \sigma_\theta = 0$ , leading to an ultimate shear failure criterion (without interaction with normal stresses) although real shear failure is plastic and a real collinear pure mode II fracture does not exist. Eq.(2.2.16) and (2.2.18) thus are in fact maximum stress conditions for the strengths in the main planes. Fracture is predicted to occur when the tensile strength is reached perpendicular to the grain and / or when the "shear strength" in this plane is reached. Thus:  $K_I \leq K_{Ic}$  and/or

$K_{II} \leq K_{IIc}$  for all stress states. This also is predicted for the n-fold higher quasi orthotropic stresses and is empirically shown to be not right (see eq.(2.2.16) and eq.(2.2.18) in Fig. 2.3.4). This also is shown by theory, eq.(2.3.10), to be not right because according to eq.(2.3.10) failure is always by the actual uniaxial maximal tangential tensile stress along the crack tip boundary, causing oblique crack extension (see fig. 2.3.1, 2.3.2, 2.4.1, 2.4.2). Thus the always applied singularity approach gives no right results for mixed mode failure. The right failure condition for combined stresses, eq.(2.3.10), is derived below in § 2.3.

The singularity approach regards  $r \rightarrow 0$ , what implies  $\sigma_t \rightarrow \infty$ , what is not possible. The strength is finite and also the radius  $r = r_0$  of the equivalent crack boundary (of the fracture process zone) is shown in § 2.3 to be constant for a constant stress intensity factor. Thus for a real singularity solution, a singular Airy stress function, is needed. This is derived and applied in § 10.2.

### 2.3. Derivation of the mixed I- II- mode equation

A general failure criterion [5] follows from the determining ultimate tensile stress which occurs at the crack boundary or better, at the elastic-plastic boundary, as plastic stress, which is necessarily along (thus tangential to) this elastic full plastic boundary (of limit analysis). By an extension of eq.(2.2.7) (by superposition) to  $p_1 = \sigma_1$  inclined at an angle  $\pi/2 + \beta$  to the Ox-axis and  $p_2 = \sigma_2$  inclined at an angle  $\beta$ , (see Fig. 2.3.1), eq.(2.2.7) turns to:

$$\sigma_t = \frac{2\sigma_y \sinh(2\xi_0) + 2\tau_{xy} [(1 + \sinh(2\xi_0)) \cdot \cot(2\beta) - \exp(2\xi_0) \cdot \cos(2(\beta - \eta)) \operatorname{cosec}(2\beta)]}{\cosh(2\xi_0) - \cos(2\eta)}, \quad (2.3.1)$$

where the stresses are given in notch coordinates with the x-axis along the crack. For small values of  $\xi_0$  and  $\eta$  (thus for flat notches), this equation becomes:

$$\sigma_t = \frac{2(\xi_0 \sigma_y - \eta \tau_{xy})}{\xi_0^2 + \eta^2} \quad (2.3.2)$$

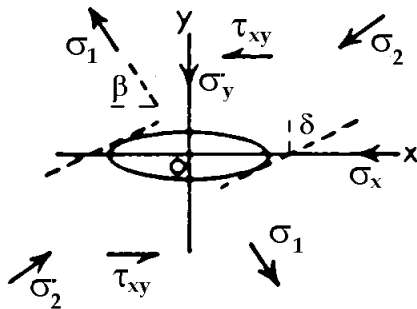


Figure 2.3.1 - Stresses in the notch plane Ox

## Exact Fracture Mechanics theory

The maximum (critical) value of the tangential tensile stress  $\sigma_t$ , for initial failure, depending on location  $\eta$ , is found by:  $d\sigma_t/d\eta = 0$ , giving the critical value of  $\eta$ :

$$-2\tau_{xy}/(\xi_0^2 + \eta^2) - (2(\xi_0\sigma_y - \eta\tau_{xy}) \cdot 2\eta)/(\xi_0^2 + \eta^2)^2 = 0, \text{ or:}$$

$$-\tau_{xy}(\xi_0^2 + \eta^2) = 2\eta(\xi_0\sigma_y - \eta\tau_{xy}) = \eta\sigma_t(\xi_0^2 + \eta^2) \quad (2.3.3)$$

where the second equality sign is due to the substitution of eq.(2.3.2).

$$\text{From the first and last term follows that: } \eta\sigma_t = -\tau_{xy} \quad (2.3.4)$$

$$\text{and from the first 2 terms: } \eta/\xi_0 = (\sigma_y \pm \sqrt{\sigma_y^2 + \tau_{xy}^2})/\tau_{xy} \quad (2.3.5)$$

Elimination of  $\eta$ , from eq.(2.3.4) and (2.26) or from eq.(2.3.5) and eq.(2.3.2) gives:

$$\xi_0\sigma_t = \sigma_y \pm \sqrt{\sigma_y^2 + \tau_{xy}^2} \quad \text{and this can be written:}$$

$$1 = \frac{\sigma_y}{\xi_0\sigma_t/2} + \frac{\tau_{xy}^2}{\xi_0^2\sigma_t^2} = \frac{\sigma_y}{f_t} + \frac{\tau_{xy}^2}{f_v^2} \quad (2.3.6)$$

This is an ultimate stress equation with strengths:  $f_t = \xi_0\sigma_t/2$  and  $f_v = \xi_0\sigma_t$ , where  $\xi_0$  depends on the structural form of the notch. For a hole, as e.g. a dislocation, is:  $2r_0 \approx c$ , or:  $\xi_0 \approx 1$  and because there is a shear movement of the dislocation,  $\sigma_t$  then is the ultimate shear stress.

Transformation from elliptic to polar coordinates by eq.(2.2.11):  $\xi_0 = \sqrt{2r_0/c} \cdot \cos(\delta)$  shows that fracture mechanics only applies when  $r_0$  and  $\sigma_t$  are constant. Thus  $r_0$  is the invariant radius of the fracture process zone near the crack tip of a flat crack. The flat crack solution leads to:

$$1 = \frac{\sigma_y \sqrt{\pi c}}{\sigma_t \sqrt{\pi r_0} / 2 \cdot \cos(\delta)} + \frac{(\tau_{xy} \sqrt{\pi c})^2}{(\sigma_t \sqrt{2\pi r_0} \cdot \cos(\delta))^2} = \frac{K_I}{K_{Ic} \cos(\delta)} + \frac{K_{II}^2}{(K_{IIc} \cos(\delta))^2} \quad (2.3.7)$$

showing that for combined (mixed mode) fracture, when  $\delta \neq 0$ , the apparent stress intensity factors of Irwin,  $K_{Ic} \cos(\delta)$ ,  $K_{IIc} \cos(\delta)$  are not constant. The value of  $\delta$  is stress dependent and depends on the combined loading according to:

$$tg(\delta) = \frac{\sigma_y}{\tau_{xy}} \pm \sqrt{\frac{\sigma_y^2}{\tau_{xy}^2} + 1} \quad (2.3.8)$$

for the stresses in the isotropic matrix.

For pure mode I:  $\delta = 0$ ,  $\tau_{xy} = 0$ , is  $K_{Ic}$  equal to the Irwin value. For pure shear loading of the isotropic matrix is  $\sigma_y = 0$  and  $\delta = 45^\circ$ , the stress intensity is lower than the Irwin value, thus:

$$K_{IIc} \cos(\pi/4) = K_{IIc} / \sqrt{2} = 0.71 \cdot K_{IIc} \quad (2.3.9)$$

This is e.g. measured in: [14] according to Fig.2.3.2, for a relatively small initial crack length, in Agathis lumber, (density  $480 \pm 10 \text{ kg/m}^3$ ; 12% m.c.  $20^\circ\text{C}$ ). The lumber had no defects, as knots or grain distortions so that the specimens consisted of clear wood.

Thus, according to the exact lower bound solution of limit analysis, is the combined- mode I – II and pure mode II fracture a matter of virtual oblique crack extension by reaching the maximal equivalent uniaxial tensile stress (at the maximal strain) along the crack tip boundary. The oblique angle  $\delta$  of eq.(2.3.8) is indicated in Fig. 2.3.3. This oblique crack extension criterion applies, (not only for clear wood) as lower bound criterion. Due to the application of virtual work and virtual displacements applies that any critical oblique direction for initial crack extension has to be regarded. For timber, with many defects, however, an approximate collinear crack extension, with

## Exact Fracture Mechanics theory

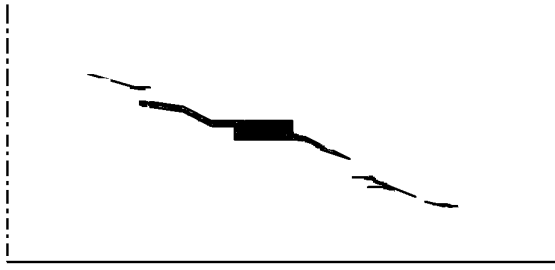


Fig. 2.3.2. Fracture by pure shear loading by oblique crack extension at the uniaxial ultimate tensile stress (opening mode) near the crack tip in the asymmetric four point bending test with small center-slit. (Sketch after photo of [14]), C(2011).

small  $\delta \approx 0$  occurs, due to the strong reinforcement, and eq.(2.3.7) becomes the Coulomb equation:

$$\frac{K_I}{K_{Ic}} + \frac{(K_{II})^2}{(K_{IIc})^2} = 1 \quad (2.3.10)$$

The fact that  $K_{IC} = \sigma_y \sqrt{\pi c_c} = \sigma_t \sqrt{\pi r_0 / 2}$  is constant, as necessary prerequisite for the existence of fracture mechanics with constant  $K_{IC}$ , indicates that  $r_0$  is the radius of the elastic-plastic boundary around the fracture process zone, (which represents a kind of crazing), which size is invariant, (related to the material inhomogenities structure). Thus micro crack behavior within the fracture process zone determines macro crack extension. This is discussed in § 3.6 and Chapter 10.

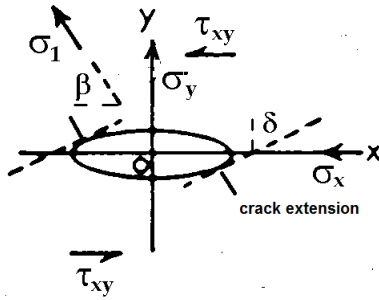


Fig.2.3.3. Uniaxial tensile failure at any mixed I-II mode fracture.

The derivation of eq.(2.3.7) also gives the relation between  $K_{Ic}$  and  $K_{IIc}$ . For the stresses in the isotropic matrix this is:

$$K_{IIc} / K_{Ic} = (\sigma_t \sqrt{2\pi r_0}) / (\sigma_t \sqrt{2\pi r_0} / 2) = 2 \quad (2.3.11)$$

The matrix stresses are also determining for e.g. Balsa wood, which is highly orthotropic, but is light, thus has a low reinforcement content and shows total failure soon after matrix failure and thus shows at failure the isotropic ratio of  $K_{IIc} / K_{Ic} \approx 2$  of the isotropic matrix material, as is verified by the measurements of Wu on Balsa by:  $K_{IIc} \approx 140 \text{ psi} \cdot \text{in}^{0.5}$  and  $K_{Ic} \approx 60 \text{ psi} \cdot \text{in}^{0.5}$  ( $K_{IIc}$  is higher than  $2 \cdot 60$  due to hardening at compression and  $K_{Ic}$  is lower than 70 due to early instability of the test rig in a tensile test, at the initial tensile strength).

Eq.(2.3.10) is generally applicable also when  $\sigma_y$  is a compression stress as e.g. follows from the measurements of Fig. 2.3.4. When the compression is high enough to close the small notches:

( $\sigma_{y,cl} \approx 2G_{xy}\xi_0$ ),  $\tau_{xy}$  has to be replaced, in eq.(2.3.6), by the effective shear stress:

$$\tau_{xy}^* = \tau_{xy} + \mu(\sigma_y - \sigma_{y,cl}) \quad (2.3.12)$$

$$\text{or: } 1 = \frac{\sigma_{y,cl}}{\xi_0 \sigma_t / 2} + \frac{(\tau_{xy}^*)^2}{\xi_0^2 \sigma_t^2}, \quad (2.3.13)$$

what fully explains fracture by compression perpendicular to the notch plane (see Fig. 2.3.4).

## Exact Fracture Mechanics theory

In these equations is  $\mu$  the friction coefficient.

For species, with denser layers than those of Balsa, a much higher value of  $K_{IIc}$  than twice the value of  $K_{Ic}$  is measured because, due to the reinforcement,  $\eta$  becomes smaller than the initial isotropic critical value of eq.(2.3.5) at further stretching. To read the equation in applied total orthotropic stress values, the matrix stress  $\tau_{iso}$  has to be replaced by  $\tau_{ort}/n_6$  and the maximum slope of the tangent, slope  $\delta$  in Fig. 2.2 of the location of the failure stress, is:

$$|\tan \delta| = |\eta_m| / \xi_0 = K_{Ic} / K_{IIc} = 1 / 2n_6 \quad (2.3.14)$$

For small values of  $\eta = -|\eta|$ , eq.(2.3.2) can be written, neglecting  $(\eta/\xi_0)^2$ :

$$\frac{\sigma_y}{\xi_0 \sigma_t / 2} = 1 + \frac{\eta^2}{\xi^2} - \frac{\tau_{xy}}{\xi_0^2 \sigma_t / (2|\eta|)} \approx 1 - \frac{\tau_{xy}}{\xi_0^2 \sigma_t / (2|\eta|)} \quad (2.3.15)$$

where  $|\eta|$  is the absolute value of negative  $\eta$ . Thus:

$$\frac{K_I}{K_{Ic}} + \frac{K_{II}}{K_{IIc}} \approx 1 \quad (2.3.16)$$

$$\text{This is a lower bound, with: } K_{IIc} = \left( \xi_0 / |\eta_m| \right) \cdot K_{Ic} \quad (2.3.17)$$

and the maximal value of  $\eta = \eta_m$  is found by measuring  $K_{Ic}$  and  $K_{IIc}$ , giving e.g. a value of about  $\xi_0 / \eta_m \approx 7.7$ , showing that the disregard of  $(\eta / \xi_0)^2 = 0.017$  with respect to 1 is possible.

Measurements between the lines eq.(2.3.10) and (2.3.16) in Fig. 2.3.4, thus indicate a strong difference between  $K_{IIc}$  and  $K_{Ic}$  of the local structure that is crossed by the propagating crack.

As mentioned, to obtain real orthotropic stresses,  $\tau_{iso} = \tau_{ort} / n_6$  has to be inserted in eq.(2.3.6):

$$\text{Giving: } 1 = \frac{\sigma_y}{\xi_0 \sigma_t / 2} + \frac{\tau_{iso}^2}{\xi_0^2 \sigma_t^2} = \frac{\sigma_y}{\xi_0 \sigma_t / 2} + \frac{\tau_{ort}^2}{\xi_0^2 \sigma_t^2 n_6^2} = \frac{K_I}{K_{Ic}} + \frac{(K_{II})^2}{(K_{IIc})^2} \quad (2.3.18)$$

$$\text{and it follows that: } \frac{K_{IIc}}{K_{Ic}} = \frac{\xi_0 \sigma_t n_6}{\xi_0 \sigma_t / 2} = 2n_6 \quad (2.3.19)$$

according to eq.(2.1.15) is e.g. for small clear specimens:

$$2n_6 = 2 \cdot (2 + \nu_{21} + \nu_{12}) \cdot (G_{xy} / E_y) = 2(2 + 0.57)/0.67 = 7.7 \text{ for Spruce and: } = 2(2 + 0.48)/0.64 = 7.7 \text{ for Douglas Fir in TL-direction. (densities: respectively 0.37 and 0.50; moisture content of 12 \%)}$$

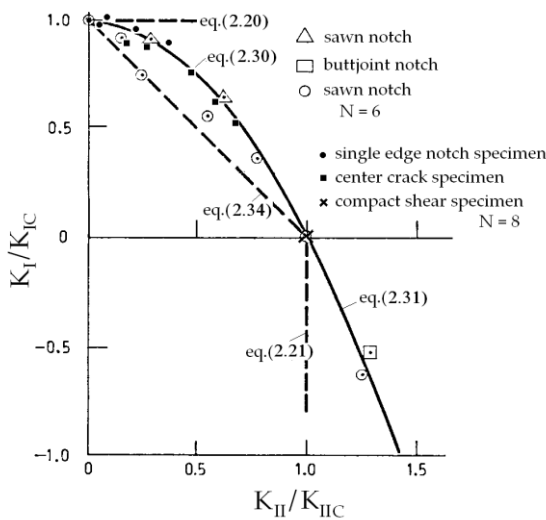


Fig. 2.3.4. Combined mode I-II fracture strength

Thus, for  $K_{Ic} \approx 265 \text{ kN/m}^{1.5}$  is

$$K_{IIc} = 7.7 \cdot 265 = 2041 \text{ kN/m}^{1.5} \text{ in TL - direction.}$$

This agrees with measurements [1]. In RL-direction this factor is 3.3 to 4.4. Thus, , when  $K_{IIc}$  is the same as in the TL-direction, the strength in RL-direction is predicted to be a factor 1.7 to 2.3 higher with respect to the TL-direction. This however applies at high crack velocities (“elastic” failure) and is also dependent on the site of the notch. At common loading rates a factor lower than:  $410/260 = 1.6$  is measured [1] and at lower [7],[1] cracking speeds, this strength factor is expected to be about 1 when fracture is in the “isotropic” middle lamella. It then thus is

independent of the TL and RL-direction according to the local stiffness and rigidity values. To know the mean influence, it is necessary to analyze fracture strength data dependent on the density and the elastic constants of  $n_6$ . From the rate dependency of the strength follows an influence of viscous and viscoelastic processes. This has to be analyzed according to Deformation Kinetics theory [8]. A general problem is further the possible early instability of the mode I-test equipment. In that case constants should be compared with the related mode II data.

Empirical verification of the above derived theory equation, eq.(2.3.18), which is a Coulomb equation, called Wu-equation for wood, is not only obtained by [6], but also by tests of [10], done at the TL-system on eastern red spruce at normal climate conditions using different kinds of test specimens. The usual finite element simulations provided the geometric correction factors, and the stress intensity factors. The lack of fit test was performed on these data, at the for wood usual variability, assuming the five different, often suggested failure equations of Table 2.1. The statistical lack of fit values in the table show, that only the Wu-failure criterion, the third equation of Table 2.1, cannot be rejected due to lack of fit. The Wu-equation is shown to fit also clear wood and timber strength data in [11] and [12], as expected from theory.

**Table 2.1. - Lack of fit values for different failure criteria [10]**

Failure criterion	<i>p</i> -value
$K_I / K_{Ic} = 1$	0.0001
$K_I / K_{Ic} + K_{II} / K_{IIc} = 1$	0.0001
$K_I / K_{Ic} + (K_{II} / K_{IIc})^2 = 1$	0.5629
$(K_I / K_{Ic})^2 + K_{II} / K_{IIc} = 1$	0.0784
$(K_I / K_{Ic})^2 + (K_{II} / K_{IIc})^2 = 1$	0.0001

**2.4. Remarks regarding crack propagation**

Because the mixed mode failure criterion shows that cracks tend to propagate in the direction perpendicular to greatest principal tangential tensile stress in the crack boundary, as shown in Fig. 2.3.2 and 2.3.3, the following modes occur:

In fig. 2.4.1-b, the mixed mode crack propagation starts at an angle with its plane (due to initial matrix failure), but, (due to the reinforcement), may bend back along the fractured zone. Stage b of this crack propagation is due to small-cracks merging in the fractured zone, which propagate to the

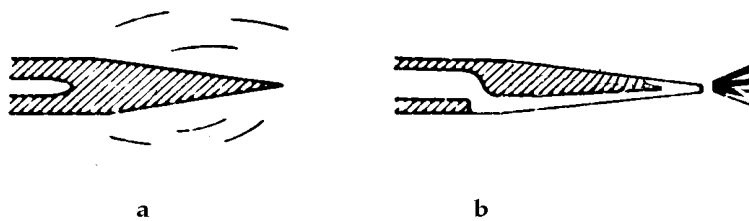


Figure 2.4.1.– a) Craze at the crack tip and: b) Possible crack extension along the fractured zone

in glassy polymers  
: macro-crack tip. For wood, stage b occurs in a parallel crack plane as e.g. given by Fig. 2.4.2. This skipping across fibers is a form of oblique crack extension in a zigzag way, jumping when the equilibrium crack length is reached for the unloading stress level. Real collinear shear crack extension does not exist because the tensile stress there is zero and then thus only plastic shear sliding is possible at a much higher ultimate shear stress.

## Exact Fracture Mechanics theory

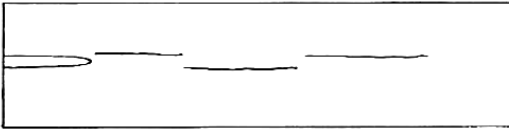


Fig. 2.4.2 Scheme of Wu, of crack extension by skipping across fibers at pure shear loading, showing “mode” II failure to be a tensile failure outside the collinear plane of pure maximal shear stress. (This also can be regarded as a zig zag, small oblique angle, tensile crack propagation, in accordance with theory).

For small- crack extension, collinear crack extension is possible by interference of tensile stresses, causing tensile failure in the weakest plane (along the grain) as is given by Fig. 2.4.3, by crack merging, where each small crack is propagating in the two directions towards the neighboring cracks. This is the principle of the small crack merging mechanism of [13], discussed in § 3.6.

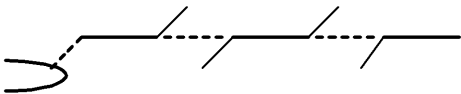


Fig. 2.4.3. Collinear small crack merging.

Figure 2.4.4 explains why, in the mode II standard test, under shear loading, not a sliding mode II, but elastic, sliding unloading, occurs, after an opening mode I tensile failure.

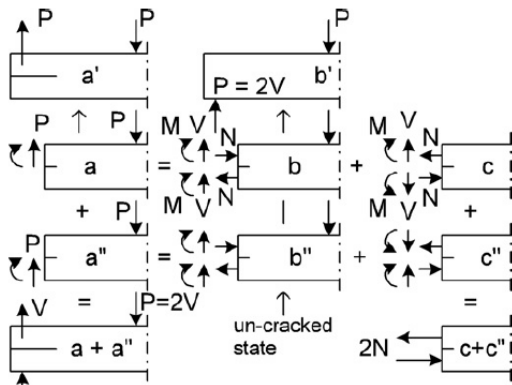


Fig. 2.4.4. Mode II standard test loading of the single end notch beam

This “mode II” test is represented by case  $a + a''$ . If the sign of the lower reaction force  $V$  of this case is reversed and  $P = 0$ , the loading of the mode I, double cantilever beam (DCB) test is obtained, identical to loading case  $c$  with  $N = 0$ . In Fig. 2.4.4, case  $a + a''$  is split in case  $a$  and in case  $a''$ , as loading of the upper and the lower cantilever. Case  $a$  is identical to case  $a'$  which is similar to end-notched beams discussed in [13], Chapter 6. This case behaves like the mode I fracture test as can be seen by loading case  $c$ . The loading near the crack tip, given by case  $a$ , can be seen as the result of superposition of the stresses of cases  $b$  and  $c$ , where the loading of case  $b$  is such, that the un-cracked state of the beam, case  $b'$ , occurs. The loading of case  $c$  is such that the sum of cases  $b$  and  $c$  gives loading case  $a$ . Case  $c$  is the real crack problem and the critical value of strain energy release rate  $G_c$  can be found by calculating the differences of elastic strain energies between case  $a'$  and  $b'$ , the cracked and un-cracked system [13]. Case  $c$  shows the loading of the mode I – DCB-test by  $V$  and  $M$ , combined with shear loading by  $N$  and the energy release rate thus will be somewhat smaller (by this combination with  $N$ ) than the value of the pure DCB-test. For the loading case  $a''$ , the same stresses occur as in case  $a$ , however with opposite directions of  $M$  and  $V$  with respect to those of case  $c$ , according to case  $c''$ , causing crack closure  $c''$ , and friction, dominate above crack opening  $c$ , the crack slit has to be filled with a

## Exact Fracture Mechanics theory

Teflon sheet. By superposition of cases  $c$  and  $c''$ , case  $c + c''$  of shear loading of pure mode II occurs, as crack problem due to the total loading. The normal load couple of  $2N$  is just the amount to close the horizontal shift of both beam ends with respect to each other at that loading stage. This explains the applicability of the virtual crack closure (VCC-) technique. Because the upper cantilever is stronger for shear than the lower cantilever, because of higher compression perpendicular and along the grain (see fig. 5.1 and 5.2, for the, with compression parabolic increasing shear strength), mechanism  $c$  will dominate above  $c''$ , when the lower cantilever start to flow in shear or fails at the support. Thus mode I, case  $c$ , tensile failure occurs.

### 2.5. Remarks regarding the empirical confirmation

Measurements are given in Fig. 2.3.4. The points are mean values of series of 6 or 8 specimens. The theoretical line eq.(2.3.10) is also the mean value of the data of Wu on extended material properties. Only the Australian sawn notch data deviate from this parabolic line and lie between eq.(2.3.10) and the theoretical lower bound eq.(2.3.16). This is explained by the theory by a too high  $K_{IIc}/K_{Ic}$ -ratio, indicating a manufacturing mistake. Using general mean values of the constants, the prediction that  $K_{IIc}/K_{Ic} = 2 \cdot (2 + \nu_{21} + \nu_{12}) \cdot (G_{xy}/E_y)$  agrees with the measurements. However, precise local values of the constants at the notches are not measurable and there is an influence of the loading rate and cracking speed. Thus safe lower bound values have to be used in practice. Fig. 2.3.4 shows that all measurements, including compression, are explained by the theory.

### 2.6. References

- [1] RILEM state of the art report on fracture mechanics, Espoo, 1991.
- [2] R.H. Leicester, Design specifications for notched beams in AS 1720, CIB-W18/38-6-1, meeting 38, Karlsruhe, Germany, August 2005.
- [3] Timoshenko S. and Goodier J.N., Theory of elasticity, McGraw-Hill book comp., N.Y. 1951, 179-204.
- [4] van der Put T.A.C.M., A new fracture mechanics theory for orthotropic materials like wood, Engin. Fract. Mech. 74, (2007) 771-781. – C(2007b)
- [5] van der Put, T.A.C.M., Explanation of the mixed mode interaction equation, COST 508 workshop 2, Bordeaux, April 1992
- [6] Wu E.M., Application of fracture mechanics to anisotropic plates, ASME J. Appl. Mech. Series E, 34 4, Dec. 1967, pp. 967-974..
- [7] Leicester R.H., Fracture strength of wood, First Australian Conf. on Engin. Materials, Univ. of New South Wales, 1974.
- [8] van der Put, T.A.C.M., Deformation and damage processes in wood, Delft Univers. press, 1989.
- [9] Bostrom, L., Method for determination of the softening behaviour of wood etc. Thesis, Report TVBM-1012, Lund, Sweden, 1992.
- [10] Mall S., Murphy J.F., Shottafer J.E., Criterion for Mixed Mode Fracture in Wood, J. Eng. Mech. 109(3) 680-690, June 1983.
- [11] van der Put T.A.C.M., A continuum failure criterion applicable to wood, J Wood Sci (2009) 55:315–322. A(2009)
- [12] van der Put T.A.C.M., A general failure criterion for wood, van der Put T.A.C.M. Proceed. 15th CIB-IUFRO Timber Eng. Group Meeting, Boras, 1982, Sweden.
- [13] van der Put T.A.C.M., A new fracture mechanics theory of wood, Nova Science Publishers, Inc. New York, C(2011a), or more complete: T.A.C.M. van der Put Exact and complete Fracture Mechanics of wood. Theory extension and synthesis of all series C publications
- [14] Susanti CME, Nakao N., Yoshihara H. Examination of the Mode II fracture behavior of wood with a short crack in an asymmetric four-point bending test Eng. Fract. Mech. 78, 16 2011) p 2775-2788.

### 3. Softening- called yield drop, by hardening behavior

#### 3.1 Introduction

A derivation is given of the yield drop curve, the occurring stable part of the Griffith locus. It follows from the derivation that strain softening does not exist.

For long over-critical initial crack lengths, the elastic crack closure energy is not equal, but less than the critical energy release rate and the clear wood ultimate stress criterion applies for the still intact, ultimate loaded clear wood material adjacent to the macro-crack. Thus micro-crack extension then is determining for failure.

The derivation of yield drop is discussed and it is shown in § 3.4 that the area under the load-displacement yield drop curve of e.g. Fig. 3.4.1, 3.4.2, 3.6 or 3.7, divided by the crack area, is not the fracture energy, but the total external work on the specimen. The fracture energy follows from half this area under the loading curve, what is equal to the critical strain energy release rate at the start of yield drop, which is the start of macro-crack extension. For wood this correctly is applied for mode II, see Fig. 3.4.3, where the elastic part of stored energy is subtracted from the total applied energy, given by the loading curve, to get the right nominal fracture energy. For mode I however, wrongly the total area is regarded to be the fracture energy e.g. by fictitious crack models.

#### 3.2. Mode I apparent “softening” behavior, explained by “hardening” behavior

Apparent softening- like yield drop, only exists for the nominal stress. Thus for the actual elastic stress far outside the fracture plane. The Griffith stress, eq.(3.2.8), is a nominal stress, acting on the section  $b \cdot t$  of Fig. 3.1. This actual stress, on the intact part of this specimen, outside the fracture plane, shows “softening- like” yield drop, following the Griffith locus, what thus is not strain softening (at failure) but is elastic unloading of intact, undamaged material, due to the reduction of intact, ultimate loaded, material in the fracture plane. The actual stress at the fractured section shows hardening and quasi hardening by stress spreading and thus no softening as will be derived below. The same applies for the necked actual cross section area of a steel rod (and for reduced fracture area of other materials). Clearly the term strain softening has to be replaced by “elastic unloading”, occurring when the unloading damage process is faster than the loading rate by the constant strain rate test. Because of sufficient plasticity, limit analysis applies and linear elastic fracture mechanics can be applied up to the ultimate stress at the elastic-plastic boundary around the crack tip. The dissipation by micro cracking, plastic deformation and friction within this boundary, called fracture process zone, then is regarded as part of the fracture energy of the macro crack extension. Thus the limit analysis, lower bound, equilibrium method is applicable.

When a specimen is loaded until just before the start of yield drop and then unloaded and reloaded, the behavior has become elastic-full plastic, and the real stress differs an internal equilibrium system with linear elastic loading stresses. Because limit analysis applies, based on virtual

displacements, this internal equilibrium system and other initial stresses and displacements have no influence on the value of the ultimate load and should not be regarded. Therefore also, the Code calculations can be based on a reduced  $E$ -modulus, up to the ultimate state and therefore also replacement in e.g. [2] of  $1/E_1$  by: the bad fit:

$\sqrt{a_{11}a_{22}/2} \cdot \left( \sqrt{a_{22}/a_{11}} + (2a_{12} + a_{66}) / (2a_{11}) \right)^{0.5}$  is not needed and therefore also the derivation below, of the yield drop curve of the fractured specimen, based on the effective  $E$ -modulus, is appropriate.

In Fig. 3.1, a mode I, center notched test specimen is given with a length “ $l$ ”, a width “ $b$ ” and thickness “ $t$ ”, loaded by a stress  $\sigma$  showing

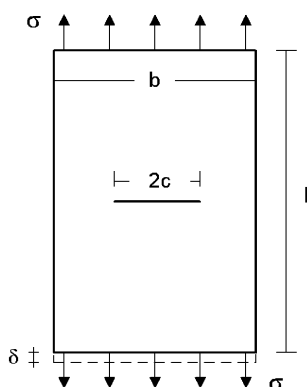


Figure 3.1 – Center notched specimen  $b \times l$  and thickness  $t$ , containing a flat crack of  $2c$ .

## Exact Fracture Mechanics theory

a displacement increase  $\delta$  of the loaded boundary due to a small crack extension. The work done by the constant external stress  $\sigma$  on this specimen, during this crack extension is equal to:

$$\sigma \cdot b \cdot t \cdot \delta = 2W = 2(\sigma \cdot b \cdot t \cdot \delta / 2) \quad (3.2.1)$$

This is twice the increase of the strain energy  $W$  of the specimen. Thus the other half of the external work, equal to the amount  $W$ , is the fracture energy, used for crack extension. Thus the fracture energy is equal to half the applied external energy which is equal to the strain energy increase  $W$  and follows, for the total crack length, from the difference of the strain energy of a body containing a crack and of the same body without a crack:

$$\frac{\sigma^2}{2E_{eff}} b l t - \frac{\sigma^2}{2E} b l t = W \quad (3.2.2)$$

The fracture energy is also equal to the strain energy decrease at fixed grips conditions when  $\delta = 0$ :

$$W = t \sigma \int_{-c}^{+c} v da = \pi \sigma^2 c^2 t / E \quad (3.2.3)$$

where the last two terms give the strain energy to open (or to close) the flat elliptical crack of length  $2c$  and where “ $v$ ” is the displacement of the crack surface in the direction of  $\sigma$ .

From eq.(3.2.2) and eq.(3.2.3) follows that:

$$\frac{\sigma^2}{2E_{eff}} b l t - \frac{\sigma^2}{2E} b l t = \pi \sigma^2 c^2 t / E \quad (3.2.4)$$

Thus the effective Young's modulus of the specimen of Fig.3.1, containing a crack of  $2c$ , is:

$$E_{eff} = \frac{E}{1 + 2\pi c^2 / b l} \quad (3.2.5)$$

The energy equilibrium condition of the critical crack length is:

$$\frac{\partial}{\partial c} (W - G_c 2ct) = 0 \quad (3.2.6)$$

where  $G_c$  is the fracture energy for the formation of the crack surface per unit crack area.

With  $W$  of eq.(3.2.2) or of eq.(3.2.3), eq.(3.2.6) becomes:

$$\frac{\partial}{\partial c} \left[ \frac{\pi \sigma^2 c^2 t}{E} - G_c 2ct \right] = 0, \quad \text{or:} \quad \frac{\partial}{\partial c} \left[ \frac{\sigma^2 b l t}{2E} \left( 1 + \frac{2\pi c^2}{b l} \right) - \frac{\sigma^2 b l t}{2E} - G_c 2ct \right] = 0 \quad (3.2.7)$$

giving both the nominal Griffith strength:

$$\sigma_g = \sqrt{\frac{G_c E}{\pi c}} \quad (3.2.8)$$

which is the actual stress  $P / bt$  outside the fractured section on the intact area  $bt$  of the specimen of Fig. 3.1. The, for strength problems, necessary real, actual stress (expressed in the nominal stress, as wanted) in the weakest actual cross section (ligament) with width:  $b - 2c$ , where fracture occurs, is:

$$\sigma_r = \sqrt{\frac{G_c E}{\pi c}} \cdot \frac{b}{b - 2c} = \sqrt{\frac{G_c E}{\pi b}} \cdot \frac{1}{(\sqrt{c/b}) \cdot (1 - 2c/b)} \quad (3.2.9)$$

and for a damage process and critical state, of the initial crack, applies:  $\partial \sigma_r / \partial c = 0$ , which is a minimum energy principle of the external applied energy. Thus applies for fracture:

$$\frac{\partial \sigma_r}{\partial (c/b)} = \sqrt{\frac{G_c E}{\pi b}} \cdot \frac{6c/b - 1}{2(c/b) \cdot (1 - 2c/b)} \geq 0, \quad (3.2.10)$$

This applies when  $c/b \geq 1/6 = 0.167$ , what always is the case for yield drop at fracture.

For larger initial cracks, the geometrical correction factor  $Y$  of § 10.2, should be accounted. Then:

$$\sigma_r = \frac{1}{Y} \sqrt{\frac{G_c E}{\pi c}} \cdot \frac{b}{b - 2c} = \sqrt{1 - (2c/b)^2} \sqrt{\frac{G_c E}{\pi b}} \cdot \frac{1}{(\sqrt{c/b}) \cdot (1 - 2c/b)} = \sqrt{\frac{G_c E}{\pi b}} \cdot \frac{\sqrt{(1 + 2c/b)}}{(\sqrt{c/b}) \cdot \sqrt{(1 - 2c/b)}},$$

## Exact Fracture Mechanics theory

and:  $\frac{\partial \sigma_r}{\partial (c/b)} > 0$  gives:  $2\frac{c^2}{b^2} + 2\frac{c}{b} - 0.5 > 0$ , or:  $\frac{c}{b} > \frac{\sqrt{2}-1}{2} = 0.207$  (3.2.11)

This applies for yield drop, because the critical value of eq.(3.3.3):  $c_c / b = 1 / \sqrt{6\pi} = 0.23$ , is higher.

The real actual stress  $\sigma_a$  increases, with the increase of the crack length, and “hardening” behavior characterizes the critical stress (not softening). However, a maximal ultimate value for this clear wood strength applies. Thus therefore, a constant maximal value of the energy release rate is basic for the Griffith theory. Then the nominal stress follows the Griffith locus, eq.(3.3.2) (see Fig. 3.6), as failure condition, which also is the condition of no damage acceleration. (Instable failure will not occur, when the testing rig is sufficient stiff). The stress for e.g. critical crack length of  $c/b = 1/6$ , of eq.(3.2.10) is:  $\sigma_c = \sqrt{G_c E / \pi c} = \sqrt{G_c E / (\pi b / 6)}$  and the actual stress at the fracture plane is:  $\sigma_{c,a} = \sqrt{G_c E / (\pi b / 6)} (b / (b - b / 3)) = 1.5 \sqrt{G_c E / (\pi b / 6)}$ . Thus is 1.5 times the nominal Griffith stress. Thus, macro crack extension demands hardening (not softening); thus demands an increase of the tensile strength. The possible tensile strength increase, follows from the exact stress spreading theory of [4]. Although derived for local compression, the sign of the shear stresses may be reversed and the same spreading rules apply for tension. For  $c/b = 1/6$ , according to Fig. 3.1, there is a spreading of the stress on  $b - 2c = 4c$  solid material to the full width:  $b = 6c$ . Thus the tensile strength is:  $1.1\sqrt{6/4} \cdot \sigma_m \approx 1.35 \cdot \sigma_m$ , thus 1.35 times the uniaxial tensile strength  $\sigma_m$ . The nominal, fully spread, stress then is  $1.1 \cdot \sqrt{4/6} \cdot \sigma_m = 0.9 \cdot \sigma_m$ . Thus  $1.5\sigma_g = 1.35\sigma_m$  or:  $\sigma_g = 0.9\sigma_m$ ,

thus:  $\sqrt{(6G_c E) / (\pi b)} = 0.9\sigma_m$ . (3.2.12)

In the same way, when the crack extends after twice this initial length, to:  $c/b = 1/3$ , then the actual stress becomes 3 times the Griffith stress, while the strength is  $1.9 \sigma_m$ , and the fully spread stress would be  $0.64 \cdot \sigma_m$ . Thus  $3\sigma_{g2} = 1.9\sigma_m$ , or  $\sigma_{g2} = 0.63\sigma_m$ , or:

$\sqrt{(3G_c E) / (\pi b)} = 0.63\sigma_m \rightarrow \sqrt{(6G_c E) / (\pi b)} = \sqrt{2} \cdot 0.63\sigma_m \approx 0.9\sigma_m$  (3.2.13)

From eq.(3.2.12) and eq.(3.2.13) follows that the nominal stress intensity  $G_c$  (fracture energy) does not decrease at the start of crack extension. This does occur when the maximal spreading is reached. Then the Griffith law for macro crack extension does not apply anymore and thus is not able to explain fracture at low stresses. This is the case below the factor 0.57 yield drop unloading level (see § 3.5). Thus total fracture can not be due to single macro crack extension. Necessary is clear wood fracture, causing micro crack extension towards the macro crack tip, to explain macro crack extension at low nominal stresses (see § 3.3). Because unloading, outside the fracture plane, follows the stiffness and strength decrease of the specimen, due to crack extension, the mathematical expression of this influence has to be discussed in the next § 3.3.

### 3.3. The “softening”- called yield drop curve

Yield drop, (wrongly called softening) is only possible for nominal stresses, thus for the stress outside the fracture plane and should be described by the limit analysis damage theory of Deformation Kinetics of [5]. But an alternative description is possible by the Griffith theory. The critical strain, of specimen of Fig.3.1, at which the initial crack will grow is, according to eq.(3.2.5):

$\varepsilon_g = \sigma_g / E_{eff} = \sigma_g \cdot (1 + 2\pi c^2 / bl) / E$  (3.3.1)

Substitution of  $c_c = G_c E / \pi \sigma_g^2$ , of the ultimate state, according to eq.(3.2.8), gives:

$\varepsilon_g = \sigma_g / E + 2G_c^2 E / \pi \sigma_g^3 bl$  (3.3.2)

This is the equation of critical (metastable) equilibrium states, representing the yield drop curve due to the Griffith stress eq.(3.2.8), which is the actual stress on the intact part of the specimen, outside the fracture plane, (and is the nominal stress at the fracture plane). It is shown by the dynamics of crack propagation that the velocity of crack propagation is zero at the initial critical crack length

## Exact Fracture Mechanics theory

and that the Griffith relation, eq.(3.2.8), is the condition for zero acceleration of crack extension. Thus the crack of Griffith length is in unstable equilibrium but does not propagate. (For crack propagation a slightly higher stress is necessary).

The “softening” called yield drop curve, eq.(3.3.2), is called “Griffith locus” and has a vertical tangent  $d\varepsilon_g / d\sigma_g = 0$ , occurring at a crack length of:

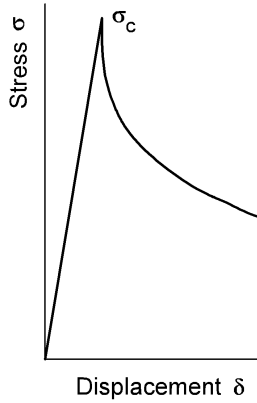
$$c_c = \sqrt{bl / 6\pi} , \quad (3.3.3)$$

which is, with  $\sigma_c$  according to eq.(3.3.5), the top of the curve of Fig. 3.2. The effective length  $l$  of the specimen of fig. 3.1, is the St. Venant distance, thus  $l \approx b$ . Thus  $c_c = \sqrt{b^2 / 6\pi} = 0.23b$ .

(For small initial cracks is  $l \approx 2c$  and  $c_c = 0.1b < b/6$ , thus acting as clear wood fracture).

Due to the steepness of the curve at the top, the first yield drop already may start earlier at:  $0.57 \cdot 0.23b = 0.13b$ , according to eq.(3.5.3). The locus below this top has a negative slope (following eq.(3.3.6)), as should be at unloading, because a positive slope, represents crack recovery, what is not possible. Eq.(3.3.2) shows, that at a positive damage rate  $d\varepsilon_g$  and negative stress rate,  $d\sigma_g$  that then necessarily  $\sigma_g \leq \sigma_c$ . Thus  $\sigma_c$  is necessarily the top of the yield drop curve.

For a distribution of (small) cracks applies, that when their distance is higher than 2 times the St.



Venant distance, the strength of the plate is about the same as when each small crack was alone in the plate. Thus for a critical distribution of small cracks in a repeating pattern,  $b$  and  $l$  in eq.(3.3.3) are the St Venant crack distances and the critical crack distance for extension therefore is about 2.2 times the crack length, because when  $b \approx 2.2 \cdot (2c_c)$  and:  $l \approx 2.2 \cdot (2c_c)$ , then  $bl = b^2 \approx 19c_c^2 \approx 6\pi c_c^2$ , according to eq.(3.3.3). This also applies for a single crack, or extended small cracks after merging to one crack, because the stress flow around the crack needs the St Venant's distance below and above the crack to be on full stress, to be able to extend the, there present, small cracks further. Thus the critical crack density, for the start of yield drop, is reached, when

Fig. 3.2.- Yield drop curve according to eq.(3.3.2) for specimens of Fig. 3.1 or Fig. 3.5.

the intermediate crack distance is about the crack length. This critical distance also is predicted by Deformation Kinetics, discussed in § 4.5, and is used in § 3.6 to explain yield drop by small-crack propagation in clear wood, at the fracture plane (the ligament). Thus, when the intermediate crack distance is the St Venant distance, the stress and strength is about the same as if the crack is alone in an infinite plate. This critical density is given by row A of fig. 3.8, what determines the critical crack density, because a lower crack distance (e.g. due to crack extension) then reduces the strength and starts yield drop. According to eq.(3.3.3), the yield drop line, eq.(3.3.2), can be written:

$$\varepsilon_g = \frac{\sigma_g}{E} \left( 1 + \frac{\sigma_c^4}{3\sigma_g^4} \right), \quad (3.3.4)$$

$$\text{where: } \sigma_c = \sqrt{EG_c / \pi c_c} \quad (3.3.5)$$

is the ultimate load with  $c_c$  according to eq.(3.3.3). The negative slope of the “stable” part of the Griffith locus, being the yield drop line, then is:

$$\frac{\partial \sigma_g}{\partial \varepsilon_g} = - \frac{E}{\frac{\sigma_c^4}{\sigma_g^4} - 1} \quad (3.3.6)$$

Vertical yield drop occurs at the top at  $\sigma_g = \sigma_c$ , and the strain then is:  $\varepsilon_{gc} = (\sigma_c / E) \cdot (1 + 1/3)$  and

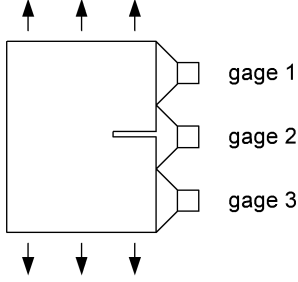
eq.(3.3.4) becomes:

$$\frac{\varepsilon_g}{\varepsilon_{gc}} = 0.75 \cdot \left( \frac{\sigma_g}{\sigma_c} + \frac{\sigma_c^3}{3\sigma_g^3} \right), \quad (3.3.7)$$

More in general eq.(3.3.4) can be written, when related to a chosen stress level  $\sigma_{g1}$ :

$$\frac{\varepsilon_g}{\varepsilon_{g1}} = \frac{\sigma_g}{\sigma_{g1}} \cdot \frac{1 + \sigma_c^4 / 3\sigma_g^4}{1 + \sigma_c^4 / 3\sigma_{g1}^4} \quad (3.3.8)$$

When the occurring yield drop curve starts to differ from the Griffith locus,  $\sigma_c$  decreases, causing a steeper decline of the curve. This failure by a small-crack merging mechanism is discussed in § 3.6.



To measure the fracture energy as area under the yield drop curve, the displacement of the loading jack due to the mean deformation of the specimen has to be known. This can not be obtained by measuring the gage displacement over a crack (see Fig. 3.3), because it is not known what then is measured and this local unloading around the open crack is mainly proportional to the crack length itself, and to possible rotation and is not simply related to the constant ultimate stress state of the ligament and to the decreasing external loading.

Fig. 3.3. Measuring nonsense data at gage 2, (see[6])

### 3.4. Fracture energy as area under the yield drop curve

The basic theory of the energy method, leading to eq.(3.2.1) and eq.(3.2.2), is of course confirmed by the loading curve (Fig. 3.4.1 and 3.4.2). When a test specimen is mechanical conditioned, the effective stiffness is obtained, given e.g. by the lines OA and OC in Fig. 3.4.1 and 3.4.2. In Fig. 3.4.1, the area OAB, written as  $A_{OAB}$ , is the strain energy of the specimen of Fig. 3.1 with a central crack or with two side cracks according to Fig. 3.5 (or Fig. 3.2) with a width “ $b$ ”, length “ $l$ ” and thickness “ $t$ ”, loaded to the stress  $\sigma$ . During the quasi static crack extension from B to D in Fig. 3.4.1, the constant external load  $\sigma$  does work on the specimen of:  $\sigma \cdot b \cdot t \cdot \Delta\varepsilon_{BD} \cdot l = \sigma \cdot b \cdot t \cdot \delta_{BD} = A_{ABDC}$ , where  $\Delta\varepsilon_{BD}$  is the strain increase due to the cracking and  $\delta_{BD}$  the corresponding displacement. The strain energy after the crack extension is  $A_{OCD}$  and the strain energy increase by the crack extension thus is in Fig. 3.4.1:

$A_{OCD} - A_{OAB} = A_{OCD} - A_{OCB} = A_{CBD} = A_{ABDC} / 2$ . Thus half of the external energy:

$A_{ABDC} = \sigma \cdot b \cdot t \cdot \delta_{BD} / 2$  is the amount of increase of the strain energy due to the elongation by  $\delta$ , and the other half thus is the fracture energy which is equal to this increase of strain energy. The same follows at unloading at yield drop. Because every point of the yield drop curve gives the Griffith strength, which decreases with increasing crack length, unloading is necessary to maintain equilibrium. The fracture with unloading step AC in Fig. 3.4.2 is energetic equivalent to the unloading steps AE and FC and the fracturing step EF at constant stress  $EB = FD = (AB + DC)/2$ . Thus  $A_{ABDC} = A_{EBDF}$ . Identical to the first case of Fig. 3.4.1, the increase in strain energy due to crack extension is:

$A_{ODF} - A_{OBE} = A_{ODF} - A_{OBF} = A_{BFD} = 0.5 \cdot A_{EBDF} = 0.5 \cdot A_{ABDC}$ ,

equal to half the work done by the external stresses during crack propagation and thus also equal to the other half, the work of crack extension. It thus is shown that half the area under the load-displacement curve represents the fracture energy. For mode II, only line OACO in Fig. 3.4.1 is measured and  $A_{OAC}$  is regarded to be the fracture energy. Because  $A_{OAC} = A_{BAC} = 0.5 \cdot A_{ABDC}$ , thus equal to half the area under the load displacement curve, the right value is measured and mode II data needs no correction. Because eq.(3.2.2) is based on the total crack length and the strength is a Griffith stress, the initial value  $2c$  of the crack length has to be accounted and  $\sigma$  and  $G_c$  has to be

## Exact Fracture Mechanics theory

related to the whole crack length, including the initial value  $2c$ , and thus should be related to the whole specimen width  $b$  and not to the reduced width of the fracture plane:  $b - 2c$  as is done now and leads to an energy, dependent on the choice of the initial value of  $2c$ . Only for the Griffith stress, the energy method of § 6 and §7 applies for initial failure, based on the energy difference of the cracked and un-cracked state. This has to be corrected together with the correction by a factor 2

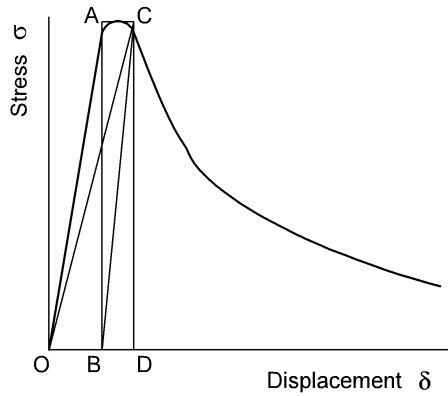


Figure 3.4.1.- Stress – displacement curve for tension, of the specimen of Fig. 3.5.

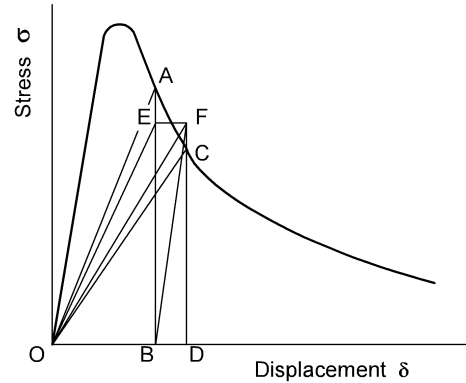


Figure 3.4.2 - Descending branch of the stress – displacement curve of Fig. 3.4.1.

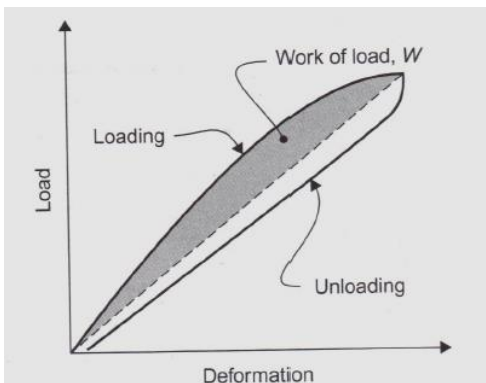


Fig. 3.4.3.

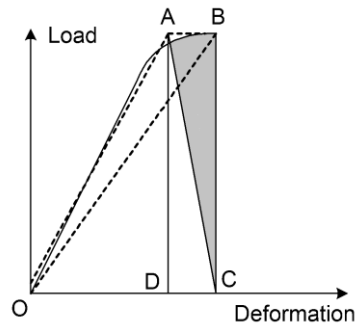


Fig. 3.4.3. Mode II fracture energy (and similarly start mode I) Area:  $OAB = CAB = ABCD/2$

for the mode I fracture energy  $G_c$ . A third correction occurs when  $\sigma_c$  of eq.(3.3.4) changes. The decrease of the mean  $G_c$ -value, starting half way the yield drop stage, shows the decrease of the nominal value of the constant  $G_c$ , due to the formation of an overcritical crack length by the decrease of intact area at the fracture plane. This is discussed in § 3.6.

In [7], not  $A_{ABDC}/2$  is regarded as fracture energy but the amount  $A_{OACO}$  of Fig 3.4.2. This is the irreversible energy of a loading cycle by a crack increment in the specimen. This consists of:  $A_{OEAO} + A_{OEFO} - A_{OFCO} = A_{OEFO} = 0.5 \cdot A_{BEFD} = 0.5 \cdot A_{ABDC}$ , thus again half the area under the load-displacement curve. As discussed in [1], the measurements of [7] indicate the presence of a mechanosorptive process, acting in the whole specimen. It thus should be realized, that the area under the loading curve as:  $A_{OACO}$  gives no separate information on the fracture process alone, of the still intact part of the fracture plane. Other viscoelastic and visco-plastic processes will dominate, what has to be corrected by deformation kinetics [5] by determination of the activation energy of all acting processes. After correction, as first lower bound solution, the fracture energy can be regarded to be constant per unit crack length and then the area below the yield drop curve is

a measure of the amount of intact ultimate loaded material at the increasing crack extension.

### 3.5. Explanation of mode I data and the empirical yield drop curve

The measurements of [3] are complete by measuring the whole loading and yield drop curve and using the compact tension tests as control, being a control by the different loading case.

The graphs of [3], Fig. 3.6 and 3.7, are the result of tension tests on the specimen of Fig. 3.5.

The length of the specimen was  $l = 3$  mm, the width and thickness:  $b = t = 20$  mm and the notch length  $2c = 2 \times 5 = 10$  mm with a notch width of 0.5 mm.

In figures 3.6 and 3.7, the measured stress-displacement is given together with the lines 1 and 2 according to the Griffith locus eq.(3.3.7). The strain  $\varepsilon_g$  follows from the displacements at the  $x$ -axis of the figures divided through 3 mm, the measuring length and length of the specimen. Because of

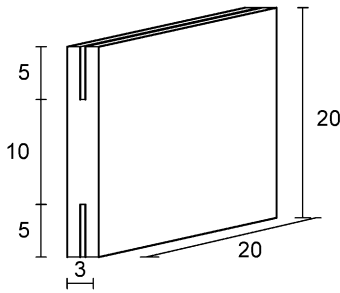


Figure 3.5 - Geometry of specimens [3]

the small length of 3 mm, not the whole width  $b$  of the specimen is active. Assuming a possible spreading of: 1.2:1, through the thickness of 1.25 mm above and below the side notches, the working width  $b_{eff}$  is equal to the length of the fracture plane plus 2 times 1.2 x 1.25 or:  $b_{eff} = 10 + 3 = 13$  mm.

Thus the notch lengths in Fig. 3.5 should be regarded to be 1.5 mm in stead of 5 mm. The stresses in the figures 3.6 and 3.7 of [3], are related to the length of the fracture plane and not to the width  $b_{eff}$ ,

according to the nominal Griffith stress. Thus the actual stresses have to be reduced by a factor  $10/13 = 0.77$ . The standard compact tension tests of [3] showed a stress intensity  $K_{Ic}$  of:  $330 \text{ kNm}^{-3/2}$ .

This value also should follow from the area under the yield drop curve of that compact tension test. When half the area of that diagram is taken to be the fracture energy, in stead of the total area, then  $K_{Ic}$ , mentioned in [3], indeed is corrected to the right value of:  $467/\sqrt{2} = 330 \text{ kNm}^{-3/2}$  giving an empirical verification of the theory.

Regarding the short double edge notched specimens of Fig. 3.5, the measured E-modulus should be related to the effective width of 13 mm in stead of the width of 10 mm of the fracture plane and therefore is  $E = 700 \times 10/13 = 700 \times 0.77 = 539$  MPa. The critical energy release rate then is:

$$G_c = K_{Ic}^2 / E = 330^2 / 539 = 200 \text{ N/m} \quad (3.5.1)$$

The measured value of  $G_c$  from the area under the stress-displacement curve is given in [3] to be 515 N/m. But, because half this area should have been taken and this value is wrongly related to the length of the fracture plane in stead of on  $b_{eff}$ , the corrected value is:

$G_c = 1/2 \times 515 \times 0.77 = 200$  N/m, as found above, eq.(3.5.1), giving again an empirical verification of the theory, now by the tests on the short double edge notched specimens.

As shown before, the yield drop curve of Fig. 3.6 has (as Fig.3.2) a vertical tangent at the top

$d\sigma_g / d\varepsilon_g = \infty$ . The critical crack length for yield drop:  $c_c = \sqrt{bl} / 6\pi$  according to eq.(3.3.3) is:

$$c_c = \sqrt{(b_{eff}l) / (6 \cdot \pi)} = \sqrt{(13 \cdot 3) / (6 \cdot \pi)} \cdot 10^{-3} = 1.4 \cdot 10^{-3} = 1.4 \text{ mm} \quad (3.5.2)$$

This confirms the mentioned initial St. Venant crack length to be as small as about 1.5 mm.

In Fig. 3.6, at the Griffith maximal stress of  $(0.77) \cdot 7 = 5.39$  MPa, is:  $K_{Ic} = \sigma \sqrt{\pi c}$  or:

$$K_{Ic} = 5.39 \cdot \sqrt{\pi \cdot 1.4 \cdot 10^{-3}} = 0.36 \text{ MNm}^{-3/2}, (> 0.33 \text{ MNm}^{-3/2}), \text{ for this strong specimen.}$$

The strength level above 4 (to 4.6) Mpa, given by Fig. 3.7, is measured in 3 of the 10 specimens of the discussed series: T1309/2309 of [3] and Fig. 3.6, shows the highest level, thus the total curve, as given by Fig. 3.2, indicating that this strength of the fracture plane, according to crack-pattern A of fig. 3.8, was determining for yield drop. The other specimens of this series did show lower strength

## Exact Fracture Mechanics theory

values than  $\sim 4$  MPa, as applies for further unloading due to already extended small cracks. At § 3.3 and § 4.5 is shown that for the critical small crack density of eq.(3.3.3), the crack distance is about the crack length, as given by row A of Fig. 3.8. Line 1 of Fig. 3.6 gives the primary crack extension, eq.(3.3.7), by this critical crack density. Curve 1 levels off from the measurements at  $\sigma = 4$  Mpa, where the next process starts, given by line 2 of Fig. 2.6. This thus happens when the crack length has become about 3 times the initial critical value  $c_{c,0}$ , because then:

$$\sigma_g = \sqrt{\frac{EG_c}{\pi 3c_{c,0}}} = 0.57 \cdot 7 = 4 \text{ MPa} \quad (3.5.3)$$

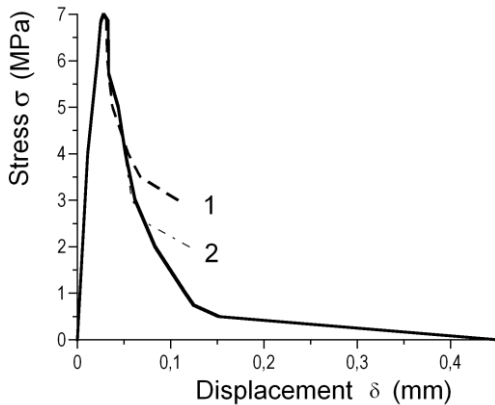


Figure 3.6 - Stress - displacement of specimen T 1409 of [3].

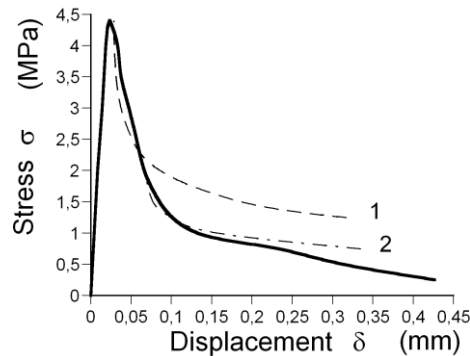


Figure 3.7 - Stress - displacement of specimen T 1509 of [3]

This 3 times larger crack length is given by crack row B of Fig. 3.8. The top value  $\sigma_c$  of the first process on row A, is  $\sigma_c = 7$  Mpa, for all values of  $\sigma_g$  between 4 and 7 Mpa. The top value of the second process B on  $3c_{c,0}$  cracks, is:  $\sigma_c = 4$  MPa. This process ends, where cracks of  $7c_{c,0}$  lengths remain, according to row C of Fig. 3.8. Thus when:

$$\sigma_g = \sqrt{\frac{EG_c}{\pi 7c_c}} = \frac{1}{\sqrt{7}} \sqrt{\frac{EG_c}{\pi c_c}} = \frac{1}{\sqrt{7}} \cdot 7 = 0.378 \cdot 7 = 2.65 \text{ Mpa} \quad (3.5.4)$$

This is where line 2 of Fig. 3.6 levels off from the data line. This stress is equal to top value  $\sigma_c$  of the next process C, on  $7c_{c,0}$  cracks, given below line 2 in Fig. 3.6. This ends at:

$(1/\sqrt{15}) \cdot 7 = 0.258 \cdot 7 = 1.81$  Mpa, where the process on  $15c_{c,0}$  starts. However, processes towards the longer cracks of 15, 31 and 63  $c_{c,0}$  are not distinct and it is probable that, due to the high actual stress, failure may occur at any point of the still intact part of the ligament.

The Griffith law is apparently paradoxical. At a certain stress level there is enough energy to fracture a critical crack length of  $2c$ . But at crack extension the stress level lowers, thus there is not enough energy to extent the longer crack. Thus initial and further crack extension is impossible. The reason of this paradox is that nominal stresses are regarded, while fracture laws only can apply in real-, thus in actual stresses. After the first process of row A, half of the intact material is fractured, but the stress level is not halved, but 0.57 times lower. The next steps to rows B and C. show respectively stress levels of 0.378 and 0.258, thus more than 0.25 and 0.125 needed to fracture the remaining 0.25 and 0.125 intact material. The proof of the increasing sufficient stress level for further fracture is given by eq.(3.2.10), because not only the first derivative but also the second derivative is positive for when  $c/b > 1/6$ . An alternative description of the process, is to regard micro-crack extension in the high loaded clear wood parts of  $2c$  lengths (see fig. 3.8). This happens from the start to the end of the process. Thus to regard clear wood failure. Although, weakest



## Exact Fracture Mechanics theory

parts of 2c length of rows A, B or C are determining for failure. Thus micro crack formation and propagation in the remaining high loaded intact, clear wood, part of the ligament is determining. This determining clear wood failure, also applies from the beginning (as discussed in e.g. § 3.7), so that fracture always is due to the same micro crack extension. This damage process acts in all these parts at the same time during the whole fracture process. Thus, for the whole fracture process, from the beginning to full separation, may apply, that micro-cracking in the intact part (b - 2c) of Fig. 3.1, of the ligament is determining, and that the concentration is not determined by the merged macro crack length:  $c_c = \sqrt{lb/6\pi} = 0.23b$ , but by the merged, clear wood, micro crack length of:

$$c_c' = \sqrt{(b-2c)^2/6\pi} = 0.23 \cdot (b-2c). \quad (3.6.3)$$

For every successive process applies optimal, that every crack merges with one neighbor by extension at one side over a distance of  $1c_0$ , leading to halving of the solid area of the ligament, and to an increase of the crack length by:

$$2c_{n+1} = 2 \cdot 2c_n + 2c_0, \text{ giving } 2c_1 = 6c_0 \text{ and } 2c_2 = 2 \cdot 2c_1 + 2c_0 = 14c_0. \quad (3.6.4)$$

$$\text{The increase of the crack length is: } \Delta(2c)' = 2c_{n+1} - 2c_n = 2c_n + 2c_0. \quad (3.6.5)$$

Including the initial crack length of  $2c_0$ , the increase of the total crack length is:

$$\Delta(2c) = 2c_{n+1} - 2c_n - 2c_0 = 2c_n. \quad (3.6.6)$$

More general for all merging cracks at any distance during time  $\Delta t$  this is:

$$\Delta(c) = \beta_1 \cdot c \cdot \Delta t \quad (3.6.7)$$

and as the determining damage deformation kinetics [5] equation this is (see § 5, eq.5.3):

$$dc/dt = \beta_2 \cdot c_0 \cdot \exp(\sigma\varphi), \quad (3.6.8)$$

when the initial site concentration  $c_0$  is high, (zero-order reaction) as applies for row A of Fig. 3.

This equation can be written:  $\ln(\dot{c}) = \ln(C) + \phi\sigma_v$ , or, because  $\phi\sigma_{v0} = n$ , is constant, independent of stress, due to the time stress equivalence, [5], is:

$$\frac{\sigma_v}{\sigma_{v0}} = 1 + \frac{1}{n} \ln\left(\frac{\dot{c}}{c_0}\right) \quad (3.6.9)$$

showing that the combined Griffith – crack-merging model is identical to common damage behavior. Fracture is caused by accumulation of broken bonds, thus follows a thermal activated process [5], as also applies for the following micro-crack formation and large cracks formation due to coalescence of micro-cracks, (in a coupled process). Normally, when no large cracks are present, micro-cracks are formed randomly through the loaded body independently of one another. When the critical density is reached, coalescence and initial crack formation occurs. However, when the loaded body contains an initial crack, micro-cracks formation occurs in the vicinity of the crack tip (due to the high stress). Then the density of micro-cracks does not increase, outside this region where the micro-crack joins the larger crack, at formation, as part of the crack merging process. The kinetics, however, shows the same behavior as for clear wood, indicating that always the same micro-crack propagation is determining. As shown in [5], always two coupled processes act, showing the same time-temperature and the same time-stress equivalence of both. (A high concentration of micro-cracks delivers the sites for the low concentration of macro-cracks). The reaction thus is autocatalytic, what means that one of the reaction products is also reactant and therefore a catalyst in the coupled reaction. The mode I notched specimen, discussed here, shows the coupled low concentration reaction of the macro-crack extension, by its property of a strong yield drop behavior of the nominal stress. The coupled processes occur for the crack merging processes, where the initial crack length is the reactant and the reaction product is the newly formed crack length what also applies for macro-crack extension due to the micro-crack merging process. The numerous small-cracks, growing towards each other and to the macro notch, provide the site for the macro crack to grow as coupled second low-concentration reaction process. The kinetics of this bond breaking process is discussed in [5].

### 3.7. Mode II yield drop behavior

As shown before, for mode I, yield drop occurs when the rate of the damage process is faster than the rate of loading in a constant strain rate test. This causes unloading, what has nothing to do with softening behavior. Analysis of tests on overcritical crack lengths is necessary to know properties of yield drop behavior. Therefore first, in paragraph 3.7.1, a prediction of the mode II critical crack length is discussed. This critical length causes the start of yield drop, thus represents the top of the yield drop curve.

#### 3.7.1. Derivation of the mode II critical crack length for yield drop

Analogous to the mode I derivation in paragraph 3.2, is the fracture energy equal to the strain energy increase  $W$ :

$$\frac{2(1+\nu)\tau^2}{2E_{eff}}blt - \frac{2(1+\nu)\tau^2}{2E}blt = W, \quad (3.7.1.1)$$

and is, analogues to eq.(3.2.3) and eq.(3.2.2):

$$W = \pi(\sigma^2 + \tau^2)c^2t / E = \pi\tau^2c^2t / E, \quad (3.7.1.2)$$

for pure shear. Thus:

$$\frac{2(1+\nu)\tau^2}{2E_{eff}}blt - \frac{2(1+\nu)\tau^2}{2E}blt = \pi\tau^2c^2t / E \quad (3.7.1.3)$$

$$\text{giving: } E_{eff} = \frac{E}{1 + \pi c^2 / bl(1+\nu)} \quad (3.7.1.4)$$

The Griffith stress  $\tau_g$  follows from:

$$\frac{\partial}{\partial c}(W - G_c ct) = 0, \text{ or: } \frac{\partial}{\partial c} \left[ \frac{\pi\tau^2c^2t}{E} - G_c ct \right] = 0; \text{ or: } \tau_g = \sqrt{\frac{G_c E}{2\pi c}} \text{ or: } c_c = G_c E / (2\pi\tau^2) \quad (3.7.1.5)$$

Substitution of  $c_c = G_c E / (2\pi\tau^2)$  into:  $\gamma = \tau / G_{eff} = 2(1+\nu)\tau / E_{eff}$  gives:

$$\gamma = \frac{2(1+\nu)\tau}{E_{eff}} = \frac{2(1+\nu)\tau(1 + \pi c^2 / bl(1+\nu))}{E} = \frac{2(1+\nu)\tau}{E} \left( 1 + \frac{\pi(G_c E)^2}{(2\pi\tau^2)^2 bl(1+\nu)} \right) \quad (3.7.1.6)$$

and the top of the yield drop curve follows, as for mode I, from:  $\frac{d\gamma}{d\tau} = 0$ , giving:

$$\frac{2(1+\nu)}{E} - \frac{3G_c^2 E}{2\pi bl\tau^4} = 0 \text{ or: } \tau_c = \frac{\sqrt{G_c E}}{\sqrt{\sqrt{\pi bl(1+\nu)}^{4/3}}} = \frac{\sqrt{G_c E}}{\sqrt{\pi c_c}}. \text{ Thus:} \quad (3.7.1.7)$$

$$c_c = \sqrt{4(1+\nu)bl / 3\pi} = \sqrt{bl / 0.5\pi} = \sqrt{0.62bl} = 0.785\sqrt{bl}$$

This value of  $c_c$  is applied as  $a_c$  in paragraph 3.7.2.

#### 3.7.2. Mode II fracture strength criterion

In [8], [9], results of mode II tests, called asymmetric four point bending tests, are given (see Fig. 3.9), applied on very long over-critical initial crack lengths, which clearly represent an identical state of a former yield drop stage, because the measured  $K_{IIC}$ -values were a factor 2.5 to 4 lower than normal thus much lower than the control tests on standard “single edge notched beam” test-specimens. The, by the numerical VCC- test, found, too low, value of  $G_{IIC}$  is not the critical energy release rate, but simply the elastic energy for elastic crack closure, (per unit crack length) of the existing very long overcritical crack length, which closure energy, per unit crack length, is lower than the apparent surface energy. In [8], [9], is stated that the compliance method delivers identical values of  $G_{IIC}$  as follow from the VCC- method. The compliance method therefore wrongly gets crack geometry factors,  $f(a/W)$ , identical to those of the VCC- method. This of course can not be

## Exact Fracture Mechanics theory

right.  $f(a/W)$  thus is nothing more than an empirical coupling factor. Because of the zero moment in the middle of the beam, at the location of the cracked, glued-in, specimen (see Fig. 3.9), only shear stress loading and energy should be regarded as also follows from the VCC-method. Starting point in [8],[9] is the Griffith eq.(3.7.2.1) giving:

$$K_{IIc} = \tau_c \sqrt{\pi a_i} \cdot f(a/W) = \left( \sqrt{EG_{IIc}} \right), \quad (3.7.2.1)$$

In this equation  $G_{IIc}$  is found by the crack closure method;  $\tau_c$ , the nominal critical shear stress, is measured;  $a_i$ , the initial crack length, is wrongly regarded to be the critical crack length and  $f(a/W)$  connects empirically  $\tau_c$ ,  $a_i$ , and  $G_{IIc}$ . The nominal eq.(3.7.2.1) has to be corrected for the real critical  $a_c$  and actual stress  $\tau_{a,c}$  values which apply at the fracture site. Thus:

$$\begin{aligned} \tau_{a,c} \sqrt{\pi a_c} \cdot f(a/W) &= \sqrt{EG_{IIc} (a_c / a_i) (\tau_{a,c}^2 / \tau_c^2)} = \sqrt{EG_{IIa,c}} = K_{IIa,c}, \quad \text{or:} \\ \sqrt{\pi a_c} \cdot f(a/W) &= \frac{K_{IIa,c}}{\tau_{a,c}} = C_1 \quad (\text{constant}) \end{aligned} \quad (3.7.2.2)$$

where  $\tau_{a,c}$  is the actual ultimate shear stress and  $K_{IIa,c}$  the real critical value of the stress intensity at the critical initial crack length  $a_c$ .  $C_1$  is only dependent on dimensions and stiffness factors of the specimen. For instance, eq.(6.7), which is based on a compliance method for only shear loading and shear deformation, shows  $C_1 = K_{IIc} / \tau_{a,c} = \sqrt{0.27 \cdot h(\alpha - \alpha^2) \cdot E / G}$ , (3.7.2.3) which is constant, independent of the crack length  $\beta h$ . The common empirical estimation in [8],[9], wrongly based on nominal stress and on initial crack lengths  $a_i$  in stead of critical crack lengths  $a_c$ , resulted in a not constant  $C_1$ , but on a strong dependence of  $C_1$  on the crack length  $a/W$  which therefor was a factor 2 higher at  $a/W = 0.9$ , with respect to the value at  $a/W = 0.7$ . The found, factors 2.5 to 4 too low, not critical, not constant, values of  $G_c$  are mainly due to the assumption that the overcritical crack length of  $a/W = 0.7, 0.8$ , and  $0.9$ , are the right initial critical crack lengths of the Griffith theory. According to fig.12 of [9], there is no difference (by volume effect) between the data for  $W = 40$  and  $20$  mm, thus in the following mean data values of both are regarded. This is necessary because the measured values of  $\tau_c$ , dependent on  $W$ , are not published in [8], [9]. Because the applied initial crack length is overcritical, the clear wood strength, thus micro crack extension, is determining in the still available intact area of:  $(W - a) (W - a)$ , adjacent to the long (overcritical) initial cracks  $a_i$ . Then the equivalent merged, critical macro-crack length according to eq.(3.3.3) is, (for a constant  $W$  in all tests):

$$a_c = 0.78\sqrt{bl} = 0.78\sqrt{(W(1-a/W) \cdot W(1-a/W))} = 0.78 \cdot W \cdot (1-a/W), \quad (3.7.2.4)$$

Thus  $C_1$  according to eq.(3.7.2.2), is, for respectively:

$$a_i / W = 0.7: \sqrt{\pi a_c} \cdot f(a/W) = \sqrt{2.46 \cdot W} \sqrt{(1-a/W)} \quad f(a/W) = \sqrt{2.46 \cdot W} \cdot \sqrt{0.3} \cdot 1.0 = 0.85 \cdot \sqrt{W} \quad (3.7.2.5)$$

$$a_i / W = 0.8: \sqrt{\pi a_c} \cdot f(a/W) = \sqrt{2.46 \cdot W} \sqrt{(1-a/W)} \quad f(a/W) = \sqrt{2.46 \cdot W} \cdot \sqrt{0.2} \cdot 1.2 = 0.84 \cdot \sqrt{W} \quad (3.7.2.6)$$

$$a_i / W = 0.9: \sqrt{\pi a_c} \cdot f(a/W) = \sqrt{2.46 \cdot W} \sqrt{(1-a/W)} \quad f(a/W) = \sqrt{2.46 \cdot W} \cdot \sqrt{0.1} \cdot 1.67 = 0.83 \sqrt{W} \quad (3.7.2.7)$$

giving the necessary constant value of  $C_1$  of eq.(3.7.2.2), for shear loading. The equations show that only eq.(3.7.2.5) gives the right value of  $a_c$  because  $f(a/W) = 1$ . Therefore the smaller fracture planes need correction factors (respectively of 1.2 and 1.67) to obtain the same determining ultimate shear strength, given by eq.(3.7.2.11) to eq.(3.7.2.13). Therefore is:

$$a_c = a_{c,0} (f(a/W))^2 \quad (3.7.2.8)$$

Thus also is shown that not the initial crack length is critical, but the actual shear strength is determining for yield drop. The actual stress of actual, still intact material, follows from the nominal Griffith stress, corrected by a factor:  $W / (W - a)$ . This stress is determining for all clear wood failure. It thus is necessary that the so found actual clear wood shear strength is the same for

## Exact Fracture Mechanics theory

the above 3 overcritical cases. Thus, similar to eq.(3.2.9), eq.(3.7.2.1) can be written:

$$\tau_u = \frac{K_{II}}{\sqrt{\pi a} \cdot f(a/W)} \cdot \frac{W}{W-a} = \frac{K_{II}}{\sqrt{\pi a} \cdot (1-a/W) \cdot f(a/W)} = \frac{K_{II} / \sqrt{\pi W}}{\sqrt{a/W} \cdot (1-a/W) \cdot f(a/W)} \quad (3.7.2.9)$$

$$\text{or: } \tau_u \sqrt{\pi W} = \frac{K_{II}}{\sqrt{a/W} \cdot (1-a/W) \cdot f(a/W)} \quad (3.7.2.10)$$

This is constant independent of  $a/W$  because not the crack closure value of  $K_{IIc}$  of: 0.79, 0.71 and 0.52 are determining in this case, but the ultimate shear stress, which is as:  $\tau_u \sqrt{\pi W}$  equal to:

$$\text{For } a/W = 0.7: \frac{K_{II}}{\sqrt{a/W} \cdot (1-a/W) \cdot f(a/W)} = \frac{0.79}{\sqrt{0.7} \cdot 0.3 \cdot 1} = 3.2 \quad (3.7.2.11)$$

$$\text{For } a/W = 0.8: \frac{K_{II}}{\sqrt{a/W} \cdot (1-a/W) \cdot f(a/W)} = \frac{0.71}{\sqrt{0.8} \cdot 0.2 \cdot 1.2} = 3.3 \quad (3.7.2.12)$$

$$\text{For } a/W = 0.9: \frac{K_{II}}{\sqrt{a/W} \cdot (1-a/W) \cdot f(a/W)} = \frac{0.52}{\sqrt{0.9} \cdot 0.1 \cdot 1.67} = 3.3, \quad (3.7.2.13)$$

giving a mean value of:  $\tau_u \sqrt{\pi W} = 3.25 \text{ MPa} \sqrt{\text{m}}$ , and with  $\bar{W} = 30 \text{ mm}$ , this is  $\bar{\tau}_u = 10 \text{ Mpa}$  of the clear wood strength of the tested small clear specimen of  $30 \times 10 \times 15 \text{ mm}^3$  glued in the centre of the beam specimen (see Fig.3.9).

The real value of  $K_{IIc}$  follows from eq.(3.7.2.2) and eq.(3.7.2.5):  $\sqrt{\pi a_c} = K_{IIa,c} / \tau_{a,c}$  or:

$$K_{IIa,c} = \tau_{a,c} \sqrt{\pi a_c} = (3.25 / \sqrt{\pi W}) 0.85 \sqrt{W} = 3.25 \cdot 0.85 / \sqrt{\pi} = 1.56 \text{ MPa} \sqrt{\text{m}}, \quad (3.7.2.14)$$

as lower bound. This is equal to the in [9], fig. 12, given value of  $1.6 \text{ MPa} \sqrt{\text{m}}$ , which is measured by the single-edge notched beam test, as control on the data of the asymmetric four point bending tests of [9]. All measured values are at the low side in [8], [9], because the start of non-linearity is regarded to be already the ultimate state.

It thus is confirmed by the data of [8], [9], that the actual mean shear strength of the intact part of the fracture plane is determining and not the, on the macro crack length based, apparent critical  $K_{II}$  -

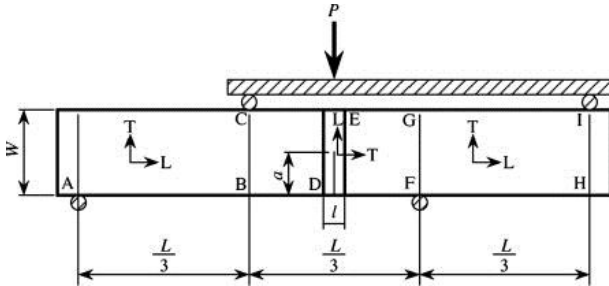


Fig. 3.9. Mode II tests, called “asymmetric four point bending tests” of [8], [9].

crack closure value, which is not constant and too low for macro-crack extension. Macro crack extension is thus due to ultimate clear wood shear strength failure, thus occurs by small crack merging and extension towards the macro-crack tip.

As shown in chapter 2, there is no principal difference between mode I and mode II fracture, because failure for any stress combination, is due to reaching the ultimate, uniaxial, tensile strength at the crack-boundary near the crack tip. Virtual, oblique, crack extension in the isotropic wood matrix applies for shear strength and all combined mode I – II failure cases as lower bound solution, which is exact, being equal to the empirical Wu-fracture criterion [7], and thus is the real solution.

### 3.8. References

- [1] T.A.C.M van der Put, A new fracture mechanics theory of wood, Nova Science Publishers NY, 2011 C(2011a) or: A new fracture mechanics theory of orthotropic materials like wood, Engin. Fract. Mech. 74/5 (2007) pp 771-781. C(2007b).
- [2] G.H. Valentin, L. Bostrom, P.J. Gustafsson, A. Ranta-Maunus, S. Gowda, RILEM state-of-the-

art report on fracture mechanics, VTT Report 1262, Espoo, Finland July 1991

- [3] L. Boström, Method for determination of the “softening” behaviour of wood etc. Thesis, Report TVBM-1012, Lund, Sweden, (1992).
- [4] T.A.C.M. van der Put, Derivation of the bearing strength perpendicular to the grain of locally loaded timber blocks, Holz Roh Werkst (2008) 66: 409–417, D(2008a).
- [5] T.A.C.M van der Put, Deformation and damage processes in wood, Delft University Press, The Netherlands, (1989). B(1989a).
- [6] I. Smith, E. Landis, M. Gong, Fracture and Fatigue in Wood, J. Wiley & Sns, 2003.
- [7] Y.W.May, On the velocity-dependent fracture toughness of wood, Wood Science July 1975
- [8] Yoshihara, H. (2012) Mode II critical stress intensity factor of wood measured by the asymmetric four-point bending test of single-edge-notched specimen while considering an additional crack length, Holzforschung, 66, pp 989-992.
- [9] Yoshihara H. (2008) Mode II fracture mechanics properties of wood measured by the asymmetric four-point bending test using a single-edge-notched specimen, Eng. Frac. Mech. 75 pp.4727-4739.

### 4. Attempted corrections of the singularity approach

#### 4.1. Introduction

Only the in chapter 2 given non-singularity approach is exact, by applying an statically admissible equilibrium system, which suffices compatibility and boundary conditions and nowhere violates the failure criterion. The singularity approximation, applies not at, but in, the neighborhood of the singularity, and is based on collinear crack extension and is therefore not able to satisfy the right failure criterion. Corrective models are further needed to remove the infinite stresses at the singularities. These models, based on plasticity by crack bridging, are known as non-linear fracture mechanics, and are only applicable to singularity solutions. An applied correction is the construction of the R-curve, to explain e.g. instable crack propagation. The stress spreading hardening effect; viscoelastic; plastic; and other structural change processes in beam type specimens at loading, (which are known from molecular deformation kinetics [1]), are wrongly regarded as response of one toughening fracture process. This results in many meaningless mutual different R-curves depending on the specimen structure and loading cases. Stable crack propagation always is possible when the testing rig with sample is stiff enough, as e.g. in the tests of [7]. Dynamic analysis (based on Griffiths theory) also predicts that always meta stable crack propagation occurs when the stress is raised to the Griffith stress. The need of an R-curve, which depends on the stiffness of the testing rig, thus is questionable, especially for overcritical macro crack lengths, when clear wood micro crack extension is determining. The decrease of the nominal stress at yield drop is wrongly regarded to be a decrease of the actual stress in the fracture plane, what leads to the assumption of physical impossible strain softening behavior at crack extension. To correct the wrong ultimate uniaxial stress criterion following from collinear crack extension, additional models are applied to constitute the ultimate state as, e.g. given by energy methods; numerical crack closure techniques; J-integral, or M-  $\theta$ - integral, to determine the initial strain energy release rate as ultimate state criterion. This does not remove the infinite singularity peak stresses, what is tried to be corrected by crack bridging by the fictitious crack models (Dugdale, Barenblatt, Hillerborg). This is discussed in § 4.2. The dynamic crack growth models and critical energy criteria are discussed in § 4.3. However, these approximations of the singularity approximation, are superfluous, because in chapter 2 the exact limit analysis approach without the questionable singularities is presented.

#### 4.2. The fictitious crack models

The fictitious crack model is based on a fictive crack length extension, which is loaded by a cohesive flow stress, over such a length that the singularity due to this cohesive flow stress neutralizes the singularity due to the field stress at the extended crack tip. The extended crack

## Exact Fracture Mechanics theory

length is however not fictitious, but real, because only then, there is a real singularity possible at a real extended crack tip, which can be neutralized. The singularity is not neutralized at the actual existing crack tip when this crack extension would not be real. Calculated thus is the strength of an extended crack length in an external stress field, loaded also by a physical and structural not possible internal opposite applied, diluting viscous stress field near the crack tips. Although the aim of the fictitious crack models (Dugdale, Barenblatt, Hillerborg) initially was, to remove the infinite high stresses of the singularity approach, it later was assumed, (against the boundary value solution) that by the questionable fictive softening boundary condition, the strength, of the real crack tip singularity, approaches zero, in stead of going to infinity according to the exact airy stress function solution. These approximation models, with arbitrary outcomes (due to the impossible, arbitrary chosen, softening boundary condition and wrong failure criterion), should not be followed. The exact boundary value limit analysis approach, without singularities, leading to the therefore exact, Wu-failure criterion, is already known. The same criterion can not be derived by the, singularity method, which leads to uniaxial ultimate stress criteria (thus with a possible 100 % overestimation). The most near to exact, for uniaxial loading only, is, (according to elastic-plastic limit analysis), the Dugdale model, and the results can be compared with the results of the exact solution. Then, the length of that enlarged plastic zone  $r_p$  of the extended crack length, according to the Dugdale model is given by eq.(4.2.1).

$$r_p = \frac{\pi}{8} \cdot \left( \frac{K_{Ic}}{\sigma_f} \right)^2 = \frac{\pi^2 \sigma^2 c}{8 \sigma_f^2} \quad (4.2.1)$$

where  $\sigma_f$  is the yield stress or is regarded to be a cohesive stress.

This leads to a maximal crack opening displacement  $\delta_c$  at the crack tip of:

$$\delta_c = \frac{8}{\pi E} \cdot \sigma_f \cdot r_p = \frac{K_{Ic}^2}{E \sigma_f} = \frac{\pi \sigma^2 c}{E \sigma_f} \quad (4.2.2)$$

when  $r_p$  from eq.(4.2.1) is substituted. This result, based on singularity equations, was necessarily based on very small values of  $r$  and  $r_0$  in § 2.2.2, so that all terms containing not the factor  $r_0^{-0.5}$  were neglected at the derivation of the equation. For finite values of  $r_0$  this should not be done for a correct result. According to the theory, Chapter 2, applies for Mode I, at the crack tip boundary  $r_0$ , at the start of flow, the condition:  $r_0 = 2c \left( \sigma / \sigma_f \right)^2$  according to eq.(2.3.7) for the elliptic crack tip.

This is approximately  $r_0 = c \sigma^2 / 2 \sigma_f^2$  according to eq.(2.2.16) for the circular crack tip of the singularity approach, showing a difference by a factor 4. The form of the crack tip determines the value of the tangential tensile stress along the crack-tip boundary. The Dugdale numerical factor:  $\pi^2 / 8 = 1.23$  (based on an enlarged crack length) is between the values of 0.5 and 2, but is too far away from the elliptic value 2, which applies as highest lower bound of limit analysis (which bound is equal to the measurements, thus is the solution). Also the theoretical elastic elliptic crack opening displacement of  $\delta_c = (2\sigma c) / E$  is far above the Dugdale value. The Dugdale model thus shows a not exact, too low, and thus rejectable lower bound of the strength, which only applies for uniaxial tensile loading perpendicular to crack and grain direction.

The Dugdale model thus is based on a real, not fictive, extended crack length. Thus the superposed compression closing stress is an impossible, not existing, external load on the specimen. This is not comparable with the crack problem, which is not loaded perpendicular to the crack boundary by a stress depending on the crack opening, but failure is independent of this, by the tangential stress in the crack boundary surface (see Chapter 2). This strength determining stress is much higher than the regarded maximal stresses of the fictitious crack models, which thus don't satisfy the right, determining, failure criterion.

## Exact Fracture Mechanics theory

The same thus applies for the Hillerborg model, which is based on closing stresses, proportional to the yield drop curve, thus proportional to the lowering mean elastic stress far outside the fracture plane and not proportional to the actual, by stress spreading increased actual stress, at the fracture plane. Therefore a zero tangential stress is found at the location of the highest (strength determining) tangential tensile stress. This error is of course opposite from right because the increasing stress and hardening at the fracture plane, (see § 3.2), are opposite to assumed softening.

### 4.3. Applied crack growth models

The acknowledged, in principle identical crack growth models for wood, of Williams, Nielsen and Schapery, mentioned in [2], are based on linear viscoelasticity and on the Dugdale-Barenblatt model in order to try to derive the empirical crack rate equation:

$$\frac{da}{dt} = A \cdot K_I^n \quad (4.3.1)$$

The followed procedure is contrary to the normal one, and can not lead to a real solution, because the rate equations are constitutive and has to follow from Deformation Kinetics theory, (see § 4.5 and Section B, [1], [3]) which applies for all materials and is the only way to account for time and temperature dependent behavior. Constitutive equations only can follow from theory and not from general thermodynamic considerations. In [2] is stated that Fig 4.1 of [2], represents eq.(4.3.1).

However, eq.(4.3.1) is a straight line on a double log-plot, while Fig. 4.1 gives the semi-log-plot which confirms the applicability of the damage equation of Deformation Kinetics [1] in the form:

$$\dot{a} \approx C \cdot \exp(\phi \sigma_v), \quad \text{or:} \quad \ln(\dot{a}) = \ln(C) + \phi \sigma_v \quad (4.3.2)$$

This equation is equal to eq.(3.6.9), discussed in § 3.6. More appropriate forms of the exact damage equations and power law forms, with the solutions as e.g. the yield drop at the constant strain rate test, are discussed in [1] and the meaning of the power law equation, eq.(4.3.1), is discussed below. The impossibility of the derivation of the fracture rate equation from the Dugdale-Barenblatt equations follows e.g. from the derivation in [2, § 2.2] of eq.(4.3.3):

$$K_{Ic} = E_0 \cdot \dot{a}^n \cdot \sqrt{\delta_c \varepsilon_y} \cdot r_p^{-n} \quad (4.3.3)$$

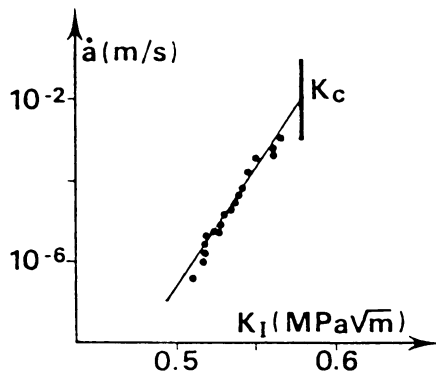


Figure 4.1 – Crack growth tests of Mindess (fig. 10 of [2])

based on the relations:  $\varepsilon_y = \sigma_c / E$  and  $K_{Ic} = \sqrt{E \sigma_c \delta_c}$ , with  $E = E_0 \cdot t^{-n}$  and  $r_p = \dot{a} \cdot t$ . These four (interlinked) relations thus also can be used now to eliminate at least 4 parameters, e.g.  $K_{Ic}$ ,  $\varepsilon_y$ ,  $r_p$  and  $E_0$  to obtain an equation in  $E$ ,  $t$ ,  $\dot{a}$ ,  $\sigma_c$  and  $\delta_c$ . When this is done, eq.(4.3.3) turns to an identity:  $E = E$ , and eq.(4.3.3) thus is not a new derived crack rate equation but an alternative writing of the four relations. The same follows for the other models of § 2.2 of [2] showing comparable parameter manipulations of many critical parameter values which can not be applied independently because they are part of the same failure condition. The models further are based on linear viscoelasticity which does not exist for polymers. It is shown in e.g. [1], page 97, and by the zero creep and zero relaxation tests at page 119, that a spectrum of retardation or relaxation times

does not exist. The superposition integral eq.(28) or eq.(51) of [2]:

$$\varepsilon(t) = \int_{-\infty}^t C(t-\tau) \frac{d\sigma(\tau)}{d\tau} d\tau \quad (4.3.4)$$

thus has no physical meaning. This also applies for the power law models of time and power law eq.(4.3.1), which only apply in a limited range, making predictions and extrapolations outer the fitted range of the data impossible. It thus is necessary to apply the exact theory of Section B, (see iews.nl) for the kinetics of damage and crack growth processes.

#### 4.4. Continuum damage mechanics

Continuum damage mechanics [4], is a simplified application of needed Deformation Kinetics analysis (of [1]), leading to the most elementary damage kinetics equations. But not all possible processes can be given in this simplified form. Regarding fracture mechanics of [4], the analysis is based on the fractured (lost) area  $A$  of an initially undamaged section  $A_0$ , leading to the variable:

$$\psi = \frac{A_0 - A}{A_0} \quad (4.4.1)$$

The actual stress  $\sigma_a$  on the material then is (expressed, as wanted, in the nominal stress  $\sigma$ ):

$$\sigma_a = \frac{P}{A_0 - A} = \frac{P}{A_0 \psi} = \frac{\sigma}{\psi} \quad (4.4.2)$$

where  $\sigma$  is the nominal stress and  $\sigma_a$  the actual stress on still undamaged (=actual) area of the section. Now:

- 1. The actual stress on the actual area evidently determines the rate of damage growth, and:
- 2. The strain increase due to damage is caused by the actual stress at the damage location.

Thus, the stress-strain behavior of the damaged material can be represented by the constitutive equation of the virgin, undamaged, material with the stress, in it, replaced by the actual stress. Thus:

$$\varepsilon = \frac{\sigma_a}{E} = \frac{1}{E} \cdot \frac{\sigma}{\psi} = \frac{\sigma}{E'} \quad (4.4.3)$$

with:  $E' = E\psi$ . A simple form of the deformation kinetics damage equation for uniaxial tension is:

$$\frac{d\psi}{dt} = -C \left( \frac{\sigma}{\psi} \right)^n \quad (4.4.4)$$

This is comparable with the deformation kinetics equation of § 4.5:

$$\frac{dN}{dt} = -CN_0 \exp\left(\frac{\sigma \lambda'}{kN}\right), \quad (4.4.5)$$

for a forward zero order reaction due to a high reactant concentration and high stress, where this exponential equation is replaced, in eq.(4.4.4), by its power law representation (derived in § 4.6). Because the stress is high, the sinh(x) -form is changed to exp(x) -form in the equation and initially also  $\sigma / N = \sigma_0 / N_0$  is constant, independent of the value of  $\sigma_0$  and independent of temperature, explaining the time temperature and time stress equivalence. Because the pre-exponential concentration term  $N$  is high and does not change much during the reaction, the value of  $N_0$  can be used and the reaction then is of zero order at the start and the solution eq.(4.5.4) then applies for initial failure. After a delay time of relatively small change, eq.(4.4.4), can be used for further failure at high enough stress, leading, after integration, for a rod, loaded by a constant tensile stress  $\sigma_0$ , at the initial boundary condition for virgin material:  $\psi = 1$  at  $t = 0$ , and at:  $\psi = 0$  for complete fracture, to a time to failure of:  $t' = [C(n+1)\sigma_0^n]^{-1}$ , and for stepwise loading then follows:

$$\sum_{k=1}^s \frac{\Delta t_k}{t'_k} = 1; \quad t'_k = [C(n+1)\sigma_k^n]^{-1} \quad \text{with: } \Delta t_k = t_k - t_{k-1}, \quad k = 1, 2, \dots, s. \quad (4.4.6)$$

which is Miner's rule, or the principle of linear summation, which evidently also applies for wood and timber. Important conclusions now are:

## Exact Fracture Mechanics theory

1. It is necessary to apply the actual stress in damage equations, for right results, as is applied in [4], [3] and [1], for all existing solutions, which all are empirically verified by tests, and:
  2. Limit analysis deformation kinetics, (developed in [1]), has to be applied, (e.g. in continuum mechanics), for exact solutions.
  3. The determining micro-crack equation, which produces macro-crack extension, can be based on an initially high concentration, high loaded, zero order reaction equation.
- This is applied and discussed in chapter 3 and in next paragraphs.

### 4.5. Deformation kinetics of fracture processes

The basic equations for fracture according to the limit analysis equilibrium theory of molecular deformation kinetics are given in § 4.4 of [1]. The basic concept of this, fundamental theory is to regard plastic flow as a matter of molecular bond breaking and bond reformation in a shifted position, what is the same as to state that flow is the result of a chemical reaction like isomerization. Thus not the composition changes, but only the bond structure of the molecules. Damage occurs when not all broken side bonds reform, providing the sites for a damage process.

The general theory, developed in [1], is based on the limit analysis equilibrium method and is, as such, an exact approach, which is able to predict all aspects of time dependent behavior of materials by the same constitutive equation, because the mathematical derivation of this general theory is solely based on the reaction equations of the bond-breaking and bond- reformation processes at the deformation sites due to the local stresses in the elastic material around these sites. The form of the parameters in the rate equations, are according to the general equilibrium requirements of thermodynamics. By expressing the concentration and work terms of the rate equation in the number and dimensions of the flow units, the expressions for the strain rate, fracture, flow, hardening and delay time are directly derived without any assumptions. To obtain simplifications, series expansion of the potential energy curve is applied, leading to the generalized flow theory, thus to a proof of this general flow model, and showing the hypotheses of this generalized theory, to be consequences of the series expansion. This theory thus applies generally, also for structural changes, giving an explanation of the existing phenomenological models and laws of fracture.

The rate equation for fracture then can be given, for high stress, as always applies for fracture, by:

$$-\frac{d\rho}{dt} = \frac{2\rho}{t_r} \sinh\left(\frac{W}{kT}\right) \approx \frac{\rho}{t_r} \exp\left(\frac{W}{kT}\right) \quad (4.5.1)$$

where the concentration of activated units per unit volume  $\rho$  can be written:  $\rho = N\lambda A / \lambda_1$ . with:  $N$  flow units per unit area of a cross section, each at a distance  $\lambda_1$  behind each other, with  $\lambda$  as jump distance and  $A$  as area of the flow unit. The work of a flow unit  $W$ , with area  $A$  moving over a barrier, over a distance  $\lambda$  is:

$W = fA\lambda = \sigma\lambda / N$ . Because of equilibrium, per unit area, of the external load  $\sigma \cdot 1 \cdot 1$  with the force on the  $N$  flow units:  $NfA$ . Thus  $\sigma = NfA$  and eq.(4.5.1) becomes, expressed in the nominal, macro, engineering stress  $\sigma$ , which is the part of the total external stress, that acts on  $N$ , to be found from tests with different loading paths:

$$-\frac{d}{dt}\left(\frac{N\lambda}{\lambda_1}\right) = \frac{N\lambda}{\lambda_1 t_r} \exp\left(\frac{\sigma\lambda}{NkT}\right), \quad (4.5.2)$$

In this equation is  $t_r$  the relaxation time. The value of  $A$  can be regarded constant because any change is compensated by an corrected value of  $f$  and a corrected value of  $\lambda$  to obtain a correct load on the flow unit and its correct volume. Eq.(4.5.2) can be written, with  $N' = N / \lambda_1$  (the number of flow units per unit volume):  $-d(N'\lambda) / dt = (N'\lambda / t_r) \exp(\sigma\lambda / NkT)$ , or:

$$\frac{d}{dt}\left(\frac{\lambda}{N'}\right) = \frac{\lambda}{N' t_r} \exp\left(\frac{\sigma\lambda}{NkT}\right) \quad (4.5.3)$$

For this zero order reaction in wood, when the very high initial reactant concentration does not

## Exact Fracture Mechanics theory

change much, and initially also  $\sigma / N = \sigma_0 / N_0$  is constant, the solution is:

$$\frac{\lambda}{N'} = \frac{\lambda t_f}{N_0' t_r} \exp\left(\frac{\sigma \lambda}{N_0 k T}\right) + \frac{\lambda}{N_0'}, \text{ or:}$$

$$\left(\frac{\lambda}{N'} - \frac{\lambda}{N_0'}\right) \cdot \frac{N_0'}{\lambda} = \frac{t_f}{t_r} = \frac{t_f}{t_0} \cdot \frac{kT}{\nu h} \exp\left(-\frac{E}{kT} + \frac{\sigma \lambda}{N_0 k T}\right) = \frac{t_f}{t_0} \cdot \exp\left(-\frac{E}{kT} + \frac{\sigma \lambda}{N_0 k T}\right) \text{ or (with } \frac{kT}{\nu h} = 1):$$

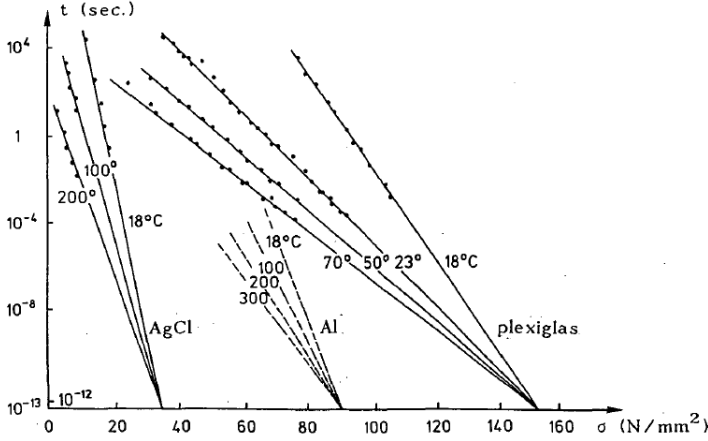


Figure 5. Stress and temperature dependence of the lifetime for structural materials [1]

$$\frac{E}{kT} - \frac{\sigma \lambda}{N_0 k T} = \ln\left(\frac{t_f}{t_0}\right) - \ln\left(\frac{N_0'}{N_f'} - 1\right) = \ln\left(\frac{t_f}{t_0}\right), \quad (4.5.4)$$

This last, according to Fig. 5, which applies for structural materials. Thus  $N_f' = 0.5 \cdot N_0'$  as also experimentally found for fracture, i.e. the crack length is about the crack distance, or the intact area has reduced to 0.5 times the initial area when macro-crack propagation starts due to small crack merging behavior, which explains the measured mode I and mode II final nominal yield drop behavior of fracture.

### 4.6. Derivation of the power law:

The power law equation may represent any function  $f(x)$ , as follows from the following derivation. It therefore also may represent, in a limited time range, a real damage equation giving then a meaning of the power  $n$  of the power law eq.(4.4.4). This is applied in § 4.4.

Any function  $f(x)$  always can be written in a reduced variable  $x/x_0$

$$f(x) = f_1(x/x_0) \quad (4.6.1)$$

and can be given in the power of a function:

$$f(x) = f_1(x/x_0) = \left(\left(f_1(x/x_0)\right)^{1/n}\right)^n \text{ and expanded into the row:}$$

$$f(x) = f(x_0) + \frac{x-x_0}{1!} \cdot f'(x_0) + \frac{(x-x_0)^2}{2!} \cdot f''(x_0) + \dots, \text{ giving:}$$

$$f(x) = \left[ \left\{ f_1(1) \right\}^{1/n} + \frac{x-x_0}{x_0} \frac{1}{n} \left\{ f_1(1) \right\}^{1/n-1} \cdot f'(1) + \dots \right]^n = f_1(1) \cdot \left( \frac{x}{x_0} \right)^n \quad (4.6.2)$$

$$\text{when: } \left( f_1(1) \right)^{1/n} = \frac{1}{n} \left( f_1(1) \right)^{1/n-1} \cdot f'(1) \quad \text{or: } n = f'(1) / f_1(1),$$

$$\text{where: } f_1'(1) = \left( \partial f_1(x/x_0) / \partial (x/x_0) \right)_{(x/x_0)=1} \quad \text{and} \quad f_1(1) = f(x_0)$$

## Exact Fracture Mechanics theory

$$\text{Thus: } f(x) = f(x_0) \cdot \left( \frac{x}{x_0} \right)^n \quad \text{with} \quad n = \frac{f_1'(1)}{f_1(1)} = \frac{f'(x_0)}{f(x_0)} \quad (4.6.3)$$

Thus the derivation of the power law, using only the first 2 expanded terms, shows that eq.(4.6.3) only applies in a limited range of  $x$  around  $x_0$ . (Using one  $x_0$  is not limiting for strength problems). Using this approach on equation:  $\dot{a} = 2C \cdot \sinh(\phi\sigma) \approx C \exp(\phi\sigma)$ , (for high stresses), gives:

$$\dot{a} = C \cdot \exp(\phi\sigma) \approx \dot{a}_0 \cdot \left( \frac{\sigma}{\sigma_0} \right)^{\phi\sigma_0} \quad (4.6.4)$$

The power  $n = \phi\sigma_0$  of the power law equation follows from the slope of the double log-plot:

$$\ln(\dot{a}) = \ln(\dot{a}_0) + n \cdot \ln(\sigma / \sigma_0) \quad (4.6.5)$$

Thus:  $n = d \ln(\dot{a}) / d \ln(\sigma / \sigma_0)$  and  $n = \phi\sigma_0$  gives a meaning of  $n$  as the activation volume parameter  $\phi\sigma_0$  of the exact equation. The values of “ $n$ ” and the matching activation energies of the different creep and damage processes in wood, with the dependency on stress moisture content and temperature, are given in [1]. The constancy of the initial value of the parameter  $\phi\sigma_0$ , independent of applied stress  $\sigma_0$ , explains the time-temperature and time- stress equivalence and explains, by the physical processes, why and when at high stresses, the in [2] mentioned value of  $n + 1 \approx 60$  is measured and at lower stresses, half this value (see [1]).

### 4.7. J-integral application

Path-independent integrals are used in physics to calculate the intensity of a singularity of a field quantity without knowing the exact shape of this field in the vicinity of the singularity. They are derived from conservation laws. For the singularity method of wood the  $J$ -integral (Rice integral) and  $M$ - $\theta$ -integral are applied for estimation of the energy release rate. However, even the finite element applications for wood, appear to lead to quite different outcomes by different authors at different situations, showing the application to be not exact, as also follows from remarks from [5]:  $J$  (near a crack singularity) is the component along the crack-line of a vector integral, having a meaning for not oblique, (thus *invalid* for mode II and mixed mode I-II) and (*only for mode I possible*) incipient self-similar growth of a crack in a (nonlinear) elastic material. In this case,  $J$  has the meaning of the rate of energy-release per unit of crack-extension. The path-independency of  $J$  can be established only, when the strain energy density (or stress working density) of the material is a single valued function of strain. In a deformation theory of plasticity, which is valid for radial monotonic loading but *precludes unloading* and which is mathematically equivalent to a nonlinear theory of elasticity,  $J$  still characterizes the crack-tip field and is still a path-independent integral. However, in this case,  $J$  does not have the meaning of an energy-release rate; it is simply the total potential-energy difference between two identical and identically (monotonically) loaded cracked bodies which differ in crack lengths by a differential amount. Further, in a flow theory of plasticity (*as applies for wood*), even under monotonic loading, the path-independence of  $J$  cannot be established. Also, under arbitrary load histories which may include loading and unloading,  $J$  is not only not path-independent, but also does not have any physical meaning. The blunting of the top of the loading curve and formation of the fracture zone and the main amount of crack growth with crazing and small crack formation in, (and outside), the process zone, means unloading and non-proportional plastic deformation which also invalidates the deformation theory of plasticity. Thus the  $J$ -integral method, of the singularity approach, does not apply to wood (and other structural materials [6]). It is shown in § 2.3 and § 2.4, that oblique crack extension in the isotropic matrix and skipping across fibers, is necessary for mode II and mixed mode I-II crack extension.

## 4.8 References

- [1] van der Put, T.A.C.M., Deformation and damage processes in wood, Delft University press, 1989. B(1989a).
- [2] G.H. Valentin, L. Bostrom, P.J. Gustafsson, A. Ranta-Maunus, S. Gowda, RILEM state-of-the-art report on fracture mechanics, VTT Report 1262, Espoo, Finland July 1991
- [3] van der Put, T.A.C.M., Transformations in wood, Delft University, Stevin-laboratory Research Report 2003-3/ME-2. B(2005).
- [4] L.M. Kachanov. Introduction to Continuum Damage Mechanics, , Martinus Nijhoff Publishers, Dordrecht
- [5] S. N. Atluri, T. Nishioka and M. Nakagaki, Incremental Path-independent integrals in inelastic and dynamic fracture mechanics, Engin. Frac. Mech. Vol. 20, No. 2, pp. 209-244, 1984
- [6] van der Put T.A.C.M. (1974) Breukcriterium voor beton als ondergrens van de sterkte bepaald volgens de evenwichtsmethode, Cement (1974) XXVI No10 pp 420-421 (for concrete).
- [7] Bostrom, L., Method for determination of the softening behaviour of wood etc. Thesis, Report TVBM-1012, Lund, Sweden, 1992.

## 5. Energy theory of fracture

### 5.1 Introduction

The failure criterion of clear wood, i.e. wood with small defects, is the same as the failure criterion of notched wood, showing again that the small-crack is dominating and extension towards the macro-crack tip is the cause of macro-crack propagation. This small-crack failure criterion thus delivers essential information on macro-crack behavior as discussed in this chapter. The limit analysis derivation of the boundary value problem and applied Airy stress function of small crack extension are given in Chapter 10.

### 5.2. Critical distortional energy as fracture criterion

The failure criterion of wood consists of an anisotropic third degree tensor polynomial (see [1], Section A), which, for the same loading case, is identical to the Wu-mixed mode I-II-equation [2], eq.(5.3). The second degree polynomial part of the failure criterion, eq.(5.1), is shown to be the orthotropic critical distortional energy principle for initial yield [3] showing, also empirically, the start of energy dissipation, what is not yet, incorporated in the finite element method [4]. By this dissipation according to the incompressibility condition, the minimum energy principle is followed, providing therefore the exact initial yield criterion as (see Section A):

$$\frac{\sigma_x^2}{XX'} + \frac{\sigma_x}{X} - \frac{\sigma_x}{X'} - 2F_{12}\sigma_x\sigma_y + \frac{\sigma_y^2}{YY'} + \frac{\sigma_y}{Y} - \frac{\sigma_y}{Y'} + \frac{\tau^2}{S^2} = 1 \quad (5.2.1) \quad (5.1)$$

where  $X, Y$  are the tension strengths and  $X', Y'$  the compression strength in the main directions and  $S$  is the shear strength and:  $2F_{12} = 1/\sqrt{XX'YY'}$

This value of  $F_{12}$  is necessary for the elastic state which also applies at the starting point of initial stress redistribution and micro-cracking of the matrix. After further straining,  $F_{12}$  becomes zero,  $F_{12} \approx 0$ , at final failure initiation. The absence of this coupling term  $F_{12}$  between the normal stresses indicates symmetry, thus (possible random oriented) initial small-cracks are extended during loading to their critical length in the weak planes, the planes of symmetry, only. Then, when these small-cracks arrive at their critical crack-density (discussed in § 3.6) and start to extend further, a type of hardening occurs because the reinforcement prevents crack extension in the matrix in the most critical direction. Then, due to hardening,  $F_{12}$  and all third degree coupling terms of the tensor polynomial become proportional to the hardening state constants [3] and therefore also dependent on the stability of the test and equipment. For the mixed I-II-loading of the crack plane by tension  $\sigma_2$  and shear  $\sigma_6$ , the polynomial failure criterion reduces to:

## Exact Fracture Mechanics theory

$$F_2\sigma_2 + F_{22}\sigma_2^2 + F_{66}\sigma_6^2 + 3F_{266}\sigma_2\sigma_6^2 = 1 \quad \text{or:} \quad \frac{\sigma_6}{S} = \sqrt{\frac{(1-\sigma_2/Y) \cdot (1+\sigma_2/Y)}{1+c\sigma_2/Y'}} \quad (5.2)$$

with:  $c = 3F_{266}Y'S^2 \approx 0.9$  to  $0.99$ , depending on the stability of the test. When, due to hardening,  $c$  approaches to  $c \approx 1$ , eq.(5.2) becomes eq.(5.3), the in § 2.3 exact, theoretically explained, Coulomb- or Wu-equation, with a cut off by the line:  $\sigma_2 = Y$ .

Full hardening is possible when the test rig is stiff enough to remain stable during test. The solution of the crack problem of Irwin as summation of in plane and antiplane solutions in order to use, isotropic stress functions for the orthotropic case, and to apply descriptions in the three different modes and to sum the result for a general mixed mode case is not right for wood because it misses the stress interaction terms and because the failure equation, eq.(5.2), is not orthotropic, by being not quadratic, but contains a third degree term and thus does not show orthotropic symmetric. This hardening coupling term is absent in the general accepted solutions. The stress function which leads directly to the Wu-equation, eq.(5.3), is given here in § 2.3 and in [5].

$$\left(\frac{\sigma_6}{S}\right)^2 + \frac{\sigma_2}{Y} \approx 1 \quad \text{or:} \quad \frac{K_{II}^2}{K_{IIc}^2} + \frac{K_I}{K_{Ic}} = 1 \quad (5.3)$$

Wrongly, and against the lack of fit test of Table 2.1, is for wood and other orthotropic materials, eq.(5.2) generally replaced in literature by:

$$\frac{\sigma_2^2}{Y^2} + \frac{\tau^2}{S^2} = 1, \quad \text{written as:} \quad \frac{K_I^2}{K_{Ic}^2} + \frac{K_{II}^2}{K_{IIc}^2} = 1, \quad (5.4)$$

which surely is not a summation of energies, as is stated, but is identical to eq.(5.1) when it wrongly is assumed that the compression and tension strength are equal for wood and orthotropic materials. To know the mode of failure, the stresses at the crack boundary should be known. This follows from the exact derivation in [5] and is applied by the VCC- technique of finite element simulation. According to the method of Sih, Paris, the sum of separate solutions for the 3

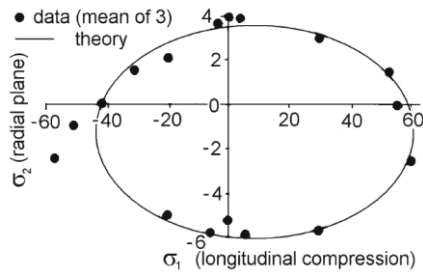


Fig. 5.1. Eq.(5.2), influence of  $3F_{266}\sigma_2\sigma_6^2$ , giving data outside the elliptic curve.

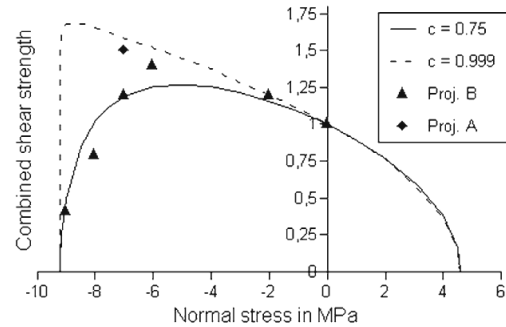


Fig. 5.2. Also same hardening at compression with dashed parabolic limit eq.(5.3)

modes, without interactions, is assumed to be determining, based on assumed isotropic and orthotropic symmetry. This however is against eq.(5.2) because the important coupling between normal and by shear stresses, as given by  $3F_{266}\sigma_2\sigma_6^2$  in eq.(5.2), is not present in the existing methods and the “mixed mode” interactions as given by Fig. 5.1 and 5.2 can not be described by other methods, because it is not quadratic but contains a third degree term and thus does not show to be orthotropic.

### 5.3. Revision of the critical energy release rate equation.

Based on the failure criterion of § 5.2, adaption of the energy release equation is necessary.

The Griffith strength equation, eq.(3.2.8) of § 3:  $\sigma_y^2 = G_c E_y / \pi c$  can be extended by superposition

## Exact Fracture Mechanics theory

$$\text{to: } \sigma_y^2 + \tau_{xy}^2 = G_c E_y / \pi c \quad (5.5)$$

This only is right, when  $G_c$  is not constant but may reach values between  $G_{Ic}$  and  $G_{IIc}$  depending on  $\sigma_y / \tau_{xy}$ , because  $G_c$  also has to satisfy the failure criterion eq.(5.3).

In orthotropic stresses, eq.( 5.5) is:  $\sigma_y^2 + \tau_{xy}^2 / n_6^2 = G_f E_y / \pi c$  and when  $\tau_{xy} = 0$ , is

$$G_f = G_{Ic} \text{ and } K_{Ic} = \sqrt{E_y G_{Ic}}. \text{ When } \sigma_y = 0 \text{ is: } \tau_{xy}^2 \pi c = n_6^2 G_{IIc} E_y = 4n_6^2 G_{Ic} E_y, \text{ because } K_{IIc} = 2n_6 K_{Ic} \text{ (eq.(2.3.19)). Thus: } K_{IIc} = n_6 \sqrt{E_y G_{IIc}} = 2n_6 \sqrt{E_y G_{Ic}} \text{ or: } G_{IIc} = 4G_{Ic} \quad (5.6)$$

The failure condition eq.(5.3) can be written in fracture energies:

$$\frac{K_I}{K_{Ic}} + \frac{(K_{II})^2}{(K_{IIc})^2} = 1 = \frac{\sqrt{G_I}}{\sqrt{G_{Ic}}} + \frac{G_{II}}{G_{IIc}} = \frac{\sqrt{\gamma \cdot G_f}}{\sqrt{G_{Ic}}} + \frac{(1-\gamma) \cdot G_f}{G_{IIc}} \quad (5.7)$$

$$\text{where, according to eq.(5.5): } G_f = G_I + G_{II} = \gamma \cdot G_f + (1-\gamma) \cdot G_f \quad (5.8)$$

$$\text{Thus: } \frac{\gamma G_f}{(1-\gamma) G_f} = \frac{K_I^2}{K_{II}^2} \text{ or: } \gamma = \frac{1}{1 + \frac{K_{II}^2}{K_I^2}} = \frac{1}{1 + \frac{\tau_{xy}^2}{\sigma_y^2}} \quad (5.9)$$

and  $\gamma$  depends on the stress combination  $\tau_{xy} / \sigma_y$  in the region of the macro notch-tip and thus not on the stresses of fracture energy dissipation as generally postulated by the I and II failure modes. This stress combination also may follow from a chosen stress field according to the equilibrium method of limit analysis as is applied in § 6 and § 7.

With eq.(5.6):  $G_{IIc} / G_{Ic} = 4$ , eq.(5.7) becomes:

$$G_f = 4G_{Ic} / (1 + \sqrt{\gamma})^2 = G_{IIc} / (1 + \sqrt{\gamma})^2 \quad (5.10)$$

where  $\gamma$  acts as an empirical constant explaining the differences in fracture energies depending on the notch structure and shear slenderness of the beam by the different occurring  $\tau_{xy} / \sigma_y$ -values according to eq.(5.9).

Applications of the theory with the total critical fracture energy  $G_f$  are given in § 6 and § 7.

The theory is e.g. applied for beams with rectangular end notches as basis of the design rules of the Dutch Timber Structures Code and some other Codes and is a correction of the method of the Euro-Code. In the Euro-Code, an approximate compliance difference is used and a raised stiffness which does not apply for the applied Airy stress function. Further  $G_{Ic}$  is used in stead of  $G_f$  according to eq.(5.10). Important is further that the theoretical prediction  $G_{IIc} = 4G_{Ic}$  is verified by measuring  $G_{IIc} / G_{Ic} = 3.5$  (with  $R^2 = 0.64$ , thus not very precise).

At comparing results it should be realized that there is Weibull volume effect of the strength. Further is a strong hardening possible due to compression perpendicular to grain at bending failure of small clear single-edge notched specimens, what wrongly is regarded as  $G_{IIc}$  resistance increase. Eq.(5.5) is equal to eq.(5.8) and is an extension of the Griffith strength for combined loading.

### 5.4 References

- [1] van der Put, T.A.C.M. (1982) A general failure criterion for wood, CIB-W18/IUFRO meeting Boras, Sweden, A(1982).
- [2] Wu, E.M. (1967) Application of fracture mechanics to anisotropic plates, ASME J. Appl. Mech. Series E, 34 4, pp. 967-974.
- [3] van der Put T.A.C.M. (2009) A continuum failure criterion applicable to wood. J. of Wood Sci, Vol. 55 No.5. (DOI: 10.1007/s10086-009-1036-2), A(2009).
- [4] Gopu, Vijaya K. A. (1987) Validity of Distortion-Energy-Based Strength Criterion for Timber Members, J. Struc. Eng. 113, No. 12 pp. 2475-2487.

[5] van der Put T.A.C.M., A new fracture mechanics theory of wood, Nova Science Publishers, Inc. New York, C(2011a), or more complete:  
T.A.C.M. van der Put Exact and complete Fracture Mechanics of wood. Theory extension and synthesis of all series C publications

## 6. Energy approach for fracture of notched beams

### 6.1. Introduction

The theory of total fracture energy, discussed in § 5, was initially developed to obtain simple general design rules for beams with square end-notches and edge joints, loaded perpendicular to the grain design rules of square notches and joints for the Dutch Building Code and later, as correction of the method of [1], published in [2] with the extensions for high beams. Horizontal splitting in short, high beams, loaded close to the support, causes no failure because the remaining beam is strong enough to carry the load and vertical transverse crack propagation is necessary for total failure. This is not discussed here because it is shown that also the standard strength calculation is sufficient. In [3] and [4] the theory is applied to explain behaviour, leading to the final proposal for design rules for the Eurocode, given at § 7.5, and to an always reliable simple design method. In the following, the theoretical basis and implementation of the new developments of the energy approach for fracture of notched beams are given and it is shown that the predictions of the theory are verified by the measurements. The presentation of more data can be found in [2].

### 6.2. Energy balance

When crack-extension occurs over the length  $\Delta x$ , along the grain, then the work done by the constant load  $V$  is  $V \cdot \Delta \delta$ , where  $\Delta \delta$  is the increase of the deformation at  $V$ . This work is twice the

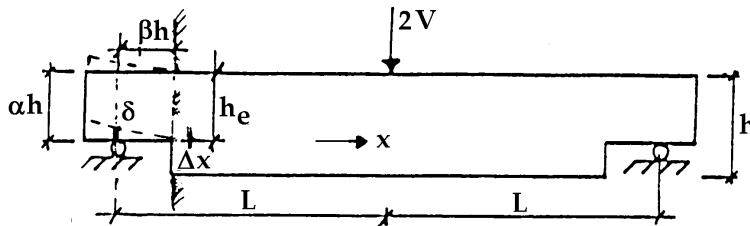


Figure 6.1. - Notched beam

increase of strain energy of the cantilever part:  $V \cdot \Delta \delta / 2$ . Thus half of the external work done at cracking is used for crack formation being thus equal to the other half, the strain energy increase. Thus in general, when the change of the potential energy  $\Delta W = V \cdot \Delta \delta / 2$  becomes equal to the energy of crack formation, crack propagation occurs. The energy of crack formation is:  $G_c b \Delta x = G_c b h \Delta \beta$ , where  $G_c$  is the crack formation energy per unit crack area. Thus crack propagation occurs at  $V = V_f$  when:  $\Delta W = V \Delta \delta / 2 = V^2 \Delta(\delta / V) / 2 = G_c b h \Delta \beta$ , thus when:

$$V_f = \sqrt{\frac{2G_c b h}{\frac{\partial(\delta / V)}{\partial \beta}}} \quad (6.1)$$

and only the increase of the compliance  $\delta / V$  has to be known.

The deflection  $\delta$  can be calculated from elementary beam theory as chosen allowable equilibrium system as a lower bound of the strength. This is close to real behaviour because, according to the theory of elasticity, the deflection can be calculated from elementary beam theory while the difference from this stress distribution is an internal equilibrium system causing no deflection of the beam and also the shear distribution can be taken to be parabolic according to this elementary theory, as only component of this polynomial expansion, contributing to the deflection.

## Exact Fracture Mechanics theory

According to the Fig. 6.2, the notch can be seen as a horizontal split, case:  $a = a'$ , and case "a" can be split in the superposition of case "b" and "c", where  $b = b'$ .

Case "c" now is the real crack problem by the reversed equal forces that can be analyzed for instance by a finite element method, etc. From the principle of energy balance it is also possible to find the critical value of case "c" by calculating the differences in strain energies or the differences in deflections  $\delta$  by  $V$  between case:  $b'$  and case  $a'$ , thus differences in deformation of the cracked and un-cracked part to find  $\Delta(\delta/V)$  for eq.(6.1).

Deformations due to the normal stresses  $N$  of case c, are of lower order in a virtual work equation and should not be accounted. It then follows that case c of Fig. 6.2 is equal to a mode I test and  $G_c = G_{Ic}$ . When the beam is turned upside down, or when  $V$  is reversed in direction, then  $M'$  and  $V'$  are reversed closing the crack and fracture only is possible by shear, identical to the mode II test and then  $G_c = G_{IIc}$ .

The change of  $\delta$  by the increase of shear deformation is, with  $h_e = \alpha \cdot h$ :

$$\delta_v = \frac{1.2}{G} \left( \frac{\beta h}{b\alpha h} - \frac{\beta h}{bh} \right) \cdot V \quad (6.2)$$

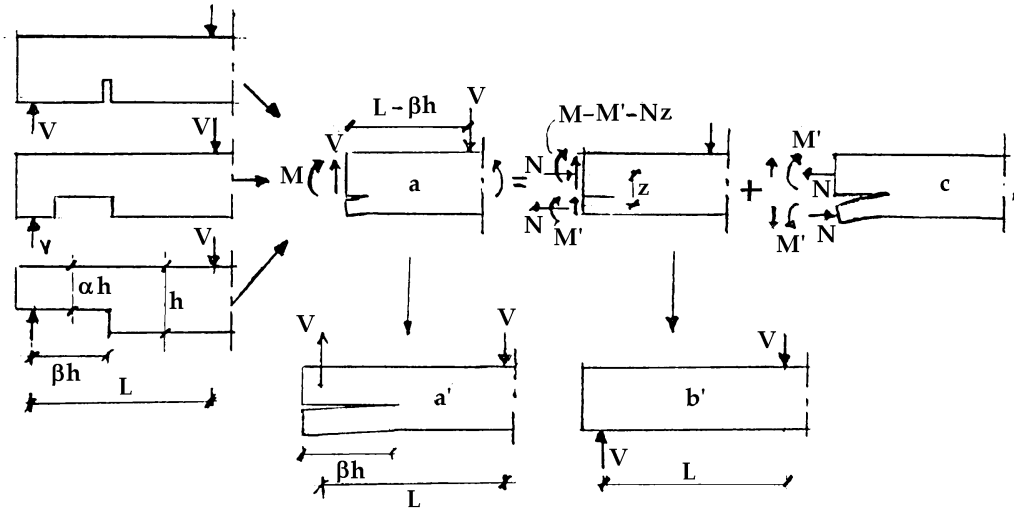


Figure 6.2 - Equivalent crack problem according to superposition

The change of  $\delta$  by the increase of the deflection is:

$$\delta_m = \frac{V(\beta h)^3}{3Eb(\alpha h)^3/12} - \frac{V(\beta h)^3}{3Eb h^3/12} = \frac{4V\beta^3}{Eb} \cdot \left( \frac{1}{\alpha^3} - 1 \right) \quad (6.3)$$

$$\text{Thus: } \frac{\partial(\delta/V)}{\partial\beta} = \frac{1.2}{Gb} \cdot \left( \frac{1}{\alpha} - 1 \right) + \frac{12\beta^2}{Eb} \cdot \left( \frac{1}{\alpha^3} - 1 \right) \quad (6.4)$$

The critical value of  $V$  thus is according to eq.(6.1):

$$V_f = \sqrt{\frac{1.67G_c h b^2}{\frac{1}{G} \left( \frac{1}{\alpha} - 1 \right) + \left( \frac{1}{\alpha^3} - 1 \right) \cdot \frac{10\beta^2}{E}}} \quad (6.5)$$

or:

$$\frac{V_f}{b\alpha h} = \frac{\alpha \sqrt{GG_c / h}}{\sqrt{0.6(\alpha^3 - \alpha^4) + 6\beta^2(\alpha - \alpha^4)G / E}} \quad (6.6)$$

For small values of  $\beta$  eq.(6.6) becomes:

$$\frac{V_f}{b\alpha h} = \frac{\sqrt{GG_c/h}}{\sqrt{0.6 \cdot (\alpha - \alpha^2)}} \quad (6.7)$$

For high values of  $\beta$ , eq.(6.6) becomes:

$$\frac{V_f}{b\alpha h} = \frac{\alpha \sqrt{EG_c/h}}{\beta \sqrt{6(\alpha - \alpha^4)}} \quad (6.8)$$

### 6.3. Experimental verification

A verification of the prediction of the theory for high values  $\beta$ , eq.(6.8), when the work by shear is negligible, is given by Table 6.1 of an investigation of Murphy, mentioned in [1], regarding a notch starting at  $\beta = 2.5$  and proceeding to  $\beta = 5.5$ . Further also beams were tested with a slit at a distance:  $\beta = 2.5$ . Because the exact eq.(6.6) gives a less than 1 % higher value, eq.(6.8) applies. ( $\sqrt{GG_c} = 11.1$  resp.  $10.9$  N/mm<sup>1.5</sup>) and:  $\sqrt{EG_c} = 48.8$  N/mm<sup>1.5</sup>. This value is used in table 6.1 for comparison of eq.(6.8) with the measurements, showing an excellent agreement between theory and measurement. For all specimens was:  $\alpha = 0.7$ ;  $\eta = L/h = 10$  ( $L$  is distance field loading to support) and  $b = 79$  mm. The other values are given in table 6.1.

Table 6.1. Strength of clear laminated Douglas fir with notches in the tensile zone in MPa

$h$ mm	$\beta$	num- ber	$V/abh$ tests	$V/abh$ eq.(6.8)
305	2.5	2	0.46	0.47
305	5.5	2	0.24	0.22
457	2.5	2	0.38	0.38
457	5.5	1	0.16	0.17

The fracture energy is:  $G_c = (48.8)^2 / 14000 = 0.17$  N/mm = 170 N/m, which agrees with values of the critical strain energy release rate. The value of  $K_{Ic}$  is about:  $K_{Ic} \approx \sqrt{0.17 \cdot 700} = 10.9$  N/mm<sup>1.5</sup> = 345 kN/m<sup>1.5</sup>, as to be expected by the high density of Douglas fir.

In table 6.2, data are given of Spruce for low values of  $\beta$ , to verify the then predicted theoretical behaviour according to eq.(6.7) with energy dissipation by shear stresses only. It appears for these data that the difference between the mean values according to eq.(6.7) and eq.(6.6) are 10 % and thus not negligible small and also the values of eq.(6.6) are given to obtain a possible correction factor. It follows from table 6.2 for Spruce that:  $\sqrt{GG_c} = 6.8$  N/mm<sup>1.5</sup> or:

$$G_c = 6.8^2 / 500 = 0.092$$
 N/mm = 92 N/m.

For Spruce is  $K_{Ic} \approx 6.3$  to 7.6 according to [5], depending on the grain orientation and then also applies:  $E_2 \approx G$  and:  $K_{Ic} = \sqrt{E_2 G_c} = 6.8$  N/mm<sup>1.5</sup>.

Although the fracture energy is shear-stress energy, failure still is by mode I (of Fig. 6.2) and not by the shear mode II, as is supposed by other models. Thus the total work contributes to failure, whether it is bending stress energy (Table 6.1) or shear stress energy (Table 6.2) and  $\gamma = 1$  (eq.(5.9) for failure of this type of notch by the high tensile stress perpendicular to the grain at the notch root. In [2] more data are given regarding the strength of square notches. The size influence, or the influence of the height of the notched beam on the strength, is tested on beams with notch parameters  $\alpha = 0.5$  and  $0.75$ ;  $\beta$  is  $0.5$  and heights  $h = 50, 100$  and  $200$  mm with  $b = 45$  mm at moisture contents of 12, 15 and 18%. The strength  $\sqrt{GG_f}$  appeared to be independent of the beam

## Exact Fracture Mechanics theory

Table 6.2. Strength of notched beams, Spruce, Mohler and Mistler.

h mm	$\alpha$	$\beta$	$\eta/\alpha$	b mm	n	V/bah N/mm <sup>2</sup>	var. coef. %	$\sqrt{GG_f}$	
								eq.(6.6)	eq.(6.7)
								N/mm <sup>1.5</sup>	
120	.917	.25	3.4	32	6	2.36	11	(5.8)	(5.5)
	.833		3.8		27	1.93	15	6.4	6.1
	.75		4.2		43	1.68	19	6.6	6.2
	.667		4.7		14	1.52	18	6.5	6.1
	.583		5.4		10	1.5	18	6.8	6.3
	.5		6.3		49	1.59	18	7.4	6.7
	.333		9.5		10	1.48	16	7.0	5.9
	<b>mean</b>								<b>6.8</b>
Testing time more than 1 min., m.c. 11%, $\rho = 510 \text{ kg/m}^3$									

depth as to be expected for macro crack extension along an always sufficient long fracture plane.

The value of  $\sqrt{GG_f}$  at moisture contents of 12, 15 and 18% was resp.: 6.7; 7.7 and 8.0 Nmm<sup>1.5</sup>.

Higher values of  $\sqrt{GG_f}$  of Spruce, given in [2], are possible for loads close to the support. Then horizontal splitting does not cause failure because the remaining beam is strong enough to carry the total load and the derivation is given by regarding vertical crack propagation necessary for total failure (bending failure of the remaining beam). For this mode I,

$$\sqrt{GG_m} = 57.5 \text{ N/mm}^{1.5} = 1818 \text{ kN/m}^{1.5} \text{ (comparable with } 1890 \text{ kN/m}^{1.5} \text{ of [5])}$$

For still higher values of  $\alpha$ , above  $\alpha = 0.875$ , compression with shear failure is determining by direct force transmission to the support.

In [3] is shown that Foschi's finite element prediction and graphs, given in [5] can be explained and are identical to eq.(6.8).

### 6.4 References

- [1] P.J. Gustafsson, A Study of Strength of Notched Beams, CIB-W18A-21-10-1, meeting 21, Parksville, Vancouver Island, Canada, Sept. 1988.
- [2] T.A.C.M. van der Put, Tension perpendicular to the grain at notches and joints. CIB-W18A-23-10-1, meeting 23, Lisbon, Portugal, Sept. 1990 C(1990)
- [3] T.A.C.M. van der Put, Modified energy approach for fracture of notched beams. Proceed. COST 508 conf. on fracture mechanics. Bordeaux, April 1992.
- [4] T.A.C.M. van der Put, A.J.M. Leijten, Evaluation of perpendicular to the grain failure of beams, caused by concentrated loads of joints. CIB-W18A/33-7-7, meeting 33, Delft, The Netherlands, August 2000, C(2000)
- [5] RILEM state of the art report on fracture mechanics, Espoo, 1991.

## 7. Energy approach for fracture of joints loaded perpendicular to the grain.

### 7.1 Introduction

It was for the first time shown in [2] that fracture mechanics applies for these type of joints. As for square end-notches, the analysis can be based on the compliance change by an infinitesimal crack increase. Because measurements show no difference in strength and fracture energy between joints at the end of a beam (Series G6.1 and G6.2 of [1]) and joints in the middle of the beam (the other G-series), and also the calculated clamping effect difference by crack extension is of lower order, this clamping effect of the fractured beam at the joint in the middle of a beam, has to be disregarded as necessity of the virtual energy equation of fracture disregard lower order terms. This is according to the limit state analysis which is based on the virtual work equations. For end-joints, the split off

part is unloaded and there is no normal force and no vierendeel-girder action at all and the situation and fracture equations are the same as for the notched beams of § 6. For joints in the middle of the beam, splitting goes in the direction of lower moments and is stable until the total splitting of the beam. The analysis in [1] and [2] shows this stable crack propagation because the terms in the denominator become smaller at crack length increase, until the shear term remains, giving the maximal value of  $V$  according to eq.(7.6), the same value as for end-joints.

It thus is not true, as is stated in the CIB/W18-discussion of [1], that the analysis and theory are incorrect when virtual lower order terms are omitted in the analysis and that splitting of joints analysis is not comparable to splitting of notched beam analysis. The proof that this neglecting of the vierendeel-action is right is given (outer the empirical proof by the measurements) by the complete analysis for this case in [3], where also the influence on the strain of normal stresses is accounted, leading to eq.(7.5) containing the negligible clamping effect term in the denominator, (based on the assumption that not total splitting of the beam is the end state).

## 7.2. Energy balance

For a simple calculation of the compliance difference of the cracked and un-cracked state, (maintaining the clamping action in the end state) half a beam is regarded, as given in Fig. 7.1, loaded by a constant load  $V$ . At the start of cracking, the deflection at  $V$  increases with  $\delta$  (see Fig. 7.2) and the work done by the force  $V$  is:  $2\Delta W = V \cdot \delta$ , which is twice the increase of the strain energy ( $\Delta W = V \cdot \delta / 2$ ) of the beam and therefore the amount  $\Delta W$  is used to increase the strain energy and the other equal amount of  $\Delta W$  is used as fracture energy. Because  $\delta$  is the difference of the cracked and "un-cracked" state, only the deformation of the cracked part  $\beta h$  minus the deformation of that same part  $\beta h$  in the un-cracked state, need to be calculated, because the deformation of all other parts of the beam by load  $V$  are the same in cracked and un-cracked state. As discussed at 6.2, the deflection  $\delta$  can be calculated from elementary beam theory of elasticity. It thus is not right to regard an additional deformation  $\delta_r$ , as is done, due to the non-linearity and clamping effect of the cantilevers  $\beta h$ , formed by the crack. The clamping effect change is of lower order at an infinitesimal crack extension. If this effect would have an influence, there should be a difference in notched beams in the splitting force for a real square notch of length  $\beta h$  and a vertical saw cut at a distance  $\beta h$  from the support, because that slit has at least twice that clamping effect (see Fig. 6.2).

For a connection at the middle of a beam the following applies after splitting (see Fig. 7.1). The part above the crack (stiffness  $I_2 = b(1-\alpha)^3 h^3 / 12$ ) carries a moment  $M_3$  and normal force  $N$  and the part below the crack (stiffness  $I_1 = b\alpha^3 h^3 / 12$ ) carries a moment  $M_1$ , normal force  $N$  and a shear force  $V$ . and at the end of the crack a negative moment of about:  $M_2 \approx -M_1$ . Further is  $M_2 = M_1 - V\lambda$ , thus  $M_1 = V\lambda / 2$ .

The deformation of beam 2 of the cracked part  $\beta h$  is equal to the un-cracked deformation  $\delta_{un}$  of that part and the deformation of beam 1 is  $\delta_{un}$  plus the crack opening  $\delta$  (see Fig. 7.1 and 7.2) and  $\delta$  is:

$$\delta = \frac{1}{2} \cdot \frac{V\lambda^2}{EI_1} \cdot \frac{2}{3} \cdot \lambda - \frac{1}{2} \cdot \frac{M_1\lambda^2}{EI_1} = \frac{1}{3} \cdot \frac{V\lambda^3}{EI_1} - \frac{1}{4} \cdot \frac{V\lambda^3}{EI_1} = \frac{1}{12} \cdot \frac{V\lambda^3}{EI_1} = \frac{V\beta^3}{bE\alpha^3} \quad (7.1)$$

The deflection difference of the cracked and un-cracked state is total:

$$\delta = \frac{1.2}{G} \left( \frac{\beta h}{b\alpha h} - \frac{\beta h}{bh} \right) \cdot V + \frac{V\beta^3}{bE\alpha^3} \quad (7.2)$$

The condition of equilibrium at crack length  $\beta$  is:

$$\partial(V \cdot \delta / 2 - G_c b \beta h) / \partial \beta = 0 \quad \text{or:} \quad \left\{ \partial(\delta / V) / \partial \beta \right\} \cdot V^2 / 2 = G_c b h \quad \text{or,}$$

with  $G_c$  as fracture energy:

## Exact Fracture Mechanics theory

$$V_f = \sqrt{\frac{2G_c b h}{\frac{\partial(\delta/V)}{\partial\beta}}} \quad (7.3)$$

where. It follows from eq.(7.2) that:

$$\frac{\partial(\delta/V)}{\partial\beta} = \frac{1.2}{bG} \left( \frac{1}{\alpha} - 1 \right) + \frac{3\beta^2}{Eb\alpha^3} \quad (7.4)$$

and eq.(7.3) becomes:

$$V_f = b\alpha h \sqrt{\frac{GG_c/h}{0.6(1-\alpha)\alpha + 1.5\beta^2 G/(\alpha E)}} \quad (7.5)$$

giving, for the always relatively small values of  $\beta$ , the previous found eq.(6.7):

$$\frac{V_f}{b\alpha h} = \frac{\sqrt{GG_c/h}}{\sqrt{0.6 \cdot (1-\alpha) \cdot \alpha}} \quad (7.6)$$

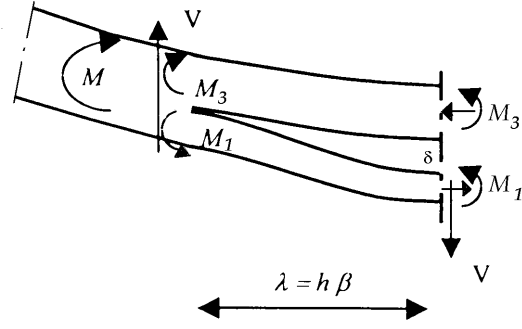
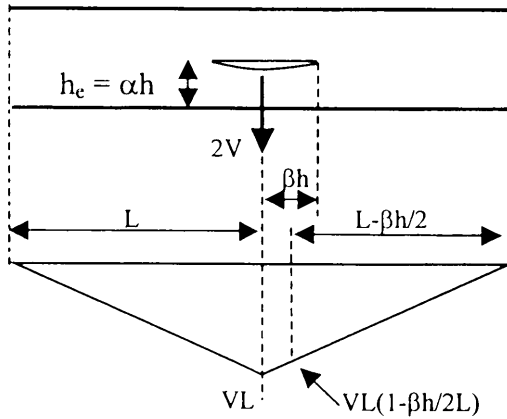


Figure 7.2 - Statics of half the crack

Figure 7.1 - Beam with crack by the dowel force of a joint and bending moment

which thus also applies for notched beams and for end-joints and verifies the lower bound of the strength, predicted by the theory of [1]. This also indicates that only work by shear stresses contributes to fracture. The fit of the equation with vierendeel action, eq.(7.5), to the data is not better than the fit by eq.(7.6) what shows that the term  $1.5\beta^2 G/\alpha E$  is small with respect to  $0.6(1-\alpha)\alpha$  and also that  $\beta$  is about proportional to  $\alpha$  and is of the same order. Comparison of eq.(7.5) and eq.(6.6) shows that the higher value of the end joint is determining for this definition of the strength and the same design rules as for notches are possible for joints when not the joint but splitting is determining. However design should be based on “flow “ of the joint before splitting of the beam and the interaction of joint failure and beam splitting has to be regarded as follows.

When crack extension starts of a cantilever beam loaded by a constant load  $V$ , giving a deflection increase of  $\delta$  at  $V$ , then the applied energy to the beam is  $V \cdot \delta$ . The energy balance equation then is:

$$V\delta = V\delta/2 + E_c \quad (7.7)$$

where  $V\delta/2$  is the increase of the elastic energy and  $E_c$  the energy of crack extension.

$$\text{Thus: } E_c = V\delta/2 \quad (7.8)$$

Thus the energy of crack extension is equal to the increase of elastic energy.

Eq.(7.8) also can be written with de incremental deflection  $\delta = du$ :

$$E_c = V^2 d(u/V)/2 = G_f b h d(\beta) \text{ or:}$$

$$V = \sqrt{\frac{2G_f b h}{\partial(u/V)/\partial\beta}} \quad (7.9)$$

where  $G_f$  is the fracture energy per unit crack surface and “ $bhd(\beta)$ ” the crack surface increase with

## Exact Fracture Mechanics theory

“ $b$ ” as width and “ $h$ ” the height of the beam with a crack length  $l = \beta h$ .

When the load on the cantilever beam, mentioned above, is prevented to move, the energy balance, eq.(7.7) becomes:

$$0 = E_e + E_c, \text{ or: } E_c = -E_e = -V\delta/2 \quad (7.10)$$

for the same crack length and now the energy of crack extension is equal to the decrease of elastic energy in the beam.

When the joint at load  $V$  becomes determining and just start to flow at  $\delta_1$  when splitting of the beam occurs, then eq.(7.7) becomes:

$$V\delta = (V\delta_1)/2 + V(\delta - \delta_1) + E_c \quad (7.11)$$

where again  $V\delta_1/2$  is the increase of the elastic energy and  $V(\delta - \delta_1)$  the plastic energy of the flow of the joint. From eq.(7.11) then follows:

$$E_c = V\delta_1/2 \quad (7.12)$$

the same as eq.(7.8), despite of the plastic deformation.

For connections, plastic deformation in the last case will not yet occur because it is coupled with crack extension. When the dowels of the joint are pressed into the wood, the crack opening increases and thus also crack extension. It can be seen in eq.(7.11), that when flow occurs, the total applied energy  $V\delta$  is used for plastic deformation. This is a comparable situation as given by eq.(7.10), and the at the plastic flow coupled crack extension will cause a decrease of the elastic energy. eq.(7.11) thus for joints is:

$$V\delta = (V\delta_1 - \delta_2)/2 + V(\delta - \delta_1) + E_s \quad (7.13)$$

where  $V\delta_2/2$  is the decrease of the elastic energy by the part of crack extension due to the plastic deformation. From eq.(7.13) now follows:

$$E_s = V(\delta_1 + \delta_2)/2 \quad (7.14)$$

and eq.(7.9) becomes:

$$V = \sqrt{\frac{2G_f bh}{\partial((u_1 + u_2)/V)/\partial\beta}} \quad (7.15)$$

From eq.(7.12) and (7.14) follows that  $V_c\delta_{1c} = V(\delta_1 + \delta_2)$ , where  $V_c\delta_{1c}$  is the amount when the connection is as strong as the beam. Thus:

$$\frac{\delta_1 + \delta_2}{\delta_{1c}} = \frac{V_c}{V} = \frac{n_c V_n}{n V_n} = \frac{n_c}{n} \quad (7.16)$$

where  $V_n$  is the ultimate load of the dowel at flow and  $n$  the number of dowels.

Substitution of eq.(7.16) into eq.(7.15) gives:

$$V = \sqrt{\frac{2G_f bh}{\partial(u_{1c}/V)/\partial\beta}} \cdot \frac{n}{n_c} \quad (7.17)$$

what is equal to  $\sqrt{n/n_c}$  times the strength according to eq.(7.9) for  $u = u_{1c}$ , thus  $\sqrt{n/n_c}$  times the splitting strength of the beam as is applied in [1].

According to eq.(7.13), the theoretical lower bound of  $V$  according to eq.(7.17) occurs at  $\delta_1 = \delta_2$ ,

Thus when  $n/n_c = 1/2$ . In [1], the empirical value of 0.5 to 0.4 is mentioned according to the data giving:

$$V = \sqrt{\frac{2G_f bh}{\partial(u_{1c}/V)/\partial\beta}} \cdot \sqrt{0,45} = \sqrt{\frac{2G_f bh}{\partial(u_{1c}/V)/\partial\beta}} \cdot 0.67 \quad (7.18)$$

This requirement for “flow” of the joint at failure:  $\sqrt{GG_f} = 0,67 \cdot 18 = 12 \text{ Nmm}^{-1.5}$  is included in the Eurocode (see § 7.5).

## Exact Fracture Mechanics theory

The condition  $\delta_1 = \delta_2$  means that there is sufficient elastic energy for total unloading and thus full crack extension with sufficient external work for plastic dissipation by the joints. According to eq.(7.13) is for that case:

$$E_c = V\delta_1 \quad (7.19)$$

### 7.3. Experimental verification

The value of  $E_c$  of eq.(7.19) is  $12 \text{ Nmm}^{-1.5}$  as follows from the test data given in [1]. In [1], first test-results of 50 beams of [4] with one or two dowel connections are given of beams of 40x100 and 40x200 mm with  $\alpha$ -values between 0.1 and 0.7 and dowel diameters of 10 and 24 mm. In all cases  $n \leq 0.5 \cdot n_c$  and not splitting but “flow” of the connection is determining for failure reaching the in [1] theoretical explained high embedding strength by hardening as to be expected for the always sufficient high spreading possibility of one- (or two-) dowel joints. The same applies for the 1 and 2 dowel joints of the Karlsruhe investigation. Splitting then is not the cause of failure but the result of post-failure behaviour due to continued extension by the testing device.

Table 7.1: TU-Karlsruhe test data No.1: Joint with nails

Type	No	$d$	rows	Col	$a=\alpha h$	$a_r$	$f_c$	$\sqrt{GG_c}$	$\eta=L/h$	$F/b\alpha h$
Test	tests		m	N			[1]	eq.(7)		
		mm			mm	mm	MPa	$\text{N/mm}^{1.5}$		MPa
beam: b.h=40.180 mm										
A1	8	3.8	5	1	28	76	3.7	13.9	2.37	7.37
A2	4	3.8	5	1	47	76	4.3	13.3	2.37	5.82
A3	3	3.8	5	1	66	76	4.2	11.3	2.37	4.52
A4	3	3.8	5	1	85	76	4.2	10.2	2.37	3.94
A5	3	3.8	5	1	104	76	5.5	11.7	2.37	4.54
beam: b.h =40.180mm						<b>mean</b>	<b>4.4</b>	<b>12.1</b>		
B1	4	3.8	5	2	47	76	3.5	15.5	2.37	6.77
B2	3	3.8	5	3	66	76	3.8	17.9	2.37	7.15
B3	3	3.8	5	4	85	76	3.3	16.1	2.37	6.21
B4	3	3.8	5	5	104	76	3.6	17.2	2.37	6.69
beam: b.h = 40.120 m						<b>mean</b>	<b>3.6</b>	<b>16.7</b>		
C1	3	3.8	2	1	28	76	6.8	15.3	2.18	8.51
C2	3	3.8	2	1	28	57	6.2	13.0	2.26	7.21
C3	3	3.8	2	1	28	38	5.6	10.9	2.34	6.07
C4	3	3.8	2	1	28	19	5.7	10.3	2.42	5.73
C5	3	3.8	1	1	28	0	6.9	11.2	2.50	6.21
C6	3	8	1	1	28	0	5.8	9.7	2.50	5.40
beam: b.h=40.180 mm						<b>mean</b>	<b>6.2</b>	<b>11.7</b>		
L8	1	8	1	1	28	0	5.0	8.8	2.50	4.64

Table 7.1 of [1] shows that for series B, splitting of the beam is determining. Whether there are 10, 15, 20 or 25 nails per shear plane, the strength is the same:  $\sqrt{GG_c} = 16.7 \text{ Nmm}^{-1.5}$ . This is confirmed by the too low value of the embedding strength of the nails  $f_c$  of series B. A more precise value of  $\sqrt{GG_c}$  follows from the mean value of  $17.1 \text{ Nmm}^{-1.5}$  of series B2 to B4. Then the value for 10 nails of series B1 is a factor  $15.5/17.1 = 0.9$  lower.

Thus  $\sqrt{n/n_c} = \sqrt{10/n_c} = 0.9$ . Thus  $n_c = 12$  for series B. This means that the number of 5 nails of

## Exact Fracture Mechanics theory

series A is below  $n_c/2 = 6$  and the measured apparent value of  $\sqrt{GG_c}$  is the minimal value of  $\sqrt{GG_c} \cdot \sqrt{0.5n_c/n_c} = 17.1 \cdot \sqrt{0.5} = 12.1 \text{ Nmm}^{-1.5}$ . The same value should have been measured for series C because the number of 3 nails also is below  $n_c/2 = 6$ . Measured is  $11.7 \text{ Nmm}^{-1.5}$ . For the 53 beams of all the series G of [1] this is  $12.0 \text{ Nmm}^{-1.5}$ . As mentioned a mean value of 12 is now the Eurocode requirement.

The value of  $0.5 \cdot n_c$ , depends on dimensioning of the joint and thus on amount of hardening by the spreading effect of embedding strength. Thin, long nails at larger distances in thick wood members are less dangerous for splitting and show a high value of  $n_c$ . For series G, with  $b = 100 \text{ mm}$ ,  $n_c/2$  is at least below 8 nails. For series V of [1] with dowels of 16 mm,  $n_c = 8.6$ . For design,  $n_c$  need not to be known. But dimensioning of the joint to meet also the requirement of  $\sqrt{GG_c} = 12 \text{ Nmm}^{-1.5}$ , will lead to the number of nails of  $n_c/2$ . This dimensioning also determines the value of  $f_c$ . The value of  $f_c = 4.4 \text{ MPa}$  of series A is lower than  $f_c = 6.2 \text{ MPa}$  of series C, in proportion to the square root of the spreading lengths per nail as expected from theory [1].

### 7.4. Design equation of the Eurocode 5

As discussed in [1], the shear capacity is (for  $h_e \leq 0.7 h$ )

$$\frac{V_u}{b\sqrt{h}} = 10.3 \sqrt{\frac{\alpha}{1-\alpha}} = 10.3 \sqrt{\frac{h_e}{h-h_e}}$$

where  $10.3 = (2/3)\sqrt{(GG_c/0.6)}$  is the characteristic value.

This can be replaced by the tangent line through this curve at point  $\alpha = 0.5$  giving:

$$\frac{V_u}{b\alpha\sqrt{h}} = 1.7\sqrt{GG_c} = 1.7 \cdot (2/3) \cdot 12 = 13.6 \text{ Nmm}^{-1.5}.$$

### 7.5. References

- [1] T.A.C.M. van der Put, A.J.M. Leijten, Evaluation of perpendicular to the grain failure of beams, caused by concentrated loads of joints. CIB-W18A/33-7-7, meeting 33, Delft, The Netherlands, August 2000. C(2000)
- [2] T.A.C.M. van der Put, Tension perpendicular to the grain at notches and joints. CIB-W18A-23-10-1, meeting 23, Lisbon, Portugal, Sept. 1990, C(1990)
- [3] T.A.C.M. van der Put, DWSF Technical note 11-7, Energy approach of fracture of beams and joints, loaded perpendicular to grain, basic equations, Series 2006, nr.1. ISSN 18-71-675X.
- [4] M. Ballerini: A set of tests on beams loaded perpendicular to the grain by dowel type of joints. CIB-W18/32-7-2. Graz. Austria.

## 8. Conclusions Chapter 1 to 7

- Strength analysis has to be based on the technical exact theory of limit analysis, at least by applying the lower bond equilibrium method, of regarding an equilibrium system which satisfies the boundary conditions and nowhere surmounts the failure criterion. Thus, accordingly, a linear elastic boundary value approach is possible up to the elastic- full plastic boundary around the crack tip.

- Wood acts as a reinforced material. The isotropic matrix fails earlier than the reinforcement and determines initial “flow” behavior. It therefore is necessary to solve the Airy stress function for the stresses in the isotropic matrix and then to derive the total (“orthotropic”) stresses from this solution. Based on this approach, the mode I and II stress intensities are:  $K_{Ic} = \sqrt{E_y G_{Ic}}$ ,

## Exact Fracture Mechanics theory

$K_{IIc} = n_6 \sqrt{E_y G_{IIc}}$ , based on the mode I and II energy release rates, which are related:  $G_{IIc} = 4G_{Ic}$  and which are for total, orthotropic stresses, for combined mode I – II failure:

$$G_f = 4G_{Ic} / (1 + \sqrt{\gamma})^2 = G_{IIc} / (1 + \sqrt{\gamma})^2 \quad \text{with : } \gamma = 1 / (1 + \tau_{xy}^2 / \sigma_y^2) \quad \text{and:}$$

$$n_6 = (2 + \nu_{21} + \nu_{12}) \cdot (G_{xy} / E_y)$$

The theoretical value of  $G_{IIc} = 4G_{Ic}$  is verified by reported measurements where ratio 3.5 is found ( $R^2 = 0.64$ ) in stead of 4. This lower measured ratio is due to the applied too high value of the fracture energy,  $G_{Ic}$ , obtained as total area under the loading curve.

If mode I and mode II values are known at combined failure, the following, (eq.(5.7)) applies:

$$\frac{K_I}{K_{Ic}} + \frac{(K_{II})^2}{(K_{IIc})^2} = 1 = \frac{\sqrt{G_I}}{\sqrt{G_{Ic}}} + \frac{G_{II}}{G_{IIc}} = \frac{\sqrt{\gamma \cdot G_f}}{\sqrt{G_{Ic}}} + \frac{(1 - \gamma) \cdot G_f}{G_{IIc}}$$

- The next stage, after initial “flow” of confined plasticity near the crack tip, also can be replaced by the equivalent linear elastic ultimate stress value. The difference is an internal equilibrium system which, as any initial displacement or initial stress, does not affect the ultimate load in accordance with the, on virtual work based, limit analysis theorems.

- Determining for the strength is the stress combination at the fracture site, which satisfies the, in Chapter 2 derived, mixed mode failure criterion, which is shown to follow the critical distortional energy criterion for initial crack extension and the Coulomb criterion after “hardening”.

This mixed mode failure criterion is the consequence of the ultimate uniaxial cohesive strength along the micro-crack boundary, causing, oblique, (virtual) crack extension. The theory therefore also explains the relations between  $K_{Ic}$  and  $K_{IIc}$  in TL- and in RL-direction and the relations between the related fracture energies and energy release rates.

- For wood, thus far, only singularity type solutions of the Airy stress function are applied in the form of:  $\sigma_{ij} = K_A \cdot F_{ij}(\theta) / (2\pi r)^{0.5}$ , while collinear crack extension is assumed. This prevents the possibility of derivation and application of the right, exact, mixed mode failure criterion.

It is shown in § 2.2.2, that this singularity solution, is a special case of the general, exact, non-singular solution.

Therefore wrongly is stated that when  $r$  in this equation goes to zero,  $\sigma$  goes to infinity, but that the product is constant by a constant  $K_A$ . There is no relation, by the applied methods, that confirms this. On the contrary, the derivation of chapter 2 shows, that  $r = r_0$  (the boundary of the fracture process zone) is constant and the cohesive strength  $\sigma$ , also is constant as necessity for fracture mechanics type solutions with constant stress intensities. The real singularity is given by:  $K_A = p\sqrt{\pi c}$ , where the applied stress  $p$  becomes infinite, when  $c$  approaches zero.

This follows from the exact derivation of the singularity equation in § 10.2, eq.(10.2.4) shows, that the external loading stress:  $(Y\sigma / \sqrt{1 - (a/x)^2})$  becomes infinite when  $x \rightarrow a$ , and the crack length:

$$\sqrt{\pi a_c} = \sqrt{\pi 2(x-a)} \rightarrow 0, \quad \text{when } x \rightarrow a. \quad \text{However, the product:}$$

$$K_I = (Y\sigma / \sqrt{1 - (a/x)^2}) \sqrt{\pi 2(x-a)} = Yx\sigma \sqrt{2\pi / (x+a)}$$

is constant, equal to  $K_I = Y\sigma \sqrt{\pi a}$  for the singularity  $x \rightarrow a$ . The smallest possible, clear wood (micro-) crack length:  $(x - a)$ , is determining for macro-crack extension due to small crack merging. It is known from testing that micro-crack multiplication and merging precedes macro-crack extension.

- As shown by Continuum Damage Mechanics, (§ 4.4), it is necessary for a right theory, that strength analysis is based on the actual stress at the actual intact area, and the strain increase is due to damage, caused by the actual stress at the damage location. This explains why approaches based on nominal stresses lead to absurdities, as e.g. the assumption of the existence of strain softening,

## Exact Fracture Mechanics theory

what is against the basic principles of science, making any strength calculation impossible.

- The Griffith stress is a nominal stress at the fracture site, what thus necessarily leads to inconsistencies. This stress acts, as actual stress, on the intact, uncracked, not ultimate, but elastic loaded section, outside the fracture plane. Thus is not related to fracture. For fracture it therefore leads to the following paradox: At fracture, the elastic energy level is just high enough to cause crack extension of the critical initial crack length. But, at crack extension, the elastic stress level (and thus the elastic energy level) goes down, while the crack length increases. Thus there is too little energy to extend this, longer, crack further. Thus: the Griffith law is not able to explain crack extension at following lower stress levels. The reason of this paradox is that nominal stresses are regarded, while fracture laws only apply in real-, thus in actual stresses. For the real stress at the fracture site, applies that, at yield drop, there is an increasingly sufficient high actual stress level for further fracture as follows from eq.(3.2.10), showing that not only the first derivative but also the second derivative is positive for fracture when critical  $c/b > 1/6$ .

- The fact that, at crack extension, the local strength of adjacent clear material increases by the stress spreading effect, and, by that, the local stress remains ultimate, is the reason that the first stage of yield drop still follows the nominal Griffith law with constant nominal  $G_{Ic}$ . The actual stress remains determining and micro-crack extension due to clear wood fracture of the always ultimate loaded intact material in the fracture plane is the real cause of crack extension and a local, ultimate, actual stress criterion, applies as shown in Chapter 3.

- The Griffith law does not apply for long overcritical initial crack lengths. The reason of this is that the Griffith law is based on the energy of elastic crack opening (or closure) what is not equal to the crack formation energy for overcritical crack lengths. The crack closure energy, per unit crack length, is lower for long cracks than for the short critical crack length. There thus is an decrease of the nominal, thus apparent, stress intensity  $G_{Ic}$ .

- It thus is shown, that strain softening does not exist. Softening called yield drop is only possible for the nominal stress, thus for the actual elastic stress outside the fracture plane and thus represent elastic unloading outside the fracture plane.

- Yield drop, only is possible in a constant strain rate test and is not possible in a constant loading rate test and not in a dead load to failure test, and is thus not a material property. The analysis shows that the actual stress at the fracture plane increases and shows hardening (by stress spreading) up to the constant ultimate level.

- The fracture energy as area under the yield drop curve should be based on half this area for mode I, as is already applied for mode II. The stress should be, as the Griffith stress, related to the whole width of the specimen, including the initial crack length, and not only to the still intact part of the fracture plane, because then, the fracture energy depends on the applied initial crack length. When the fracture energy is related to the whole width, the energy method is correctly based on the energy difference of the cracked and the fully un-cracked state of the specimen.

- The area of a loading cycle at “yield drop”, divided by the crack length, is indeed equal to the fracture energy, because this area is indeed half the area under the yield drop curve. However, this energy is proportional to the apparent activation energy of all acting processes in the whole test specimen, including visco-elastic and plastic processes, which response should be obtained by Deformation Kinetics on an uncracked specimen and then then has to be subtracted to obtain the fracture energy. Because this is not applied, and therefore leads to not crack related R-curves, this area method should not be applied anymore.

- A derivation of the mode I and II yield drop curves, according to the Griffith theory is given (chapter 3) The curve can be explained by an optimal small crack merging mechanism of increasing small crack lengths, showing that this curve also fully is explained by the ultimate state of the decreasing intact clear wood part in the fracture plane. The yield drop curve follows at the start the “stable” part of the Griffith locus. This means that every point of the yield drop curve gives the Griffith strength. This curve depends on only one parameter, the maximal critical Griffith stress  $\sigma_c$

## Exact Fracture Mechanics theory

and therefore depends on the critical crack density. This applies until half way of unloading. The fracture energy is down to this point equal to the critical energy release rate. After that, the strength of the fracture plane of the test specimen becomes determining due to a crack merging mechanism, changing the crack density and intact area of the fracture plane and therefore causing a decrease of  $\sigma_c$  (the top of the yield drop curve) and an apparent decrease of the fracture energy. The strength at every point of the “softening” curve is fully determined by the strength of the intact area of the fracture plane. yield drop thus is a matter of elastic unloading of the specimen outside the fracture zone and yield drop thus is not a material property.

- Fracture mechanics of wood and comparable materials appears to be determined by small-crack propagation towards the macro-crack tip. This follows e.g. from the same failure criterion for “clear” wood and for macro-crack extension. The presence of small-crack propagation is noticeable by the Weibull volume effect of timber strength. There is no influence on macro-crack propagation of the geometry of notches and sharpness of the macro crack-tip in wood (against orthotropic theory). Thus orthotropic fracture mechanics is not determining. This also follows from the nearly same fracture toughness and energy release rate for wide and slit notches and the minor influence of rounding the notch (also against orthotropic theory). Determining thus is the influence of small cracks in the isotropic matrix for the total behavior, having the same influence at the tip of wide, as well as, slit notches.

- It is shown, that the models applied to wood, as replacement of infinite fracture stresses of the singularity approach, as e.g. the Dugdale model, fictitious crack model, J-integral and crack growth models are not exact and have to be replaced by the general theory, derived in Chapter 2.

- The theory shows that the Eurocode design rules for beams with rectangular end notches or joints should be corrected to the right real compliance difference and the right measured uniaxial stiffness. The verification of the derived theory by measurements shows the excellent agreement. The method provides an exact solution and is shown to be generally applicable also for joints and provides as simple design equations as wanted

- Because the macro-crack kinetics is the same as for clear wood, this small-crack behavior is always determining (see last part of Section 3.6 of [2]).

- For long sub critical initial cracks as in [13], the strength of the intact part of the fracture plane is always determining and explains the measured too low apparent stress intensity.

- Small-crack merging explains precisely the yield drop curve (of [11]) by the strength (or plastic flow stress) of the intact part of the fracture plane, which is always in the ultimate state and is most probable because it requires a lower stress than single macro-crack propagation ([2], Section 3.5 and 3.6) and shows in rate form the necessary molecular deformation kinetics equation of this damage process. (see [11]).

### **9. Weibull size effect in fracture mechanics of wide angle notched timber beams.**

Because the Weibull size effect is normally not regarded as a fracture mechanics subject, this influence is discussed in a separate chapter 9.

#### **9.1. Overview**

A new explanation is given of the strength of wide angled notched timber beams by accounting for a Weibull type size effect in fracture mechanics. The strength of wood is described by the probability of critical initial small crack lengths. This effect is opposed by toughening by the probability of having a less critical crack tip curvature. The toughening effect dominates at the different wide angle notched beams showing different high stressed areas by the different notch angles and thus different influences of the volume effect. This is shown to explain the other power of the depth in eq.(9.18) and (9.19) than applies for the sharp notch value of 0.5 of eq.(9.17). It further is shown to explain why for very small dimensions, also for sharp notches, the volume effect applies. The explanation by the Weibull effect implies that the strength depends on small crack initiation and propagation, in the neighbourhood of the macro crack tip. This initial crack

population can be different for full scale members indicating that correction of the applied data is necessary and that additional toughness tests have to be done on full scale (or semi full scale) test specimens. Small cracks fracture mechanics is discussed in Chapter 10.

### 9.2. Introduction

Fracture mechanics of wood is normally restricted to fracture along the grain. Also the mixed mode crack follows the weak material axes and only may periodically jump to the next growth layer at a weak spot. Thus the direction of the collinear crack propagation is known. As shown in chapter 2, the singularity approach gives no right results in this case and the analysis has to be based on linear elastic, flat elliptic, crack extension by the maximal tensile stress at the elastic-plastic boundary around the small crack. This response at randomized stress raisers near weak spots is indicated by the volume effect of the strength. There also is no clear influence on macro-crack propagation of the crack geometry and notch form and sharpness of the macro crack tip, showing orthotropic fracture mechanics to be not decisive. This also is indicated by the not orthotropic, but isotropic relation between mode I stress intensity and strain energy release rate of wood. The determining small crack behaviour also follows from the failure criterion of common un-notched wood, being of the same form as the theoretical explained fracture mechanics criterion for notched wood.

The wood matrix is determining for initial failure and not the reinforcement. The failure criterion of unnotched wood shows no coupling term between the reinforcements in the main directions confirming the orthotropic strength schematization to be not determining. The determining small crack dimension follows from the Weibull size effect. The here treated strength of wide angle notched beams is an example of a determining size effect in fracture mechanics.

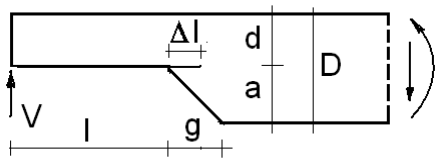


Figure 9.1 - Wide angle notched beam element

The strength analysis of [1] of wide angle notched beams, given in Fig. 9.1, was based on the orthotropic Airy stress function. However, despite of the dominant mode I loading, none of the solutions of this function are close enough to the measurements to be a real solution. The reason of this is the absence of the Weibull size effect in the equations as will be shown in this paragraph. The in [1] chosen solutions of the biharmonic Airy stress function are:

$r_1^{\pm n} \cos(n\theta_1)$ ,  $r_1^{\pm n} \sin(n\theta_1)$ ,  $r_2^{\pm n} \cos(n\theta_2)$ ,  $r_2^{\pm n} \sin(n\theta_2)$  resulting in:

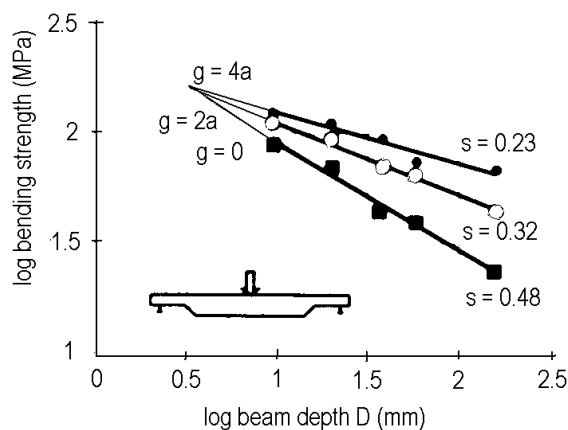


Figure 9.2 - Measured bending strengths for different sizes and notch angles

$$\{\sigma_r, \sigma_\theta, \sigma_{r\theta}\} = \frac{K_A}{(2\pi r)^n} \{f_1(n\theta), f_2(n\theta), f_3(n\theta)\} \quad (9.1)$$

where  $K_A$  is the stress intensity factor and “ $r$ ” the distance from the notch root. In the direction of crack extension, along the grain ( $\theta = 0$ ), the tensile strength perpendicular to the grain  $\sigma_\theta$  is determining for fracture. The boundary conditions, for the different notch angles  $a/g$ , provide different values of the power “ $n$ ” and thus different slopes of the lines in Fig. 9.2. However, it is theoretically not possible that these lines intersect through one point, as is measured, because the different boundary conditions by the different notch angles cannot be satisfied at the same time and the chosen mathematical solution of [1] thus has to be rejected. The fact that these lines cross one point, at the elementary volume, proves the existence of a volume effect of the strength. This is introduced in the fracture mechanics energy method calculation in § 9.4. In § 9.3, the derivation of the size effect is given to show the equivalent derivation of the toughening size effect in § 9.4.

### 9.3. Size effect

Due to the initial small crack distribution, clear wood shows a brittle like failure for tension and shear. According to the Weibull model, the probability of rupture, due to propagation of the biggest crack in an elementary volume  $V_0$  is equal to  $1 - P_0(\sigma)$ , when  $P_0$  is the probability of survival. For a volume  $V$  containing  $N = V/V_0$  elementary volumes the failure probability is:

$$1 - P_s = (1 - P_0)(1 - P_0)(1 - P_0) \dots = (1 - P_0)^N. \text{ Thus } \ln(1 - P_s) = N \ln(1 - P_0) \approx -NP_0 \text{ because } P_0 \ll 1.$$

Thus the probability of survival of a specimen with volume  $V$ , loaded by a constant tensile stress  $\sigma$ , as in the standard tensile test, is given by:

$$P_s(V) = \exp(-NP_0) = \exp\left(-\frac{V}{V_0} \left(\frac{\sigma}{\sigma_0}\right)^k\right) \quad (9.2)$$

where  $P_0(\sigma) = (\sigma/\sigma_0)^k$  is chosen, because the power law of  $\sigma$  may represent any function of  $\sigma$  around a chosen stress value as e.g. the mean failure stress (see § 4.4 for the proof).

For a stress distribution, eq.(9.2) becomes:

$$P_s(V) = \exp\left(-\int_V \left(\frac{\sigma(x, y, z)}{\sigma_0}\right)^k dx \cdot dy \cdot dz / V_0\right) \quad (9.3)$$

This specimen has an equal probability of survival as the standard test specimen eq.(9.2), when the exponents are equal thus when:

$$\int_V \left(\frac{\sigma(x, y, z)}{\sigma_0}\right)^k dV = \left(\frac{\sigma_s}{\sigma_0}\right)^k V_s \quad (9.4)$$

For a constant stress  $\sigma(x, y, z) = \sigma$ , the specimen strength thus will decrease with its volume  $V$  according to:

$$\sigma = \sigma_s \cdot \left(\frac{V_s}{V}\right)^{1/k} \quad (9.5)$$

where  $\sigma_s$  is the mean strength of the specimen with volume  $V_s$ . The power  $k$  depends on the coefficient of variation  $s/\sigma$  according to:

$$\left(\frac{s}{\sigma}\right)^2 = \frac{\Gamma(1+2/k)}{\Gamma^2(1+1/k)} - 1 \quad (9.6)$$

From the row-expansion of the Gamma-functions it can be seen that:

$$k \cdot \frac{s}{\sigma} = f\left(\frac{s}{\sigma}\right) \approx 1.2 \quad (9.7)$$

where  $f(s/\sigma)$  is normally a little varying function. Thus:  $1/k = s/(1.2 \cdot \sigma)$

For a stress distribution, eq.(9.4) becomes:

$$\int \left(\frac{\sigma_m}{\sigma_0}\right)^k \left(\frac{\sigma(x, y, z)}{\sigma_m}\right)^k dx dy dz = \left(\frac{\sigma_m}{\sigma_0}\right)^k V_{ch} = \left(\frac{\sigma_s}{\sigma_0}\right)^k V_s \quad (9.8)$$

where  $\sigma_m$  is the determining maximal stress in volume  $V$  and  $V_{ch} = \int (\sigma/\sigma_m)^k dV$ , a characteristic volume. Eq.(9.8) thus becomes:

$$\sigma_m = \sigma_s \left(\frac{V_s}{V_{ch}}\right)^{1/k} = \sigma_s \left(\frac{V_s}{V_{ch}}\right)^{s/1.2\sigma} \quad (9.9)$$

This applies for the strength of common unnotched specimens.

This strength also is determined by fracture mechanics. The tensile strength is e.g.:

$$f_t = \frac{K_{Ic}}{\sqrt{\pi c}} \quad \text{or} \quad f_t = f_{t,s} \sqrt{\frac{c_s}{c}} \quad (9.10)$$

where  $K_{Ic}$  is the stress intensity factor.

Substitution of the strength according to eq.(9.5) (or eq.(9.9)) leads to:

$$f_t = f_{t,s} \sqrt{\frac{c_s}{c}} = f_{t,s,V} \left(\frac{c_s}{c}\right)^{0.5} \left(\frac{V_s}{V}\right)^{1/k} \quad (9.11)$$

This equation gives the probability of a critical Griffith crack length  $c$  leading to fracture. Also in this case, a crack toughening mechanism is thinkable, discussed in § 9.4, leading to the opposite volume effect with a negative value of the exponent  $1/k$ . This can not be distinguished and the resultant value of  $1/k$  then is given by eq.(9.11). Because for every type of wood material the value of  $c$  is specific, determining the specimen strength, eq.(9.9), as shortcut of eq.(9.11), is applied in practice.

According to eq.(2.3.7), the stress intensity factor of eq.(9.10) is:  $K_{Ic} = \sigma_t \sqrt{\pi r}/2$  where  $\sigma_t$  is the equivalent cohesion strength at the crack tip boundary and  $r$  is the radius of the elastic-plastic boundary of the crack tip zone. A constant stress intensity factor  $K_{Ic}$  means that  $\sigma_t \sqrt{r}$  is constant and only the crack length  $c$  is a variable, as for brittle fracture. Toughening means an increase of the plastic zone, thus of  $r$  of the small cracks, within the characteristic volume. This influence is visible at the different wide angle notches as discussed in § 9.4.

Because fracture across the grain is tough and the lengths of applied beams don't vary much, the size effect of the length dimension is small and the volume effect for bending is replaced by a height effect of the beam only. It is postulated that this absence of a width effect is explained by the constant widths of  $2b'$  of 2 planes of weakness adjacent to the free sides of the beam due to the cutting action at manufacturing. Then:  $(V_s/V_{ch})^{1/k} = (2b'h_s l / 2b'hl)^{1/k} = (h_s/h)^{1/k}$ , becomes the height factor of the Codes. This width effect is applied in § 9.4.

#### 9.4. Size effect of wide notched beams

The analysis of the strength of notched beams can be based on the energy method where the critical fracture energy is found from the difference of the work done by the constant force due to its displacement by a small crack extension minus the increase of the strain energy due to this displacement. According to this approach of [3], [4], and § 6, the bending stress  $\sigma_m$  at the end of the notched beam at  $l = \beta D$  in Fig. 9.1 is:

$$\sigma_m = \frac{6V_f \beta D}{b(\alpha D)^2} \approx \frac{\sqrt{6EG_c / D}}{\sqrt{(\alpha - \alpha^4)}} \quad (9.12)$$

when the notch is not close to the support. In [1] is chosen:  $\alpha = d/D = 0.5$ , what means that  $d = a$ . Further the length is  $l = 2D$  when  $g/a = 0$  and 2, while  $l = 4D$  for  $g/a = 4$  in Fig. 9.1.  $E$  is the modulus of elasticity and  $G_c$  the critical energy release rate, given in [3]. Eq.(9.12) applies for the rectangular notch ( $g = 0$ ). For wide notch angles a more complicated expression applies because of the changing stiffness over length  $\Delta l$  of the crack extension. However, for given dimensions and loading, the basic form of the equation is the same as eq.(9.12), thus:

$$\sigma_m = B\sqrt{EG_c / D} \quad (9.13)$$

where  $B$  is a constant depending on dimensions and notch angle. According to §2 and [3] is, as mentioned,  $\sqrt{EG_c} \triangleq K_c \triangleq \sigma_t \sqrt{r}$ , where  $\sigma_t$  is the equivalent cohesion strength and the crack tip radius  $r$  is the only parameter of the notch strength. The volume effect depending on the stress follows from § 9.3 and the analysis thus can be based on the flow stress and the characteristic volume around the notch tip, For the probability of a critical value of  $r$ , of the small initial cracks within the high stressed characteristic volume around the notch tip, the probabilistic reasoning of § 9.3 can be repeated as follows. The probability of having a critical flaw curvature  $1/r$  in an elementary volume  $V_0$  is equal to  $1 - P_0(1/r)$ , when  $P_0$  is the survival probability. For a volume  $V$  containing  $N = V/V_0$  elementary volumes the survival probability is in the same way:

$$P_s(V) = \exp(-NP_0) = \exp\left(-\frac{V}{V_0} \left(\frac{r}{r_0}\right)^{-k}\right) \quad (9.14)$$

where  $P_0(1/r) = (r_0/r)^k$ , because the power law may represent any function in  $1/r$ . At “flow”, this probability is not a function of  $\sigma$ , but of the flow strain, given by a critical  $r$ . Equal exponents for the same probability of failure in two cases now lead to:

$$r = r_s (V/V_s)^{1/k} \quad (9.15)$$

and eq.(9.13) becomes:

$$\sigma_m \approx \frac{B' \sigma_t \sqrt{r_s}}{\sqrt{D}} \cdot \left(\frac{V}{V_s}\right)^{1/2k} \quad \text{or:} \quad \sigma_m = \sigma_{m0} \left(\frac{D}{D_0}\right)^{-0.5} \left(\frac{V}{V_0}\right)^{1/2k} \quad (9.16)$$

For the notch angle of  $90^\circ$ , ( $g = 0$  in Fig. 9.1), or for smaller angles, the high stressed elastic region around the crack tip is, as the fracture process zone itself, independent of the beam dimensions.

Thus in characteristic dimensions  $V = b'l'h' = V_0$  and eq.(9.16) becomes:

$$\sigma_m = \sigma_{m0} \left(\frac{D}{D_0}\right)^{-0.5} \quad (9.17)$$

independent of a volume effect. For the widest notch angle of  $166^\circ$  ( $g/a = 4$ ), there is a small stress gradient over a large area and  $V$  is proportional to the beam dimensions. Thus:  $V(:) b \cdot d \cdot l =$

$\gamma D \cdot \delta D \cdot \beta D = \gamma \cdot \beta \cdot \delta D^3$  and:  $V/V_0 = (\gamma \delta \beta D^3 / \gamma \delta \beta D_0^3) = (D/D_0)^3$ . Thus is, with  $1/k = 0.18$ :

$$\sigma_m = \sigma_{m0} \left(\frac{D}{D_0}\right)^{-0.5+3/(2k)} = \sigma_{m0} \left(\frac{D}{D_0}\right)^{-0.23} \quad (9.18)$$

For the angle of  $153.40^\circ$ , ( $g/a = 2$ ), the high stressed region dimensions becomes proportional to the dimensions  $b$  and  $D$  and:

$V/V_0 = (bdl)/(b_0 d_0 l) = (\gamma \delta D^2 / \gamma \delta D_0^2) = (D^2 / D_0^2)$  and with  $1/k = 0.18$  is:

## Exact Fracture Mechanics theory

$$\sigma_m = \sigma_{m0} \left( \frac{D}{D_0} \right)^{-0.5+2/(2k)} = \sigma_{m0} \left( \frac{D}{D_0} \right)^{-0.32} \quad (9.19)$$

It follows from Fig. 9.2, that the values of exponents of  $-0.5$ ,  $-0.32$ , and  $-0.23$  are the same as measured. The coefficient of variation of the tests must have been:  $1.2 \cdot 0.18 = 0.22$ , as common for wood. According to the incomplete solution of [1], discussed § 9.2, these values of the exponents were respectively  $-0.437$ ,  $-0.363$  and  $-0.327$ , thus, too far away from the measurements.

The explanation of no volume effect of sharp notches due to the invariant characteristic volume, independent of the beam dimensions, explains also why for very small beams, also for sharp notches, there is a volume effect because then the beam dimensions are restrictive for the characteristic volume. As known, the exponent may also change from  $-0.5$  to  $-0.23$  with decrease of the beam dimensions. This is measured and e.g. discussed at pg. 85 of [2]. The constant dimensions of the fracture process zone act as a relative increase of the plastic zone for decreasing test beam dimensions and it appears that toughening is the explanation of this volume effect. The lines in Fig. 9.2 intersect at the elementary Weibull volume wherefore the depth dimension is  $10^{0.6} = 4$  mm with a material bending strength of 147 MPa.

### 9.5. Conclusions regarding the size effect

- A new explanation is given of the strength of wide angled notched beams of [1] by introducing the Weibull type size effect in fracture mechanics, based on the critical small crack length, opposed by the toughening curvature of the initial small cracks near the high stressed macro notch tip zone.

- For sharp notch angles, up to  $90^\circ$ , there is no volume effect due to the constant characteristic volume, at the fracture process zone. For wider notch angles, the peak stresses and stress gradients become lower and are divided over a larger region and influenced by the dimensions of the specimen and thus a volume effect correction applies.

- The intersect of the three lines in Fig. 9.2, with different values of “ $n$ ” of eq.(9.1), due to different boundary conditions, which can not apply at the same time for the different notch angles, thus can not be explained by the boundary value analysis. This intersect only can be explained to be due to the volume effect of the strength indicating failure by small crack extension within the high stressed region at the notch tip.

- The measured values of the powers of the depths (or the slopes of the lines of Fig. 9.2) are precisely explained by applying the Energy approach and the volume effect correction according to:

$$\sigma_m = \sigma_{m0} \left( D / D_0 \right)^{-0.5} \left( V / V_0 \right)^{1/2k}$$

### 9.6. References

- [1] R.H. Leicester, Design specifications for notched beams in AS 1720, CIB-W18/38-6-1, meeting 38, Karlsruhe, Germany, August 2005.
- [2] I. Smith, E. Landis, M. Gong, Fracture and Fatigue in Wood, J. Wiley & Sns.
- [3] T.A.C.M. van der Put, Modified energy approach for fracture of notched beams, COST 505 workshop on Fract. Mech. Bordeaux, April 1992.
- [4] T.A.C.M. van der Put A new fracture mechanics theory of wood, Nova Science Publishers, Inc. New York, C(2011a), or more complete:  
T.A.C.M. van der Put Exact and complete Fracture Mechanics of wood. Theory extension and synthesis of all series C publications.

## 10. Small crack fracture mechanics

### 10.1. Introduction.

Because small crack behavior is a new subject and is shown to be always determining for fracture, it is discussed in a separate chapter as basis for a necessary new approach.

That small crack extension is determining is e.g. indicated by the volume effect of the strength and

by the no clear influence on macro-crack propagation of the crack geometry and sharpness of the crack-tip of notches in wood. Also the only possible explanation of yield drop and the dynamics of crack propagation by micro crack extension and small crack merging shows this behavior. The failure criterion of clear wood and of timber [1], [2], and the failure criterion by a single macro notch [3], [4], are the same, showing that small-crack extension towards the macro-crack tip is the cause of macro-crack extension. This is confirmed by the fact that the stress intensity factor is independent on the macro-form and dimensions of the notch. It also is confirmed by molecular deformation kinetics, showing the same processes in clear- and in notched wood (see discussion Annexes B on: iews.nl). Also the exact solutions given in [4] and below of the geometric correction factor and of [5] and § 3.7, of the strength behavior of long post-critical crack lengths is totally based on small crack behavior. The small-crack merging mechanism explains, in [3] and in § 3.6 and § 3.5, precisely the mode I yield drop curves of [6]. The failure criterion [1], shows no coupling term between the normal stresses at “flow”, and thus shows no dowel action of the reinforcements and there only is a direct interaction of the reinforcement with the matrix and the matrix stresses determine the stresses in the reinforcements. Because the initial small cracks in wood are in the matrix and start to extend in the matrix, the stress equilibrium condition of the isotropic matrix by the matrix-stresses has to be regarded. The isotropic solution of the matrix stresses thus has to be regarded in the end state. The total stresses, due to the reinforcement, then follow by multiplication of an elastic constants factor e.g. derived in Chapter 2 and § 2 of [3].

In [4], and in § 10.2, the exact derivation of the geometric correction factor of the center notched test specimen is given, based on small cracks merging. As known, this geometric correction factor accounts for the difference of finite specimen dimensions with respect to the notch in an infinite plate. Because, contrarily to macro-crack extension, unloading by yield drop (wrongly called “softening”) by step wise small crack merging is possible at any low mean stress level, it can be postulated that small crack merging always takes place in the high loaded zone near the macro-crack tip and that macro-crack extension is always due to small crack extension towards the macro-crack tip.

## 10.2. Derivation of the geometric correction factor of the center notched specimen

As mentioned, at eq.(2.3.10), fracture mechanics laws only apply when  $r_0$ , (process zone) and thus  $\sigma_t$ , (strength) are constant in:  $K_{Ic} = \sigma_y \sqrt{\pi c_c} = \sigma_t \sqrt{\pi r_0 / 2}$ . The singularity approach, (called LEFM), as derived in § 2.2.2, as special case of the exact solution, is thus wrongly based on  $r_0 \rightarrow 0$ , and an infinite strength  $\sigma_t \rightarrow \infty$ . Necessary thus is that  $\sigma_y \rightarrow \infty$ ,  $c_c \rightarrow 0$  at the singularity for the right solution. Therefore in the following, the necessary exact derivation of the right geometric correction factor is given:

For a crack in an infinite plate, which is loaded by a tensile stress  $\sigma$ , the stress distribution along the fracture plane, line AB of Fig. 10.2, is e.g.:

$$\sigma_{y,\infty} = \frac{\sigma}{\sqrt{1-(a/x)^2}} \quad x > a \quad (10.2.1)$$

where  $2a$  is the crack length and  $x$  is the distance from the center of the crack. This stress distribution is according to the solution of the Airy stress function of [7]. Such solution satisfies the equilibrium, compatibility and boundary conditions and thus is an exact (limit analysis) solution. To obtain the ultimate state of the specimen given in Fig. 10.1, we may cut out the specimen dimensions from the infinite plate, as is given in Fig. 10.2. Next we may multiply the stress  $\sigma_{y,\infty}$  by a (by definition stress independent) factor  $Y$  with such magnitude that the resultant shear loading  $2R$  in the planes AD and BC of Fig. 10.2 becomes zero. There remains an equilibrium system in those vertical planes giving an internal equilibrium system in the cut-out specimen which, as such, has no influence on the strength. Because limit analysis applies with virtual deformations there is no effect

## Exact Fracture Mechanics theory

of initial stresses or deformations on the limit collapse load.. As condition for zero values of  $R$ , the sum of the normal stresses in the upper plane AB should be equal and opposite to the normal stresses in the bottom plane CD, giving:

$$\sigma W = 2 \int_a^{W/2} \sigma_y dx = 2 \int_a^{W/2} \left( Y \sigma / \sqrt{1 - (a/x)^2} \right) dx = Y \sigma W \sqrt{1 - (2a/W)^2}, \quad (10.2.2)$$

and the stress multiplication factor thus is:

$$Y = 1 / \sqrt{1 - (2a/W)^2}. \quad (10.2.3)$$

The stress intensity factor  $K_I$  due to the critical small crack concentration follows from:

$$K_I = \sigma_y \sqrt{\pi a_c} = \sigma_y \sqrt{\pi 2(x-a)} = \left( Y \sigma / \sqrt{1 - (a/x)^2} \right) \sqrt{\pi 2(x-a)} = Y x \sigma \sqrt{2\pi / (x+a)} \quad (10.2.4)$$

As shown § 3.6 and in [3], the small crack merging towards the macro-crack tip causes the macro-crack extension. When the nearest, determining small crack tip is situated at a distance  $x$ , then the one sided small crack merging distance to the macro-crack tip is  $x - a$ , which is equal to half the small crack length  $c$  of row A of fig. 3.8. Thus:  $c = (x - a)$ , and total  $2(x - a)$  applies, of both sides

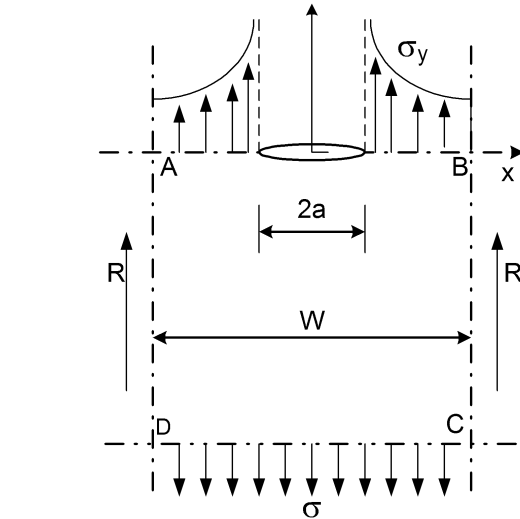
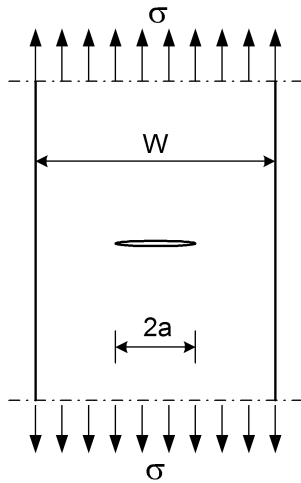


Fig. 10.1. CN test specimen

Fig. 10.2. Cut out of the specimen from the infinite plate

**Table 10.1. Comparison of linear elastic Geometric correction factors**

$2a/W$	$Y = \sqrt{\sec(\pi a/W)}$	$Y = 1/\sqrt{1 - (2a/W)^2}$	$Y = \sqrt{(W/\pi a) \cdot \tan(\pi a/W)}$
0.1	1.006	1.005	1.004
0.2	1.025	1.021	1.016
0.3	1.059	1.048	1.040
0.4	1.112	1.091	1.075
0.5	1.189	1.155	1.128
0.6	1.304	1.250	1.208
0.8	1.799	1.667	1.565
0.9	2.528	2.294	2.113
0.95	3.570	3.203	2.918
	Feddersen Koiter et al	Limit analysis solution, eq.(10.2.3)	Irwin

## Exact Fracture Mechanics theory

of two sided macro-crack extension of the initial crack length of  $2a$ . This also applies when the macro crack-tip has become sharp enough to take part in the crack merging process. Then all active crack tips extend over a distance  $c$ , which is equal to  $c = (x - a)$  in the analysis.

For  $x \rightarrow a$ , the lowest, thus first occurring, initial flow value for  $K_I$  of eq.(10.2.4), becomes:

$$K_I = Y\sigma\sqrt{\pi a} \quad (10.2.5)$$

This is identical to the results of other methods, showing the mathematical flat crack, singularity solution, to apply for the smallest initial small crack system and to represent clear wood fracture at the start of “flow” and crack extension (see also § 3.6 and § 3.10). Thus the derived geometric correction factor  $Y$  is comparable to the other solutions of Tada, Feddersen, Koiter, Isida and Irwin [8]. The exact value of  $Y$ , according to eq.(10.2.3):  $Y = 1/\sqrt{1 - (2a/W)^2}$ , lies intermediate between the, in [8] given, values of Feddersen and Koiter et al. around  $Y = \sqrt{\sec(\pi a/W)}$  and the solution of Irwin:  $\sqrt{(W/\pi a) \cdot \tan(\pi a/W)}$ . In Table 10.1, eq.(10.2.3) is compared with the solution of Irwin and the usual applied Feddersen equation. The precise description by the exact derivation shows that small crack merging does not only explains yield drop, but is the basic mechanism of all crack extension. This is discussed in chapter 3. The small crack limit behavior is derived in § 10.3. The possibilities of the singularity approach are very limited and extension of the theory for e.g. crack bridging and mixed mode loading are not possible at assumed collinear crack extension.

### 10.3. Small crack limit strength behavior

#### 10.3.1. Small crack limit dimensions

The interpretation of the strength data-line of Fig. 10.3 on geometrically similar specimens of Bazant is to regard the inclined line to represent LEFM theory, the horizontal line to be the strength theory and the curved, connecting line to follow nonlinear fracture theory. However, there is no difference between nonlinear and linear elastic (LEFM) fracture mechanics. For both the linear elastic - full plastic approach of limit analysis applies. The full-plastic zone of the elastic-full plastic approach exists as failure criterion, by a single curve in stress space as shown in Fig. 10.3. In this figure of [9], is  $d/d_0$ , the ratio of specimen size to the fracture process zone size. But, because the line is the result of volume effect tests, the initial crack length is proportional to the test-specimen length. Thus,  $d/d_0$  also can be regarded to be the ratio: initial open crack length, to the process zone size. Then, for small values of  $d$ , this  $d/d_0$  ratio also may represent the critical small crack density in a macro specimen ( $d$  also is small crack interspace). The curved line of Fig. 10.3, follows the equation:

$$\ln \sigma = \ln \sigma_0 - 0.5 \ln(1 + d/d_0) \quad (10.3.1)$$

This can be written:

$$\ln\left(\frac{\sigma}{\sigma_0}\right) = \ln\left(\frac{d_0 + d}{d_0}\right)^{-0.5} = \ln\left(\frac{d_0}{d_0 + d}\right)^{0.5} \quad (10.3.2)$$

$$\text{or: } \sigma\sqrt{\pi(d_0 + d)} = \sigma_0\sqrt{\pi d_0} = K_c, \quad (10.3.3)$$

This confirms that the curve represents the stress intensity as ultimate state with  $K_c$  as critical stress intensity factor as should be for values of  $d/d_0 \gg 1$ . For these higher values the curved line approaches the drawn straight tangent line  $\ln \sigma = \ln \sigma_0 - 0.5 \cdot \ln(1 + d/d_0) \approx \ln \sigma_0 - 0.5 \ln(d/d_0)$  with the necessary slope of the curve: (Bazant - curve)

$\frac{\partial \ln(\sigma/\sigma_0)}{\partial \ln(d/d_0)} \approx -0.5$  as limit. The real slope however is:

$$\frac{\partial \ln \sigma}{\partial \ln(d/d_0)} = \frac{\partial \ln(\sigma/\sigma_0)}{(d_0/d)\partial(d/d_0)} = \frac{d}{d_0} \frac{\partial(\ln(1 + d/d_0)^{-0.5})}{\partial(d/d_0)} = \frac{d}{d_0} \cdot \frac{-0.5}{1 + d/d_0} = \frac{-0.5}{1 + d_0/d} \quad (10.3.4)$$

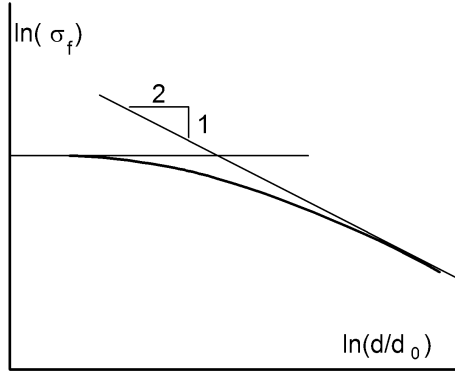


Fig. 10.3. From [9]. Limit LEFM behavior as correction of the interpretation of [9].

This slope is:  $-0.5$  for  $d \gg d_0$  and this slope is zero when  $d = 0$ .

This shows that for the whole curve LEFM applies and it is an indication that, at zero open crack dimensions, thus for:  $d = 0$ , the clear wood ultimate strength theory still follows LEFM, because it applies also for the constant initial length  $d_0$  (the fracture process zone length).

After first yield drop, to half way unloading, the strength theory further applies for further unloading by crack extension. Similar to steel, where yield drop is due to dislocation multiplication and dislocation breakaway, applies for wood, that yield drop is due to Micro-crack multiplication (as fracture zone  $d_0$ ) and micro- crack propagation and merging. The clear wood Wu-equation then may be expressed in stresses (see [2]) in stead of in stress intensities.

The in § 2.3 derived equation:

$$1 = \frac{\sigma_y}{\xi_0 \sigma_t / 2} + \frac{\tau_{xy}^2}{\xi_0^2 \sigma_t^2}, \text{ with } \xi_0 = \sqrt{2r_0 / c} \text{ for collinear crack extension, can only be written as:}$$

$$1 = \frac{\sigma_y \sqrt{\pi c}}{\sigma_t \sqrt{\pi r_0} / 2} + \frac{(\tau_{xy} \sqrt{\pi c})^2}{(\sigma_t \sqrt{2\pi r_0})^2} = \frac{K_I}{K_{Ic}} + \frac{K_{II}^2}{(K_{IIc})^2},$$

when  $r_0$ , the radius of the fracture process zone is constant. In the limit case of clear wood micro-crack failure, when  $2c \approx r_0$ , the equation becomes, with  $\tau_u = 2\sigma_t$ , for the isotropic matrix:

$$1 = \frac{\sigma_y}{\sigma_t} + \frac{\tau_{xy}^2}{\tau_u^2} \quad (10.3.4)$$

### 10.3.2. Small crack failure criterion

Softening called yield drop is explained by the crack merging mechanism and discussed for mode I and II, in Chapter 3. Because the isotropic matrix fails before the reinforcement, limit analysis has to be applied for the isotropic stresses in the isotropic matrix. This is not followed by all other fracture mechanics approaches, which therefore don't satisfy the failure criterion and are not able to give the right exact mixed mode fracture criterion. At initial "flow" of the matrix, the stresses of the still elastic reinforcement follow in proportion the matrix stresses. That the matrix is first determining follows e.g. for Balsa wood, which is highly orthotropic, but is light, thus has a low reinforcement content and shows total failure soon after matrix failure and thus shows at failure the isotropic ratio of  $K_{IIc} / K_{Ic} \approx 2$  of the isotropic matrix material. But also for strong clear wood which is failing by shear by single oblique crack extension according to Fig. 2.3.2, it appears that the start of crack extension shows the isotropic oblique angle, showing the matrix to be determining for initial failure.

The truss action, at bending failure of a beam, causes a negative contraction coefficient in the bending tension zone. This shows that the reinforcement holds, even after flow in compression and

stress redistribution, with increased tension in the reinforcement. It is therefore a requirement for an exact orthotropic solution of the total applied stress, applicable to wood, to also satisfy the isotropic flow solution of matrix-stresses and to look at possible stress redistributions.

As discussed at § 5.2 (and Section A), the (small crack) failure criterion for shear with tension is: eq.(5.1) or eq.(5.2), which becomes, as limit behavior, equal to the Wu-equation when due to full hardening  $c \rightarrow 1$  in eq.(5.2). Full hardening is possible when the test rig is stiff enough to remain stable during test. The solution of the crack problem of Irwin as summation of in plane and antiplane solutions in order to use (with minor adaptations) isotropic stress functions for the orthotropic case, and to apply descriptions in the three characteristic modes and to sum the result for the general mixed mode case, is not right for wood. It misses e.g. the interaction terms and the failure equation, eq.(5.2), is not orthotropic, because it is not quadratic but contains a third degree term and thus does not show orthotropic symmetry. This coupling term is absent in the general accepted solutions. The strong influence of compression in e.g. fig. 5.2, therefore cannot be given. The stress function which leads directly to the Wu-equation is given in § 2.3 and in [3]. Necessary are the stresses at the crack boundary to know the mode of failure. This follows from the exact derivation in chapter 2 and is applied by numerical simulation by the VCC- technique of the finite element method, and thus can not be based on a separate calculation of the energy release rates of the normal stress in the opening mode and of the shear stress in the sliding mode according to the method of Sih, Paris, Irwin by giving the sum of separate solutions of the 3 modes, without interactions, (as e.g.  $3F_{266}\sigma_2\sigma_6^2$ ) what is assumed to be possible by assumed isotropic and orthotropic symmetry. Thus the, not orthotropic, “mixed mode”, interactions, as given by Fig. 5.1 and 5.2, can not be described by other methods.

### 10.4. Conclusions regarding small crack fracture mechanics

- Part of the conclusions are given in Chapter 8.
- The right derivation is given of the geometric correction factor of the center notched specimen, based on small-crack extension to the macro-crack tip, and based on a constant finite ultimate cohesion strength and constant dimensions of the process zone and thus **not** based on an infinite tensile strength at zero process zone dimensions of the other derivation methods.
- A new interpretation is given of the transition of strength theory to fracture mechanics theory of Bazant based on tests on geometrically similar specimens. It follows that the whole curve represents LEFM (linear elastic fracture mechanics) and shows that, at zero open crack dimensions, the clear wood ultimate strength theory still follows LEFM, because it applies also for the constant initial length of the fracture process zone length.
- Eq.(10.3.3) shows that the crack length consist of an open part plus the process zone length.
- There is no difference between linear elastic- and non-linear fracture mechanics because for both approaches linear elastic behavior is regarded up to failure and plastic flow. This is possible because by the virtual work approach at the ultimate state there is no influence on the strength depending on the loading path followed and of initial stresses and internal equilibrium systems. The critical energy release rate is in both cases determined by plastic behavior. In fact always the linear full plastic approach of limit analysis applies for the boundary value approach and ultimate state at the crack-tip boundary.
- It is confirmed:
  - that limit analysis applies, with elastic-full plastic behavior and may be regarded to be elastic up to fracture, at the confined plastic zone.
  - that wood behaves as a reinforced material, and the solutions of the isotropic Airy stress function of the matrix stresses as well as the orthotropic Airy stress function of the total stresses are needed,
  - that reaction kinetics and the general applicable failure criterion indicate that, small-crack processes are always determining for fracture.
- The explanation of the failure criterion is given. All other methods are **not** able to give and explain the right failure criterion for combined “mixed mode” failure

## 10.5. References

- [1] van der Put T.A.C.M., A continuum failure criterion applicable to wood, *J Wood Sci* (2009) 55:315–322, (A(2009)).
- [2] van der Put T.A.C.M., A general failure criterion for wood, *Proc. 15<sup>th</sup> CIB-IUFRO Timber Engineering Group Meeting, Boras, May 1982*, A(1982a),
- [3] van der Put T.A.C.M., A new fracture mechanics theory of wood, Nova Science Publishers, Inc. New York, C(2011a), or more complete:  
T.A.C.M. van der Put Exact and complete Fracture Mechanics of wood. Theory extension and synthesis of all series C publications
- [4] van der Put T.A.C.M., Exact derivation of the geometric correction factor of the center notched test specimen, based on small cracks merging as explanation of yield drop; *Int. J. Comp. Eng. Res.* Vol. 04, Issue, 7, July 2014, C(2014a).
- [5] van der Put T.A.C.M., Discussion of: “Mode II fracture mechanics properties of wood measured by the asymmetric four-point bending test using a single-edge-notched specimen of H Yoshihara in *Eng. Frac. Mech.* 75 pp 4727-4739” in *Eng. Frac. Mech.* 90 pp 172-179, C(2012).
- [6] Boström L, Method for determination of the softening behavior of wood etc. Thesis, Report TVBM-1012, Lund, Sweden, (1992).
- [7] Westergaard H.M., *Trans. ASME, J. Appl. Mech.* Vol. 61, 1939, pp A49 – A53.
- [8] Tada H., Paris .P.C. and Irwin G,R. *The stress analysis of Cracks Handbook*”. Del Research Corporation, St. Louis, Missouri, 1985, H. Tada, Paris and G.R. Irwin.
- [9] I. Smith, E. Landis, M. Gong, *Fracture and Fatigue in Wood*, J. Wiley & Sns.
- [10] van der Put T.A.C.M. (2010): Failure criterion for timber beams loaded in bending, compression and shear, *Wood Material Science & Engineering*, 5:1, 41-49
- [11] van der Put T.A.C.M., *Deformation and damage processes in wood*, Delft University Press, The Netherlands, (1989), B(1989a).
- [12] Yoshihara, H. (2012) Mode II critical stress intensity factor of wood measured by the asymmetric four-point bending test of single-edge-notched specimen while considering an additional crack length, *Holzforschung*, 66, pp 989-992.
- [13] Yoshihara H. (2008) Mode II fracture mechanics properties of wood measured by the asymmetric four-point bending test using a single-edge-notched specimen, *Eng. Frac. Mech.* 75 pp.4727-4739.
- [14] van der Put T.A.C.M. (1974) Breukcriterium voor beton als ondergrens van de sterkte bepaald volgens de evenwichtsmethode *Cement* (1974) XXVI No10 pp 420-421

## 11. Conclusions overview

In chapter 8, conclusions are given regarding chapters 1 to 7.

Conclusions of chapter 9, regarding the size effect, are given in § 9.5

Conclusions of chapter 10 regarding small crack fracture are given in § 10.4.

## Appendix A:

### The dynamics of crack propagation

The dynamic extension of the Griffith theory is given by Berry in: Some kinetic considerations of the Griffith criterion for fracture I and II: *J. Mech. Phys. Solids*, 8, 194-206 and 207-216.

Regarding the test specimen of fig. 3.1, assuming plane stress, the work done by the external forces is:

$$W_i = bl\sigma_i^2 \left[ 1 + 2\pi c_i^2 / bl \right] / 2E \quad (A1)$$

Including the apparent surface energy:  $4\alpha c_i$  gives as total energy:

$$V_i = bl\sigma_i^2 \left[ 1 + 2\pi c_i^2 / bl \right] / 2E + 4\alpha c_i \quad (A2)$$

When the crack extends at constant  $\sigma_i$ , the total energy  $V$  will be

## Exact Fracture Mechanics theory

$$V = bl\sigma_i^2 \left[ 1 + 2\pi c_i^2 / bl \right] / 2E + 4\alpha c_i + K \quad (\text{A3})$$

Where  $K$  is the stored kinetic energy. The work  $W - W_i$  done by  $\sigma_i$  during the extension is:

$$W - W_i = bl\sigma_i(\varepsilon - \varepsilon_i) \quad (\text{A4})$$

where  $\varepsilon, \varepsilon_i$  are the strains corresponding to crack lengths  $c, c_i$ . Thus:

$$W - W_i = 2\pi\sigma_i^2(c^2 - c_i^2) / E \quad (\text{A5})$$

Equating this to  $V - V_i$  gives:

$$\pi\sigma_i^2(c^2 - c_i^2) / E = 4\alpha(c - c_i) + K \quad (\text{A6})$$

Writing:  $n = 4\alpha E / \pi c_i \sigma_i^2$  this is:

$$K = \pi\sigma_i^2 c^2 (1 - c_i / c) [1 - (n-1)c_i / c] / E \quad (\text{A7})$$

On dimensional grounds is:

$$K = k\rho\sigma_i^2 c^2 v_c^2 / 2E^2 \quad (\text{A8})$$

where  $v_c = dc / dt$  velocity of crack extension,  $\rho$  the density and  $k$  is a constant.

From the last 2 equations follows:

$$v_c^2 = \frac{2\pi E}{k\rho} \left( 1 - \frac{c_i}{c} \right) \left[ 1 - (n-1) \frac{c_i}{c} \right] = v_m^2 \left( 1 - \frac{c_i}{c} \right) \left[ 1 - (n-1) \frac{c_i}{c} \right] \quad (\text{A9})$$

where  $v_m = \sqrt{2\pi E / k\rho} = 0.38\sqrt{E / \rho}$  is the maximum velocity of crack extension.

Differentiating eq.(A9) gives the acceleration of the moving crack tip:

$$\frac{dv_c}{dt} = \frac{\pi E c_i}{k\rho c^2} \left[ n - 2(n-1) \frac{c_i}{c} \right] \quad (\text{A10})$$

It follows from eq.(A9) that the crack velocity is zero when  $c = c_i$  and from eq.(A10), that for  $n = 2$ , the acceleration of crack extension is zero also. For  $n = 2$  is  $\pi c_i \sigma_i^2 = 2\alpha E$ , which is the Griffith equation. Thus the crack of Griffith length is in unstable equilibrium but does not propagate. For  $n < 2$ , is  $\sigma_i > \sigma_g$ , the Griffith stress, the crack propagates.

### Appendix B:

#### Direction of crack propagation

The in Chapter 2 given derivation of the mixed mode fracture criterion was for the first time given for concrete in:

van der Put T.A.C.M. (1974) Breukcriterium voor beton als ondergrens van de sterkte bepaald volgens de evenwichtsmethode Cement (1974) XXVI No10 pp 420-421, (in Dutch). i.e.:

Fracture criterion for concrete as lower bound of the strength, determined by the limit analysis equilibrium method.

Also a dissertation was then written and handed over to prof. Bruggeling of Delft University.

Although there never was a reaction, he should be able to give information about the progress of this project.

Figure B.1, of

Fracture Mechanics of Concrete Structures, de Borst et al (eds)© 2001 Swets & Zeitlinger, Lisse, ISBN 90 2651 825 0, based on:

Shear behavior in fracture process zone of concrete; Y. Shinohara, Structural Engineering Research Center, Tokyo Institute of Technology, Tokyo, Japan

Shows oblique crack extension due to mixed mode loading.

If specimens were not pre-cracked for shear tests under constant vertical load, it was found that a diagonal cracking always nucleated and extended from the bottom of the right notch, as shown in the left of Figure B.1. According to FEM analysis stated in section 2, the maximum principal stress occurred at the right notch tip and the direction normal to it is also shown in Figure B.1. The initial

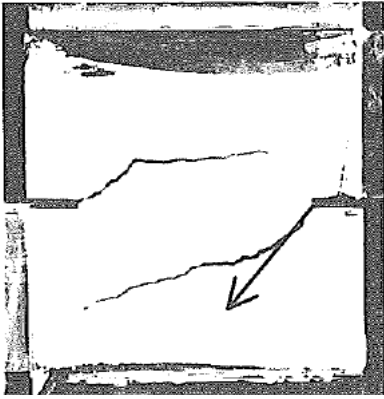


Fig. B.1. Double-edge notched specimen loaded in tension and shear, in concrete.  
Square 200x200x100 specimen

crack propagated in the direction normal to the maximum principal stress. This means the shear failure is caused by tensile stress, according to theory. The crack propagation is due to the tensile stresses and perpendicular to the direction of this principal stress. With further increasing shear displacement, the second diagonal crack ran from the top of the left notch, so that a compressive strut eventually formed in the specimen. In that case, the compressive shear load would be carried by the intact part between two diagonally overlapping cracks, as shown in the right of Figure 10.